AD-A231 722

SSC-343

GLOBAL ICE FORCES AND SHIP RESPONSE TO ICE

A SECOND SEASON

SHIP STRUCTURE COMMITTEE

1990

91 2 01 050

SHIP STRUCTURE COMMITTEE

The SHIP STRUCTURE COMMITTEE is constituted to prosecute a research program to improve the hull structures of ships and other marine structures by an extension of knowledge pertaining to design, materials, and methods of construction.

RADM J. D. Sipes, USCG, (Chairman)
Chief, Office of Marine Safety, Security and Environmental Protection
U. S. Coast Guard

Mr. Alexander Malakhoff
Director, Structural Integrity Subgroup (SEA 55Y)
Naval Sea Systems Command

Dr. Donald Liu
Senior Vice President
American Bureau of Shipping

Mr. H. T. Haller
Associate Administrator for Shipbuilding and Ship Operations
Maritime Administration

Mr. Thomas W. Allen
Engineering Officer (N7)
Military Sealift Command

CDR Michael K. Parmelee, USCG,
Secretary, Ship Structure Committee
U. S. Coast Guard

CONTRACTING OFFICER TECHNICAL REPRESENTATIVES

Mr. William J. Siekierka
SEA 55Y3
Naval Sea Systems Command

Mr. Greg D. Woods
SEA 55Y3
Naval Sea Systems Command

SHIP STRUCTURE SUBCOMMITTEE

The SHIP STRUCTURE SUBCOMMITTEE acts for the Ship Structure Committee on technical matters by providing technical coordination for determinating the goals and objectives of the program and by evaluating and interpreting the results in terms of structural design, construction, and operation.

AMERICAN BUREAU OF SHIPPING

Mr. Stephen G. Arntson (Chairman)
Mr. John F. Conlon
Mr. William Hanzalek
Mr. Philip G. Rynn

NAVAL SEA SYSTEMS COMMAND

Mr. Robert A. Sielski
Mr. Charles L. Null
Mr. W. Thomas Packard
Mr. Allen H. Engle

MILITARY SEALIFT COMMAND

Mr. Albert J. Attermeyer
Mr. Michael W. Touma
Mr. Jeffery E. Beach

U. S. COAST GUARD

CAPT T. E. Thompson
CAPT Donald S. Jensen
CDR Mark E. Noll

MARITIME ADMINISTRATION

Mr. Frederick Seibold
Mr. Norman O. Hammer
Mr. Chao H. Lin
Dr. Walter M. Maclean

SHIP STRUCTURE SUBCOMMITTEE LIAISON MEMBERS

U. S. COAST GUARD ACADEMY

LT Bruce Mustain

U. S. MERCHANT MARINE ACADEMY

Dr. C. B. Kim

U. S. NAVAL ACADEMY

Dr. Ramswar Bhattacharyya

STATE UNIVERSITY OF NEW YORK MARITIME COLLEGE

Dr. W. R. Porter

WELDING RESEARCH COUNCIL

Dr. Martin Prager

NATIONAL ACADEMY OF SCIENCES - MARINE BOARD

Mr. Alexander B. Stavovy

NATIONAL ACADEMY OF SCIENCES - COMMITTEE ON MARINE STRUCTURES

Mr. Stanley G. Stiansen

SOCIETY OF NAVAL ARCHITECTS AND MARINE ENGINEERS - HYDRODYNAMICS COMMITTEE

Dr. William Sandberg

AMERICAN IRON AND STEEL INSTITUTE

Mr. Alexander D. Wilson

Member Agencies:

United States Coast Guard
Naval Sea Systems Command
Maritime Administration
American Bureau of Shipping
Military Sealift Command

Ship Structure Committee

An Interagency Advisory Committee
Dedicated to the Improvement of Marine Structures

Address Correspondence to:

Secretary, Ship Structure Committee
U.S. Coast Guard (G-MTH)
2100 Second Street S.W.
Washington, D.C. 20593-0001
PH: (202) 267-0003
FAX: (202) 267-0025

SSC-343
SR-1320

December 3, 1990

GLOBAL ICE FORCES AND SHIP RESPONSE TO ICE
A SECOND SEASON

This report is the last in a series of six that address ice loads, ice forces, and ship response to ice. The data for these reports were obtained during deployments of the U.S. Coast Guard Icebreaker POLAR SEA. This report provides a second set of data and describes the method used to determine global ice impact forces from strain gage measurements. A comparison of results from earlier data analyses is included. The observations of global ice impact loads are combined with those from previous deployments. The other ice reports are published as SSC-329, SSC-339, SSC-340, SSC-341 and SSC-342. These six reports are a valuable contribution to the body of knowledge of ship/ice interactions and will be useful in developing ice load criteria for the design of ice breaking ship hulls.

J. D. SIPES
Rear Admiral, U.S. Coast Guard
Chairman, Ship Structure Committee

Technical Report Documentation Page

1. Report No. SSC-343	2. Government Accession No.	3. Recipient's Catalog No.
4. Title and Subtitle Global Ice Forces and Ship Response to Ice - A Second Season		5. Report Date August 1990
		6. Performing Organization Code
7. Author(s) P. Minnick, J. St. John		8. Performing Organization Report No. AEI 1298C
9. Performing Organization Name and Address ARCTEC Engineering, Inc. 9104 Red Branch Road Columbia, MD 21045		10. Work Unit No. (TRAIS)
		11. Contract or Grant No. DTMA-91-84-C-41032
12. Sponsoring Agency Name and Address Maritime Administration U.S. Department of Transportation 400 Seventh Street, SW Washington, DC 20593		13. Type of Report and Period Covered Final Report
		14. Sponsoring Agency Code MAR-760

15. Supplementary Notes
The U.S. Maritime Administration served as the sponsoring agency for the interagency Ship Structure Committee.

16. Abstract
During September of 1986 the POLAR STAR conducted ice-impact tests on ice pressure ridges and ice floes in the Alaskan portion of the Beaufort Sea. Strain gages were used to obtain measurements of the bending strain on the hull girder of the POLAR STAR during impacts with ice features. These measurements were then used to calculate the longitudinal bending moment and shear force distributions to arrive at an estimate of the vertical bow force. Compressive strains along the stem and ship acceleration and velocity measurements were also recorded. This report describes the methodology for determining the global ice impact force from the measurements and presents the results of these tests. Sample hull strain, and impact force time-histories are presented along with the longitudinal bending and shear distributions from several ramming events. A comparison of the results with other available data is also presented and the observations are combined with global ice impact loads measured on the POLAR SEA during the previous year. Results indicate that the methodology used in estimating the impact force contributes to the overall understanding of the ship-ice interaction process.

17. Key Words Design Criteria, Ice Loads, Icebreakers, Shipboard Loads Measurement	18. Distribution Statement Document is available to the U.S. Public through the National Technical Information Service, Springfield, VA 22161

19. Security Classif. (of this report) Unclassified	20. Security Classif. (of this page) Unclassified	21. No. of Pages	22. Price

Form DOT F 1700.7 (8-72) Reproduction of completed page authorized

METRIC CONVERSION FACTORS

Approximate Conversions to Metric Measures

Symbol	When You Know	Multiply by	To Find	Symbol
		LENGTH		
in	inches	*2.5	centimeters	cm
ft	feet	30	centimeters	cm
yd	yards	0.9	meters	m
mi	miles	1.6	kilometers	km
		AREA		
in^2	square inches	6.5	square centimeters	cm^2
ft^2	square feet	0.09	square meters	m^2
yd^2	square yards	0.8	square meters	m^2
mi^2	square miles	2.6	square kilometers	km^2
	acres	0.4	hectares	ha
		MASS (weight)		
oz	ounces	28	grams	g
lb	pounds	0.45	kilograms	kg
	short tons (2000 lb)	0.9	tonnes	t
		VOLUME		
tsp	teaspoons	5	milliliters	ml
Tbsp	tablespoons	15	milliliters	ml
fl oz	fluid ounces	30	milliliters	ml
c	cups	0.24	liters	l
pt	pints	0.47	liters	l
qt	quarts	0.95	liters	l
gal	gallons	3.8	liters	l
ft^3	cubic feet	0.03	cubic meters	m^3
yd^3	cubic yards	0.76	cubic meters	m^3
		TEMPERATURE (exact)		
°F	Fahrenheit temperature	5/9 (after subtracting 32)	Celsius temperature	°C

*1 in. = 2.54 cm (exactly). For other exact conversions and more detail tables see NBS Misc. Publ. 286. Units of Weight and Measures. Price $2.25 SD Catalog No. C13 10 286.

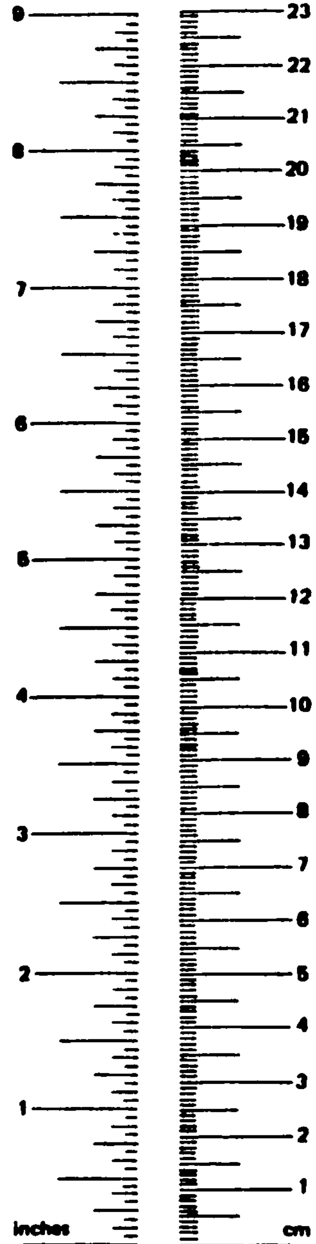

Approximate Conversions from Metric Measures

Symbol	When You Know	Multiply by	To Find	Symbol
		LENGTH		
mm	millimeters	0.04	inches	in
cm	centimeters	0.4	inches	in
m	meters	3.3	feet	ft
m	meters	1.1	yards	yd
km	kilometers	0.6	miles	mi
		AREA		
cm^2	square centimeters	0.16	square inches	in^2
m^2	square meters	1.2	square yards	yd^2
km^2	square kilometers	0.4	square miles	mi^2
ha	hectares (10,000 m^2)	2.5	acres	
		MASS (weight)		
g	grams	0.035	ounces	oz
kg	kilograms	2.2	pounds	lb
t	tonnes (1000 kg)	1.1	short tons	
		VOLUME		
ml	milliliters	0.03	fluid ounces	fl oz
l	liters	2.1	pints	pt
l	liters	1.06	quarts	qt
l	liters	0.26	gallons	gal
m^3	cubic meters	35	cubic feet	ft^3
m^3	cubic meters	1.3	cubic yards	yd^3
		TEMPERATURE (exact)		
°C	Celsius temperature	9/5 (then add 32)	Fahrenheit temperature	°F

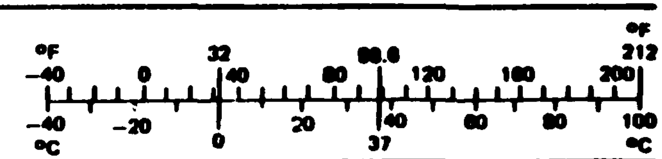

PREFACE

The overall objective of the project was to measure and analyze the global ice-hull interaction forces of a ship ramming in multi-year ice. Specific objectives were to obtain a larger data base of ice loads for the development of analytical models describing ship-ice interaction, and to analyze the effect of ship displacement and bow shape on global ice loads through comparison with the Canadian experience gained from the 1983 KIGORIAK and ROBERT LEMEUR Impact Tests [17].

The instrumentation system that was developed for measurement of global ice impact loads onboard the USCGC POLAR SEA in 1985 was adapted with only minor modifications for use on the USCGC POLAR STAR. From September 17 to September 28, 1986, the POLAR STAR conducted ice-impact tests on ice pressure ridges and ice floes in the Alaskan portion of the Beaufort Sea. Bending strain gage measurements were used to estimate the longitudinal bending moment distribution of the POLAR STAR during impacts with ice features. Compressive strains along the stem and ship acceleration and velocity measurements were also recorded. Since the methodology used was the same as that used during the previous year to measure the global ice impact loads on the POLAR SEA, both sets of observations could be combined.

TABLE OF CONTENTS

LIST OF FIGURES

LIST OF FIGURES (Continued)

LIST OF TABLES

1. INTRODUCTION

USCGC POLAR Class winter deployments sponsored by Maritime Administration (MarAd) have provided a platform to gather environmental, trafficability, and ship performance data. For this phase of the program, a deployment of the POLAR STAR in September of 1986, the Ship Structure Committee and the Maritime Administration sponsored a program to collect global ice load data. The data collected from this deployment is in a form that can be combined with the global ice load information obtained on the POLAR SEA during 1985.

The ultimate objective of this jointly funded research is to develop ice load criteria for the future design of ships. Specifically, the objective of this study was to measure the total load that ice exerts on the hull of the vessel when it rams large ice features. Other objectives included increasing the data base of ice loads for the development of analytical models describing the ship-ice interaction and for understanding the effect of ship displacement and bow shape upon the global ice loads by comparison with other available data.

The "global ice load" is defined as the net resultant of the ice loads generated at the many local contact areas around the bow during impact. These loads may generate significant bending moments in the hull girder, which may affect the structural integrity of icebreaking ships. This in turn has implications on the design of icebreaking vessels and the type of design criteria to be developed.

Since the start of commercial oil development in the Arctic a number of analytical models describing ship-ice interaction have been developed using a rigid body idealization, flexible beam elements, and three dimensional finite element models [1,2,3,4]. Full-scale impact tests have also been conducted on the icebreaking vessels M.V. CANMAR KIGORIAK [5,6], M.V. ROBERT LEMEUR [6,7], M.V. ARCTIC [8] and now the USCGC POLAR SEA [9]. General discussions of these tests can be found in References 10 and 11. Physical modelling of the ship-ice impact interaction for the M.V. ARCTIC has also been carried out by ARCTEC CANADA for the Canadian Coast Guard [12] and the Technical Research Center of Finland under a joint research program. The focus of all this work has been to provide a sound technical basis for further development of ice load design criteria to accommodate the technical and regulatory requirements of expanding maritime operations in the Arctic.

Work presented here was carried out onboard the USCGC POLAR STAR in the Alaskan Beaufort Sea between September 17 and September 28, 1986. Figure 1 shows the principal areas of operation during the deployment. This report describes data collection methods and presents an analysis of the collected data.

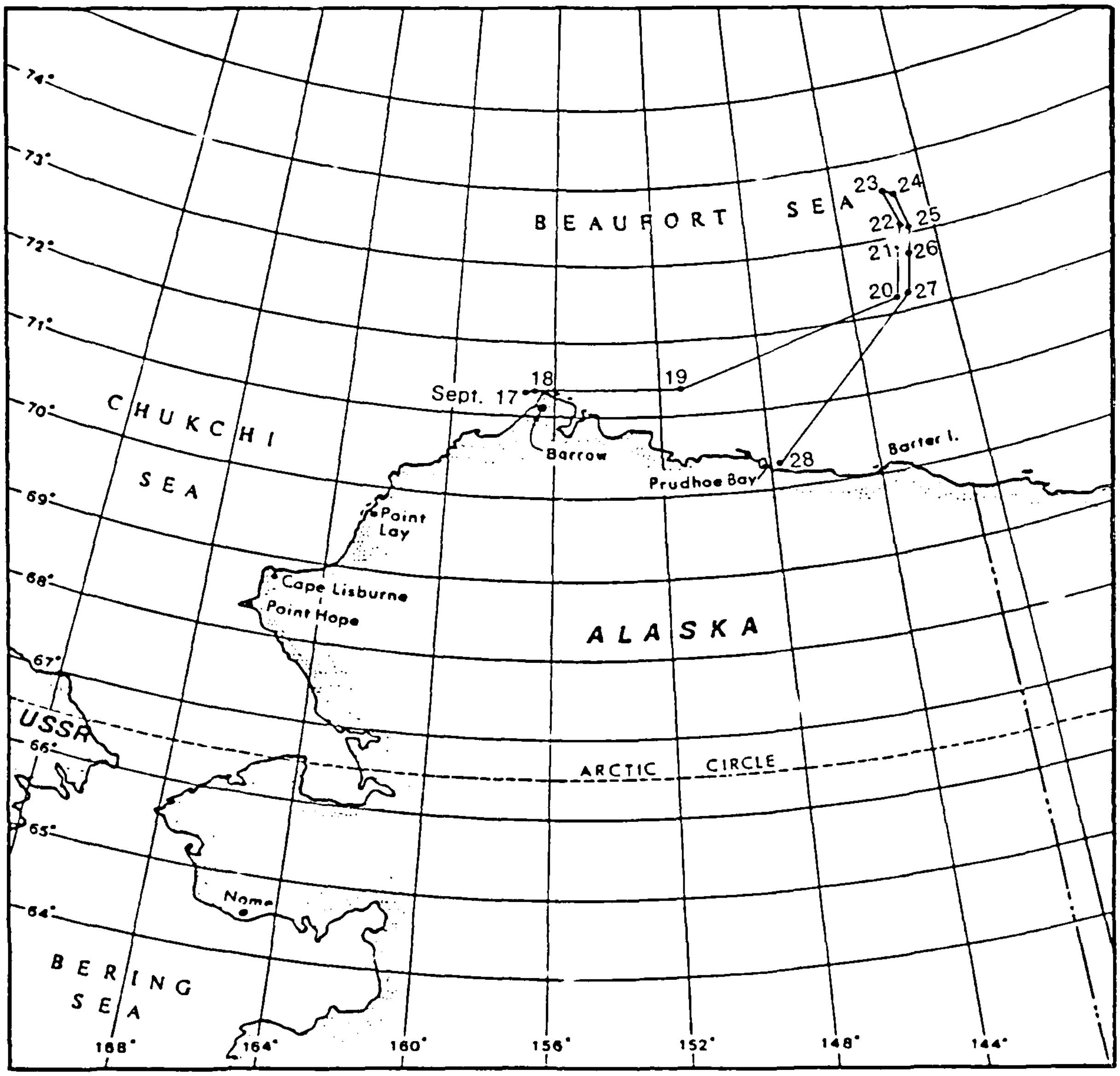

Figure 1

DAILY LOCATION OF USCGC POLAR STAR
AT 0800 LOCAL TIME

2. DESCRIPTION OF THE DATA ACQUISITION SYSTEM

An outline of the instrumentation system developed for this project is illustrated in Figure 2. The present system was adapted from the system originally developed by Canadian Marine Drilling Ltd. (Canmar) for the 1983 M.V. KIGORIAK and M.V. ROBERT LEMEUR full-scale impact tests [6] and is, with only slight modifications, the same system that was used on the POLAR SEA in 1985 [9]. There are several fundamental differences between the KIGORIAK and LEMEUR system and the system developed for use on the POLAR Class. The approach used on the POLAR Class measured the longitudinal bending strain distribution spanning the location of the ice load, whereas the Canmar system measured the shear strain in sections near the location of the ice load and the bending strain distribution aft of the location of the ice load. The POLAR Class method required fewer strain gages at each location and therefore allowed more frames along the ship to be instrumented. The result was a better definition of the longitudinal bending and shear distribution spanning the location of the load because of the larger number of instrumented frames. Secondly, in these tests the actual longitudinal location of the load was measured from compressive strain gages along the centerline bulkhead, while the Canmar system had to infer the location from other data. Additional details of the POLAR STAR system as well as an itemized channel description are presented in Appendix A.

To estimate the vertical ice force on the bow during an impact with a heavy ice feature, the shear force around the location of the load must be well defined. Figure 3 gives some idealized shear and bending moment diagrams for an icebreaker ramming into an ice feature. As the lower figure indicates, the shear force changes from negative to positive over a relatively short distance near the location of the load. Since the shear force is the negative of the slope of the bending moment diagram, the bending moment must be well defined over this same region in order to obtain an accurate estimate of the shear force. With this in mind, the majority of the frames instrumented for bending were concentrated near the anticipated location of the ice force. Figure 4 shows the location of these gages.

The bending gages along the 01 Deck, the 3rd Deck, and the 1st Platform were placed parallel to the side shell in pairs along opposite sides of the ship. Measurements taken from these gages were later transformed into the strain parallel to the centerline. (See Appendix B for the details involved in any of these conversions and computations.) In the calculation of longitudinal strain due to the ice force, data from each pair were averaged to exclude any torsional strain. Another advantage of this gage pair arrangement was the ability to observe the symmetry, or the lack thereof, in the ice loading during a ram.

The bending gages were placed on at least two levels for every location forward of frame 85. This arrangement allowed computation of the bending moment based upon a stress couple with a known separation distance. It had the further advantage of eliminating the longitudinal stress, and therefore force, from the bending moment calculation.

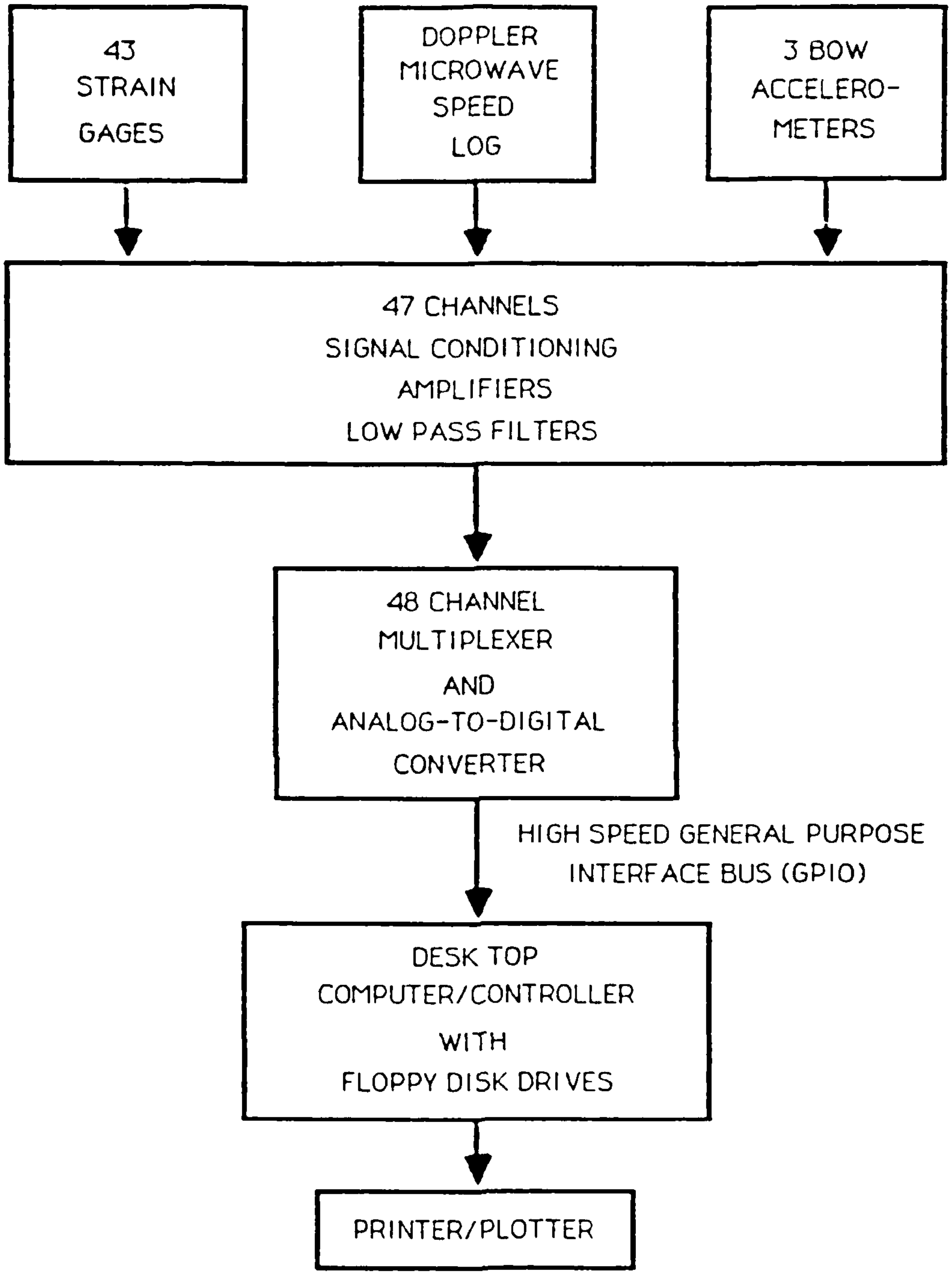

Figure 2

SCHEMATIC DIAGRAM OF THE GLOBAL LOADS
DATA ACQUISITION SYSTEM

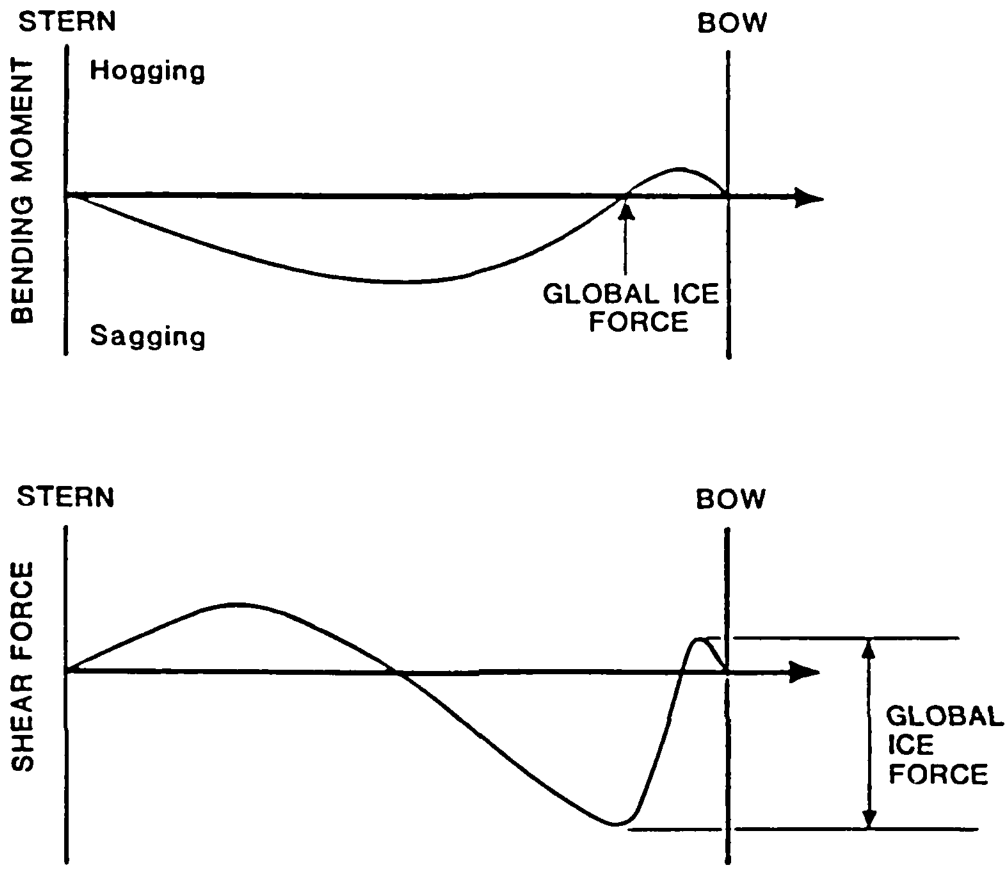

Figure 3

ESTIMATED SHEAR AND BENDING MOMENT DIAGRAMS
FOR THE USCGC POLAR STAR

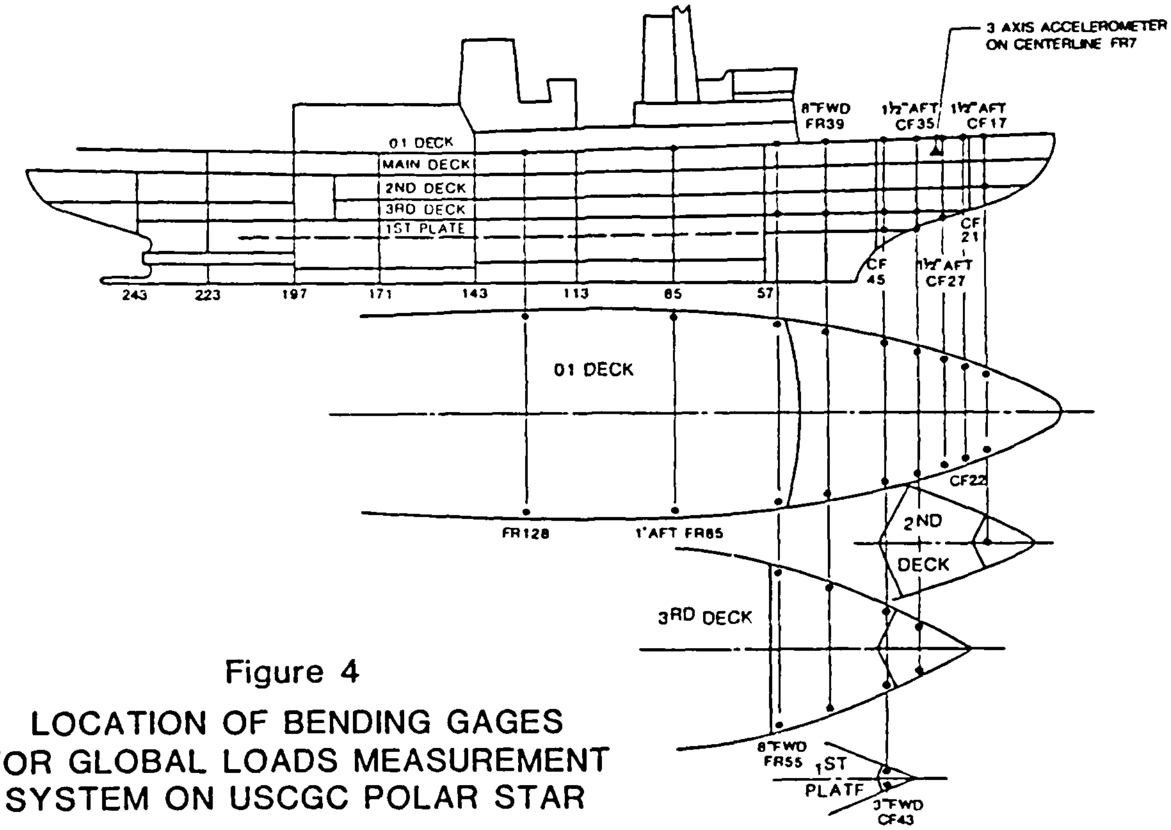

Figure 4

LOCATION OF BENDING GAGES FOR GLOBAL LOADS MEASUREMENT SYSTEM ON USCGC POLAR STAR

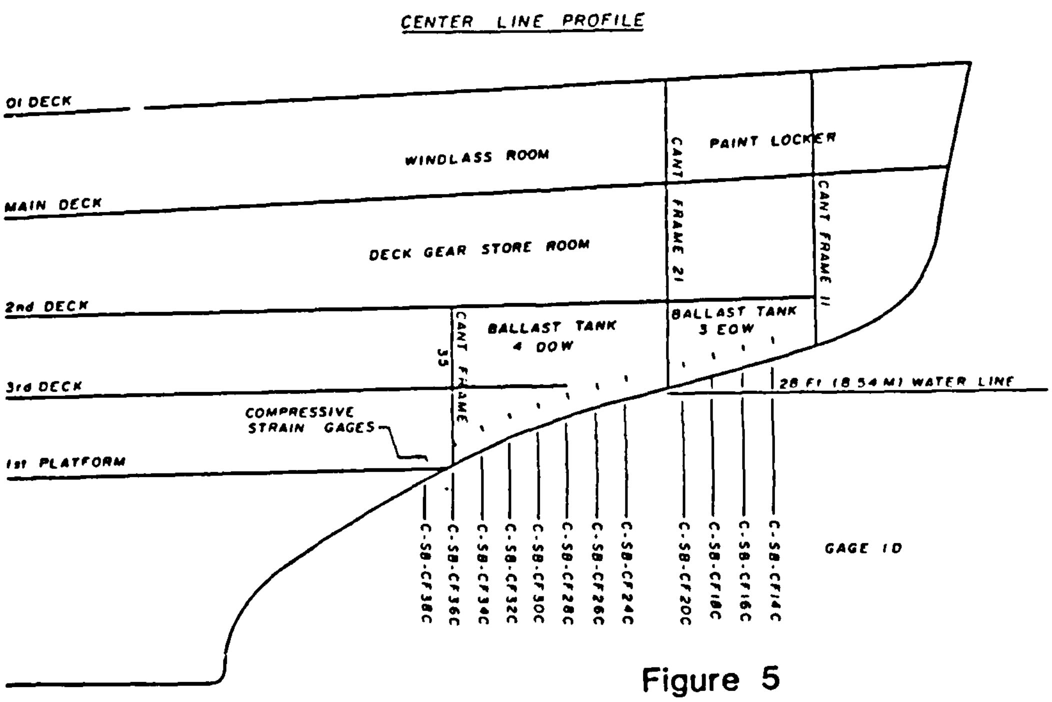

Figure 5

LOCATION OF LONGITUDINAL COMPRESSION GAGES

Compression gages for estimating the location of the load were installed from cant frame 14 to cant frame 38. They were placed on the centerline bulkhead, just forward of the cant frames and 12 to 18 inches above and perpendicular to the stem bar. Figure 5 shows these locations. The spacing of these gages enabled an accurate estimate of the center of the ice force to be made since the load could be "sensed" every 32 in (80cm) along the stem. The gage distance away from the stem bar was selected from work done on the placement of gages for measurement of local loads [13] to avoid the possibility of "dead spots" between the gages. This system also provided an estimate of the impact speed as the peak ice force moved along the stem bar.

In addition to the strain gages, three uniaxial accelerometers arranged in a triaxial array and oriented along the ship's principal axes were located in the bow area, as shown in Figure 4. The output from the yaw accelerometer was used to determine if a ram was symmetric. The accelerometer readings could also be used to provide an estimate of the inertial forces forward of the ice force and an assessment of the relative importance of the longitudinal, transverse and vertical ice forces acting on the vessel. The POLAR STAR was also equipped with a doppler microwave speed log. This radar was mounted at the waist of the vessel and oriented forward to provide an estimate of the impact velocity. The specifications and locations of all transducers used for the onboard instrumentation are described in Appendix A.

The required sampling frequency for measurement of the strain response on the POLAR Class vessels was selected based on the rate of loading and the vibrational frequency of the ship. Previous experiments have indicated that the dominant vibrational frequency is approximately 3 Hz [14]. The predicted rise time of the ice force was used to estimate the rate of loading. In this case, previous full-scale measurements indicated rise times to be as fast as 0.1 seconds [15]. If a quarter sine wave is assumed for the rise in strain, a corresponding maximum frequency of interest of 2.5 Hz results (period of 0.4 seconds). A low-pass filter frequency of 10 Hz was selected such that it was well above all the frequencies of interest. The minimum digital sampling frequency would then be 32 Hz to ensure a unique 10 Hz sine wave. This is exactly the system that was used in the local loads measurement program [13]. In this case a more sophisticated data acquisition system allowed an increase in sampling frequency over the local loads system, so 100 Hz was selected to provide at least 10 samples during the strain rise time. Data was sampled for 25 seconds, which was determined by the size of the storage medium. An increase in sampling frequency above 100 Hz, would have required the length of recording to be shorter or a larger storage medium.

3. DESCRIPTION OF THE TEST PROGRAM

Global load data were gathered during the summer deployment of the POLAR STAR to the Beaufort Sea. On Thursday, September 18, 1986, the participants for the week and a half global ice loads program arrived onboard the USCGC POLAR STAR off Barrow, Alaska. During the next two days the POLAR STAR proceeded eastward just south of the ice edge until a position near the Canadian-Alaskan border was reached. At this point the POLAR STAR turned north into the ice pack (see Figure 1 for a trackline of the ship's route).

As the POLAR STAR proceeded further north, it became apparent that the overall ice conditions were less severe than the ice conditions encountered during the 1985 POLAR SEA ice impact tests [9]. Generally the pack ice in the area was composed of medium to large first year ice floes (ice that had survived the summer) with imbedded multiyear fragments. The heaviest areas of the floes were around 15 ft (5 m) thick, but lacked structural integrity due to the rotten ice prevalent in the surrounding floe. Several photographs taken during the northward thrust into the pack ice are reproduced in Figure 6. They show the ice concentration to be around 70% with the remaining 30% consisting of partially refrozen melt ponds, polynyas and open water. These ice conditions persisted up to the northernmost extent of the POLAR STAR's route (73° 38'N) which was about 85 nautical miles into the pack from the ice edge.

Table 1 gives the general daily weather conditions experienced during the deployment including the daily average air temperature. At the start of the deployment, near Barrow and in the open water along the coast, the temperature was unseasonably warm at about 40°F (4°C). After the POLAR STAR entered the ice pack the average air temperature generally hovered around freezing, and then gradually fell to 25°F (-4°C). It was not until September 27, the last full day inside the ice pack, that the first signs of grease ice began to appear.

On the morning of September 21 a total of 13 trial rams were conducted to verify the correct operation of the data collection system. During this investigation it was discovered that two gages on the 01 Deck and one gage in the ballast tank 3-EOW were defective. These gages were either replaced or rewired during the next two days. The software was modified to delete the use of these gages in the analysis of ramming events that took place during that time.

It was anticipated that more than thirty ice impacts would be recorded during the deployment, but ice conditions were not as severe as expected. Ideal ice conditions for the tests would have been large, thick multiyear floes that could be rammed repeatedly without breaking apart. Multiyear ice was only encountered in fragments or small ridges that were imbedded in rotten first year ice. Most of the ice floes encountered had very little structural integrity and fell apart easily upon impact. Table 2 summarizes the general characteristics of each ramming event.

Figure 6

ICE CONDITIONS, BEAUFORT SEA
September, 1986

After an adequate ice feature was located the typical ramming test consisted of the following sequence of events. The icebreaker cleared a path to ram the ice feature unless the surrounding ice was weak and rotten. The vessel was then moved perpendicular to the feature and several ship lengths away before accelerating for the ram. Approximately five seconds prior to impact data acquisition was started and data were acquired for 25 seconds. Data collection was triggered by an operator viewing a a video display of the bow of the vessel and the immediate area ahead of the ship. After the ramming event, measured data were stored on a floppy disk; a process that took approximately 60 seconds. When time permitted between ramming tests, the data were analyzed and plotted.

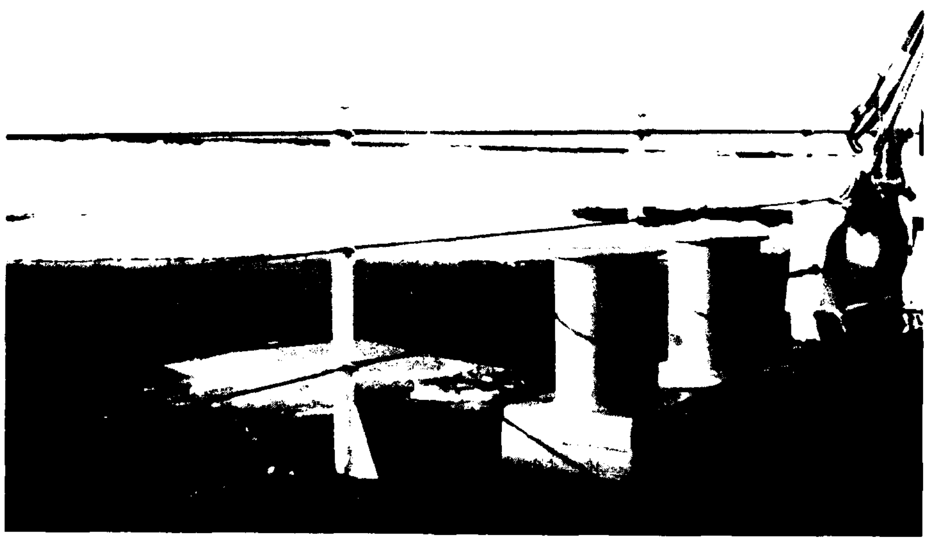

Figure 6 (continued)
ICE CONDITIONS, BEAUFORT SEA
September, 1986

TABLE 1

DAILY AVERAGE WEATHER CONDITIONS
September 17 - September 28, 1986

DATE	WIND DIRECTION TRUE	WIND FORCE (knots)	AIR TEMPERATURE (F^0)	GENERAL WEATHER
September 17	W	10	41	Fog, Overcast
September 18	SE	11	42	Overcast
September 19	SSE	9	41	Overcast, Scattered and Broken Clouds
September 20	SE	10	35	Fog, Overcast
September 12	SW	25	33	Snow, Overcast
September 22	SW	23	31	Snow, Overcast
September 23	WSW	20	29	Snow, Overcast
September 24	W	15	26	Snow, Overcast
September 25	WSW	11	26	Snow, Overcast
September 26	SW	11	29	Overcast
September 27	NW	8	28	Snow, Overcast
September 28	E	8	25	Overcast, Broken Clouds

TABLE 2

OBSERVATIONS OF RAMMING TESTS

Ram No.	Date	Symmetric	Magnitude of Measured Load	Description of Ice Feature and Comments
1-13	9/21			Test rams for system check-out
14	9/22	Y	S	Small floe with melt ponds
15	9/22	Y	S	Same small floe
16	9/22	Y	S	Small floe
17	9/22	Y	S	Small floe
18	9/22	Y	L	Same floe, brought to stop
19	9/22	Y	M	
20	9/22	Y	M	
21	9/22	Y	L	Good ram but complete ice failure
22	9/22	Y	L	
23	9/22	Y	M	Brought to stop
24	9/23	Y	S	Small floe, shattered ice
25	9/23	Stbd	M	Medium floe, (1/2 mile dia.)
26	9/23	Y	M	Same floe, brought to stop, cracks to meltponds
27	9/23	Y	S	Same floe
28	9/23	Y	M	Brought to stop
29	9/23	Port	L	
30	9/23	Port	S	Brought to stop
31	9/23	Y	S	Into meltpond
32	9/23	Y	S	
33	9/23	Y	S	Medium floe, shattered ice
34	9/25	Y	S	Small floe, shattered ice
35	9/25	Y	M	Large floe
36	9/25	Y	S	Same floe but shattered ice
37	9/25	Y	S	Floe fractured
38	9/25	Y	S	Backbone of ridge, brought to stop
39	9/25	Y	M	Same ridge
40	9/25	Y	L	Same ridge, brought to stop
41	9/25	Y	M	Same Ridge, brought to stop, fractured most of ridge
42	9/25	Y	M	Same ridge, brought to stop
43	9/25	Y	L	Same ridge, shattered remains

* S, M, L, & VL indicates small, medium, large, and very large bow force loads.

4. ANALYSIS PROCEDURES AND RESULTS

Procedures used to analyze the data from each ramming event are summarized here. Appendix B gives a more detailed description and derivations of the various equations used.

Analysis software was separate from data acquisition software. This allowed flexibility during the data collection process since several good rams could occur a few minutes apart. The separation of these functions (data acquisition and analysis) meant that the information could be collected and stored for future analysis without missing any opportunities to collect data during sequential rams.

Analysis software was derived from the program written for the KIGORIAK and ROBERT LEMEUR impact tests conducted in 1983 and was, with only minor modifications, the same software used in the 1985 POLAR SEA tests. The principal functions of the software were to calculate and plot the vertical bow force time-history acting on the POLAR STAR, and to determine the time of the maximum bow force together with the location along the stem. In addition, it was used to plot the shear force and bending moment distributions at any time-step during the 25 second sampling interval. Analysis software also performed a number of secondary calculations such as plotting the strain time-history from any of the gages, or finding the location of the neutral axis at frames instrumented on two separate levels. Appendix C contains a summary of the program's features and a flow chart showing the branching structure.

During the analysis, the deck bending stress time-history at each gage location is calculated and plotted for every ram. Zeros on all channels are determined by averaging the data obtained just prior to the impact and subtracting them from the subsequent measurements. Stresses are calculated by multiplying the results by a calibration factor and the elastic modulus. The gages that were placed parallel to the side shell of the vessel are multiplied by another transformation factor to arrive at the bending stress parallel to the centerline. Appendix A contains a listing of the gage calibration factors used, while Appendix B gives the derivation of the centerline stress transformation for each instrumented frame.

A sample plot of the bending strain at frame 85 (the highest bending stress was usually located here or at frame 39) is shown in Figure 7. During the ramming tests, the maximum bending stress was typically determined within a minute of completion of the ram. These values were always well below the yield stress of the 01 Deck which is 45,600 psi (310 MPa). A histogram of the maximum bending stress is given in Figure 8 which shows that the highest bending stress recorded was approximately 3800 psi (26 MPa). During the 1985 POLAR SEA tests a maximum bending stress of approximately 6500 psi (45 MPa) was measured at frame 39 [9].

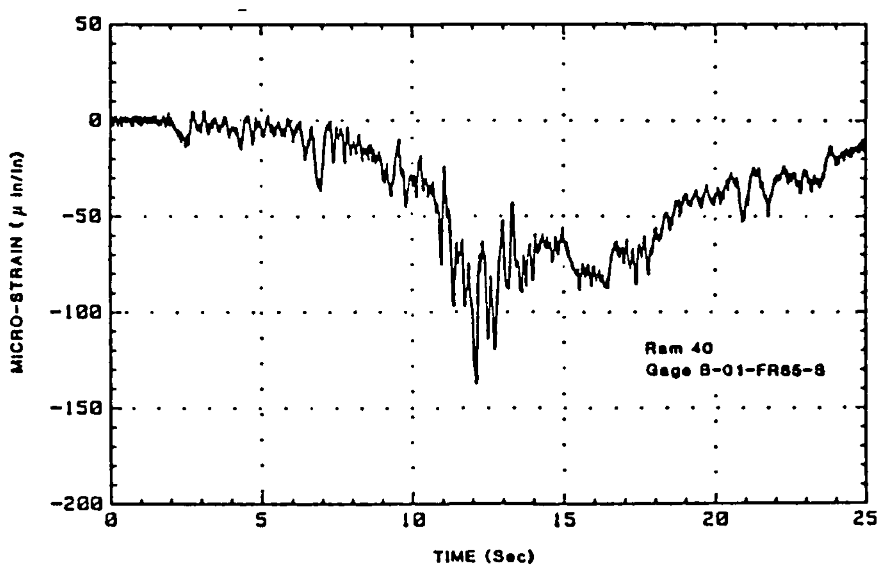

Figure 7
BENDING STRAIN TIME-HISTORY AT FRAME 85

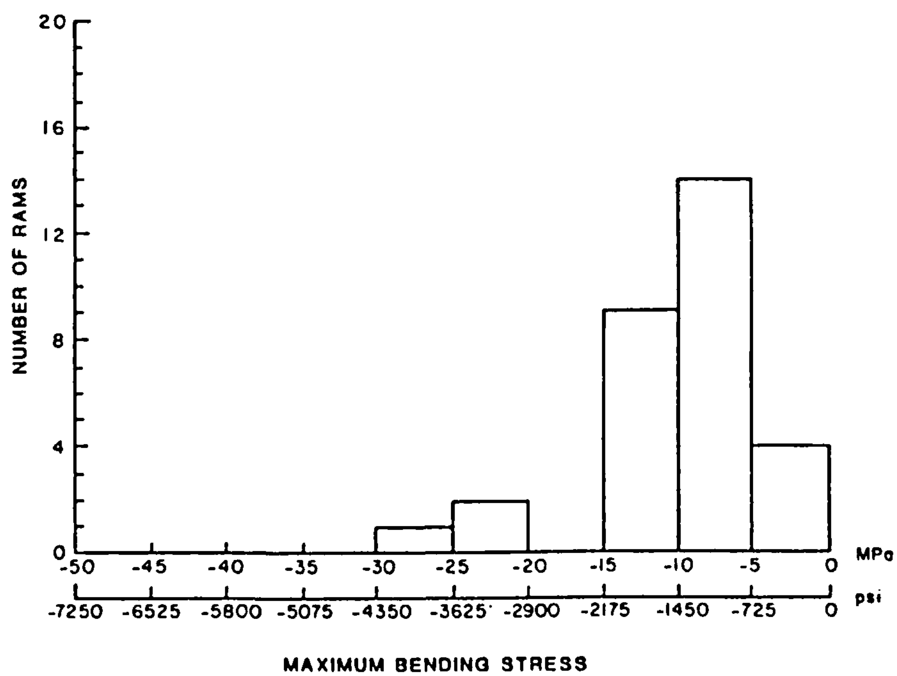

Figure 8
HISTOGRAM OF MAXIMUM BENDING STRESS

Figure 9 illustrates excitation of the first mode natural frequency of the hull girder. This figure shows the stress time-history measured by the port bending gage located at frame 128 near amidships on the 01 Deck. The measured frequency of 2.83 Hz is within 6% of the previously measured 3.0 Hz value on the POLAR SEA and very close to the 2.9 Hz computed by the finite element model constructed by ABS [9].

In order to compute a bending moment from the bending stresses, it was assumed that when the USCGC POLAR SEA impacts a heavy ice feature it responds similar to a beam for bending within the centerline plane. The bending moment at each instrumented frame was then calculated using the bending stresses and structural properties of the vessel.

$$M = \frac{\sigma \cdot I}{Y}$$

where
- σ = Bending stress = $\varepsilon \cdot E$
- ε = Strain (parallel to the centerline)
- E = Elastic modulus
- I = Transverse sectional moment of inertia
- Y = Distance between gage and neutral axis or the distance between gage pairs on the same frame

Referring again to Figure 5 which gives the locations of the bending gages, it can be seen that several of the frames offer several different methods for applying this formula. At cant frame 43, for instance, the stresses at the gages on the 01 Deck are averaged together and used in conjunction with either the gages on the Third Deck or the First Platform. The 01 Deck gages could be used alone along with their vertical distance from the neutral axis. Generally however, a gage "couple" was used except for the cases where bending gages were installed along the stem bar or the 2nd Deck centerline gage. These particular gages were found to respond to the local load of the ice moving down the stem bar or other stress concentration influences and hence were not used in the calculations.

Once the bending moment distribution along the length of the ship was obtained, the shear force was computed as the negative slope (derivative) of the longitudinal bending moment curve. Figure 3 shows, generally, how these curves appeared.

Figure 3 also shows how the global ice force is related to the shear diagram. The force on the bow was calculated by the addition of the absolute value of the greatest shear force forward and aft of the load. The location of the center of the vertical ice load was estimated from the measurements received from the compression gages arranged along the stem bar. At any instant in time, the location of the compression gage with the largest compressive strain was taken as the ice load's location.

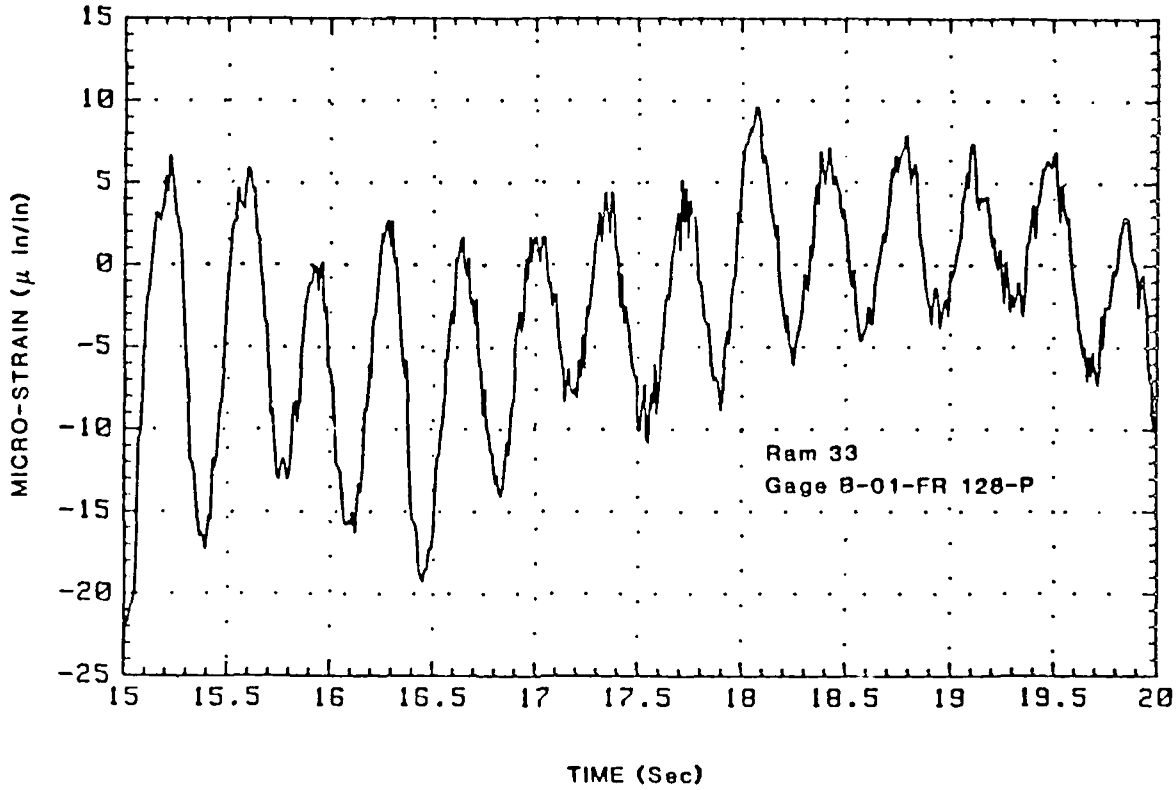

Figure 9

BENDING STRAIN TIME-HISTORY NEAR MIDSHIPS (FRAME 128)

This entire procedure was repeated for every time step (0.01 seconds) for the duration of the ramming test (25 seconds). The result of these computations was a time-history of the vertical bow force during the ramming event. Figure 10 gives a bow force time-history plot for one of the more severe impacts. Representative rams were analyzed onboard the vessel using preliminary estimates for the sectional inertias and locations of the neutral axes.

It was anticipated that if the ice load occured forward of cant frame 17, then the shear force would be estimated by the multiplication of the measured vertical acceleration and the mass of the bow section forward of the load. The maximum value for this inertial force, however, was estimated to be approximately 30 LT (0.3 MN) which is less than the uncertainty expected in computing the vertical bow force and was therefore neglected (Section 6 discusses the err analysis).

During the 1985 POLAR SEA tests the data analysis indicated that while in the ramming mode the superstructure of the POLAR SEA contributed significantly to the flexural stiffness of the vessel [9]. This was apparent when the calculated bending moment at frame 55 (using a section modulus which did not include the effect of the superstructure) was much less than that calculated at frame 39. As Figure 4 shows, frame 39 is just forward of the superstructure and only 20.6 ft (6.3 m) forward of frame 55. The bending moment distribution for this portion of the ship should have a relatively smooth shape.

The calculated bow force determined from the discontinuity in the shear curve was almost always located forward of the superstructure and hence unaffected by the sectional properties for the frames under the superstructure. Based on this observation, it was decided that "effective" sectional properties could be found for these frames for use in the final calculations [9]. The location of the effective neutral axis was calculated at frames where the bending strain was measured at two levels by assuming a linear stress distribution through the cross section. The point where this distribution passed through zero was taken to be the effective neutral axis. The moment of inertia for each of these cross-sections was recalculated from the ship's drawings based upon the new location for the neutral axis. With the assumption that the ship remains in a quasi-static equilibrium and using ram events where the shear discontinuity remains forward of the superstructure, the areas above and below the shear diagram were calculated to determine if they were equal. The sectional properties for the frames including the superstructure were then adjusted to bring the positive and negative areas of the shear graph into equilibrium.

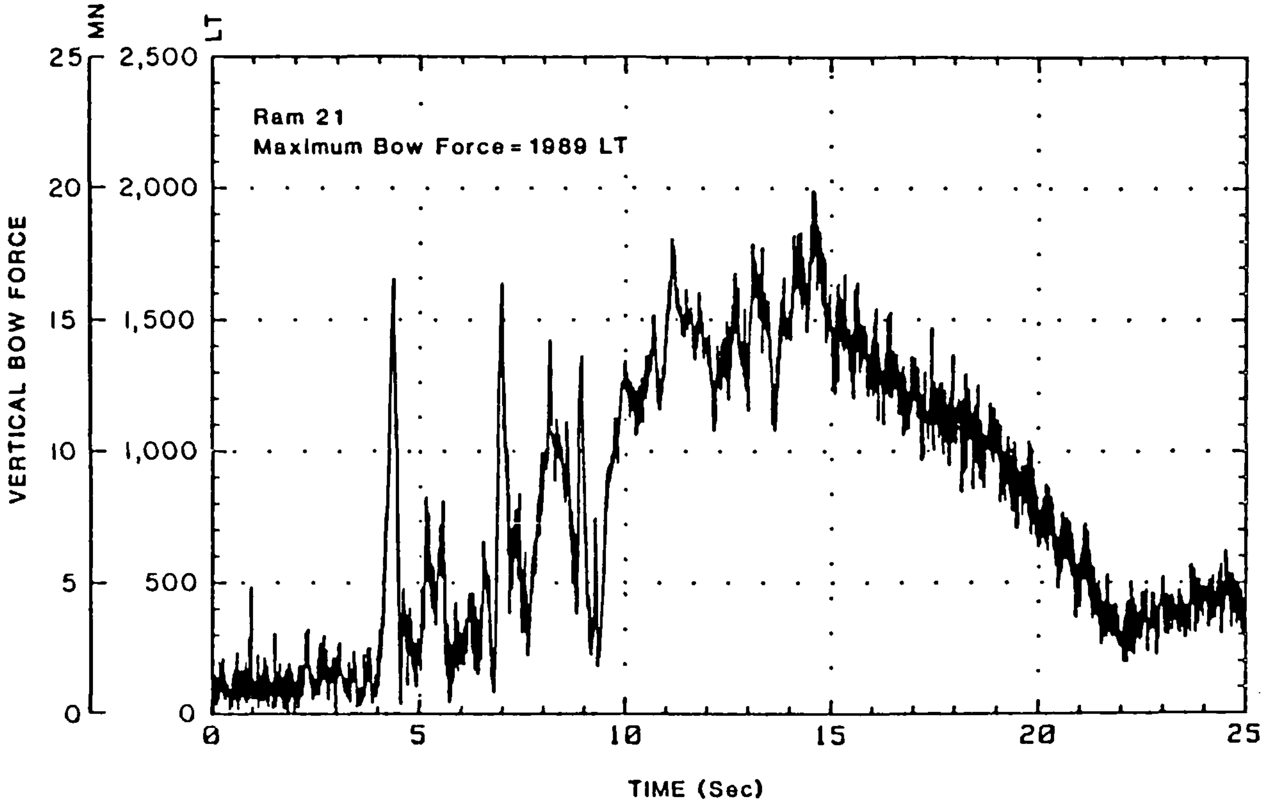

Figure 10
VERTICAL BOW FORCE TIME-HISTORY

Table 3 gives a listing of the neutral axes and moment of inertias calculated for the bow of the POLAR STAR along with the values obtained during the analysis of the POLAR SEA data for the three instrumented frames under the superstructure [9].

TABLE 3

SECTIONAL PROPERTIES FOR THE POLAR CLASS ICEBREAKERS

LOCATION	NEUTRAL AXIS ft (m)	MOMENT OF INERTIA ft^4 (m^4)
Frame 128	24.3 (7.41)	11,586 (100)
Frame 85	25.8 (7.86)	11,586 (100)
Frame 55	25.3 (7.7)	15,062 (130)
Frame 39	27.6 (8.4)	7,919.4 (68.4)
Cant Frame 43	34.3 (10.5)	3,204.2 (27.7)
Cant Frame 35	36.3 (11.1)	2,089.1 (18.0)
Cant Frame 27	39.6 (12.1)	1,186.2 (10.2)
Cant Frame 22	40.9 (12.5)	985.2 (8.5)
Cant Frame 17	42.6 (12.9)	810.3 (7.0)

The location of the center of the ice force (calculated from output of the stem bar compression gages) during ramming can be used to estimate the impact velocity. A sample plot of the calculated location of the load versus time is shown in Figure 11. The slope of a line drawn through this stepped curve is an estimate of the velocity of the ice movement along the stem bar. Correcting for the angle of the stem bar, an approximate value for the ship impact velocity is obtained. A comparison between the impact velocity calculated from the location of the load time-history and the velocity measured from the doppler speed log for several rams is shown in Table 4.

TABLE 4

COMPARISON OF IMPACT VELOCITIES

RAM NO.	DOPPLER SPEED LOG knots	(m/sec)	STEM BAR GAGES knots	(m/sec)
19	1.0	(0.5)	0.9	(0.4)
28	6.5	(3.3)	6.3	(3.2)
33	5.7	(2.9)	5.2	(2.7)
39	1.7	(0.9)	1.7	(0.9)
40	4.2	(2.2)	3.1	(1.6)
42 ride up	7.2	(3.7)	6.2	(3.2)
42 slide down	-0.8	(-0.4)	-0.7	(-0.4)

The difference in velocities is probably due to the nature of the ship-ice interaction. The ice moving down the stem bar is not exactly a point load and does experience some crushing causing the point of maximum loading to shift locations within the ice feature.

Figures 12 through 16 provide strains from all of the compression gages along the stem at a single instant of time. There is a one second interval between each of the figures. These figures give an understanding of the extent of the ice load and how it progresses down the stem bar. Comparing the first two figures in the series, it can be seen that the load spreads out from a concentrated point to cover two of the gage locations. Localized crushing of the ice after the intitial impact would account for this effect. The remaining figures in the series depict the location of the load as it continues to move aft.

Since the compression gages were mounted on the centerline bulkhead 12 to 18 inches away from the stem bar and just forward of the cant frames, it is possible to see the effect that the stiffening cant frames have on the distribution of stress in the centerline bulkhead. If the ice load is localized to one side of a cant frame causing a region of compression in the centerline bulkhead, then a region of tension will form on the other side of the cant frame.

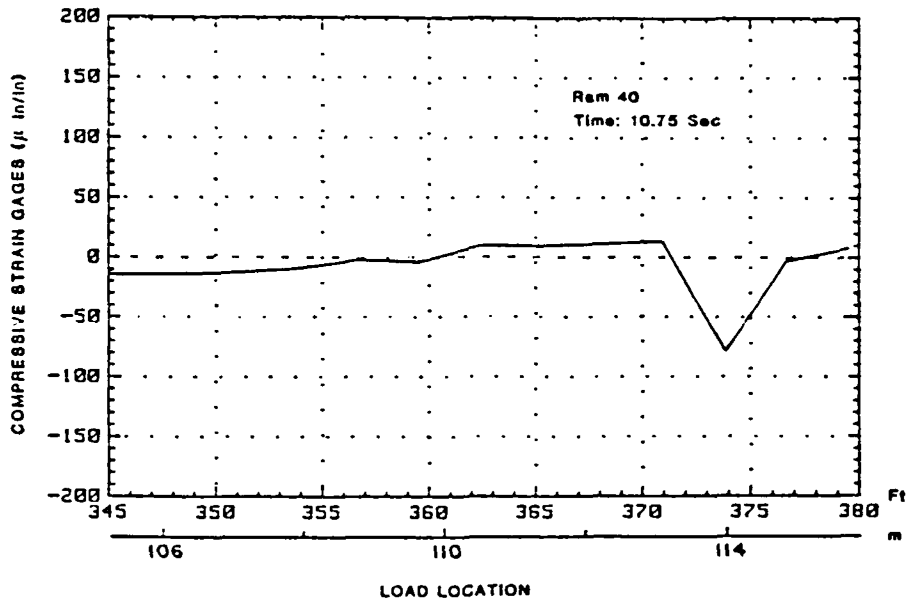

Figure 12
LOCATION OF THE LOAD FORWARD OF THE STERN

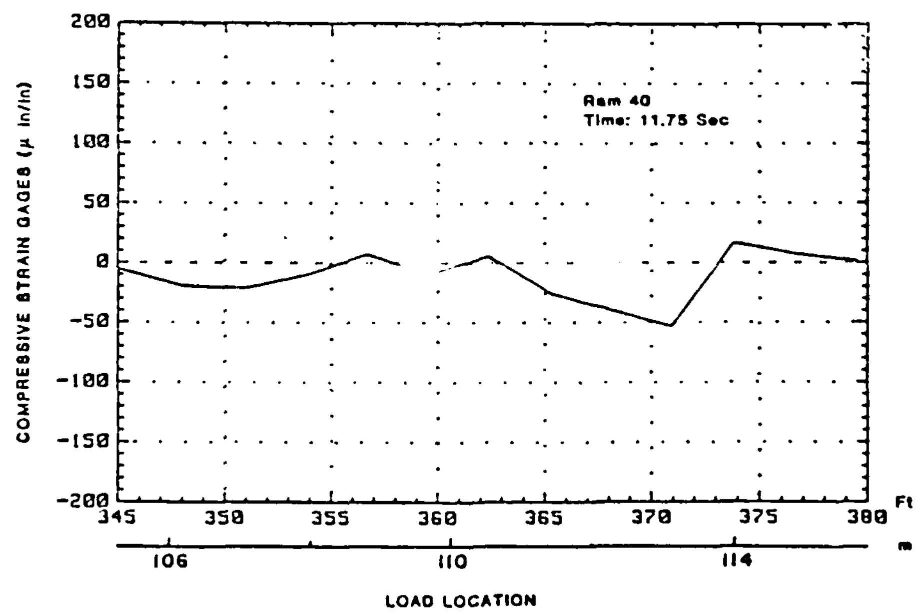

Figure 13
LOCATION OF THE LOAD FORWARD OF THE STERN

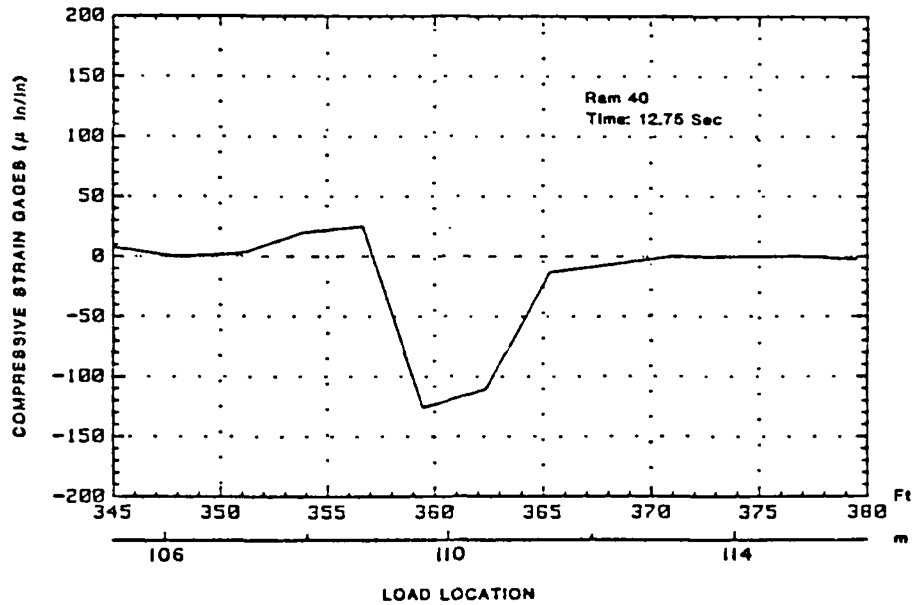

Figure 14
LOCATION OF THE LOAD FORWARD OF THE STERN

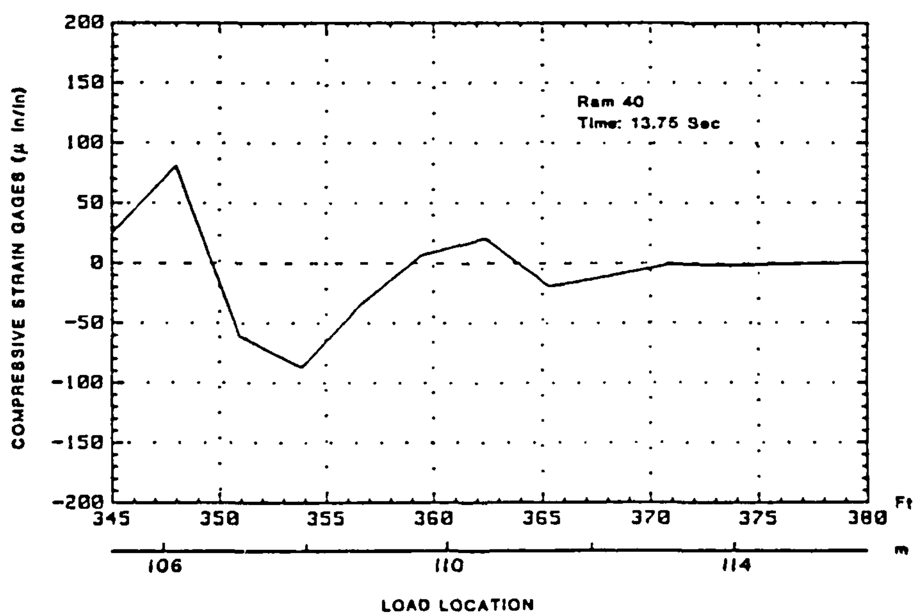

Figure 15
LOCATION OF THE LOAD FORWARD OF THE STERN

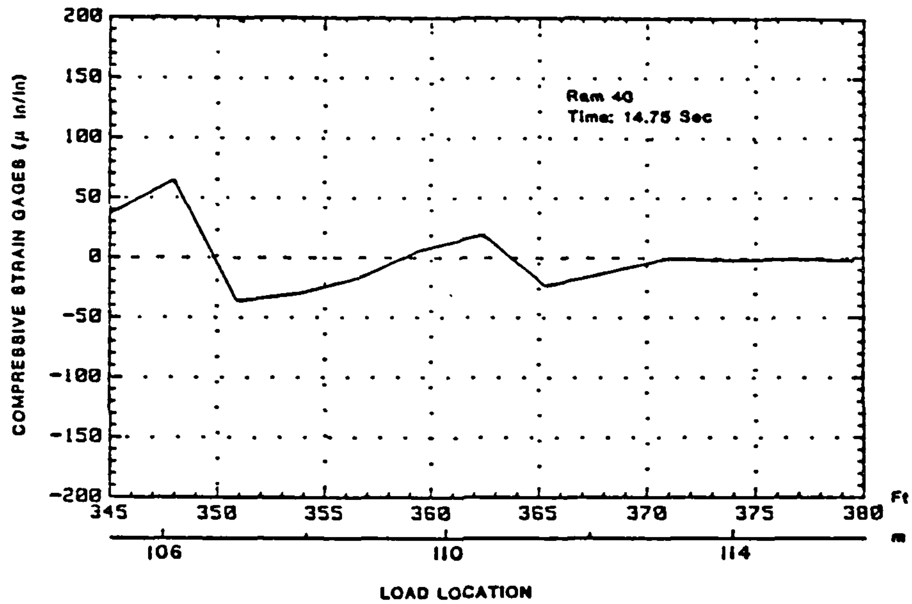

Figure 16
LOCATION OF THE LOAD FORWARD OF THE STERN

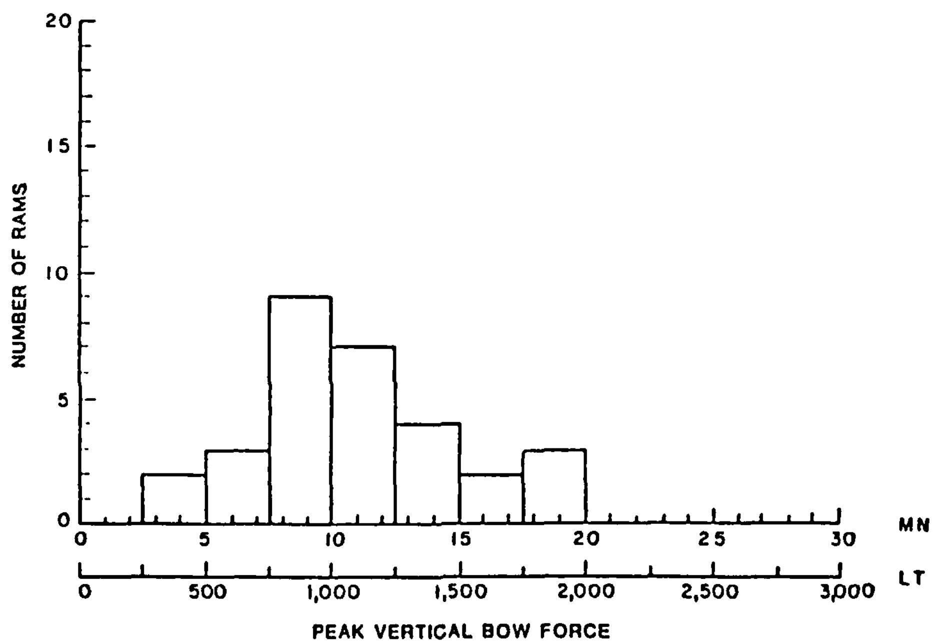

Figure 17
HISTOGRAM OF PEAK VERTICAL BOW FORCE

All strain data was analyzed using the procedure described above. Tables 5 and 6 summarize the results for all of the rams and give the impact velocity, the peak vertical bow force, and the maximum bending stress along the 01 Deck. The largest bow force encountered was 1989 LT (19.74 MN) during ram number 21 which is lower than the 2506 LT (24.97 MN) maximum experienced by the POLAR SEA in slightly more severe ice conditions [9]. A histogram of the peak vertical force is given in Figure 16.

Table 5 also gives the location of the bow force as a distance forwad of the stern from two different methods. The first method (next to the last column) uses the discontinuity in the shear distribution to estimate the longitudinal bounds of the load while the last column in the table gives the location of the stem bar compression gage undergoing the greatest compression. A comparison of the last two columns in Table 5 shows that the location given by the stem gages is usually forward of the shear discontinuity. If a ramming event took place against a larger ice feature, the time of the maximum bow force would usually occur shortly after the initial contact and the two methods of locating the load would be fairly close. However, this scenario did not usually occur during the POLAR STAR tests due to the light ice conditions. The lack of any structural integrity in the ice features frequently resulted in ice failure upon impact. As a consequence, the maximum bending moment occurred after the vessel was well inside the ice feature and not during the initial impact phase as expected. Therefore, much of the icebreaking process was taking place along both sides of the bow, i.e. aft of the stem bar.

Table 6 gives the location of the instrumented frame where the largest bending stress occurred on 01 Deck. Almost half of the entries are at frames 39 and 85. Frame 39 is just forward of the superstructure while frame 85 lies between midships and the forward end of the superstructure. Fully three quarters of the observed maximum bending stresses occurred at the three instrumented frames in the vicinity of the forward part of the superstructure: frames 39, 55, and 85. The largest bending stress was 3796 psi (26.17 MPa) at frame 39 (ram 22) which is much less than the maximum bending stress of 6078 psi (41.91 MPa) obtained on the POLAR SEA [9].

The major difference between the data acquisition systems installed on the POLAR STAR and POLAR SEA is the location of the strain gages installed on the 3rd Deck and 1st Platform. During the POLAR SEA's instrumentation most of these gages were positioned along the centerline of the ship. It was discovered later that these gages were affected by stress concentrations and thus were not used in the final analysis. One of the recommendations in the report [9] was that these gages should be moved off of the centerline to the deck edge where their measurements would be averaged during the bending moment calculation. This recommendation was followed during the instrumentation of the POLAR STAR and the gages in question were positioned 4 to 6 inches inboard of and parallel to the deck edge. No peculiar stress concentrations were noticed, however, a local load effect would sometimes occur. The 3rd Deck lies very close to the 28 ft. (8.5 m) design waterline where the bending gages would occasionally sense the movement of broken and overturned ice fragments along the side of the hull.

TABLE 5

SUMMARY OF COMPUTED VERTICAL BOW FORCES

RAM NUMBER	IMAPCT VELOCITY		MAX. VERTICAL BOW FORCE		LOCATION BY SHEAR GRAPH	LOCATION BY STEM GAGES
	kts	m/s	LT	MN	Ft Fwd. of Stern	
14	3.2	1.6	420	4.19	306-400	379
15	2.5	1.3	364	3.63	306-344	354
16	2.5	1.3	917	9.14	306-328	379
17	2.5	1.3	752	7.49	306-355	365
18	4.7	2.4	1495	14.90	306-344	365
19	2.0	1.0	1025	10.21	306-355	357
20	5.0	2.6	1034	10.30	306-355	354
21	5.2	2.7	1989	19.82	306-344	365
22	5.6	2.9	1981	19.74	344-372	379
23	4.4	2.3	1109	11.05	306-344	348
24	5.8	3.0	611	6.09	328-388	374
25	4.3	2.2	1326	13.21	306-344	354
26	4.2	2.2	1102	10.98	306-355	362
27	2.9	1.5	645	6.43	306-355	351
28	7.1	3.7	1267	12.62	274-306	---
29	6.2	3.2	1528	15.23	328-344	357
30	5.4	2.8	979	9.76	274-306	351
31	4.2	2.2	577	5.75	306-328	345
32	4.0	2.1	853	8.50	306-372	362
33	6.0	3.1	902	8.99	306-355	362
34	3.8	2.0	863	8.60	306-344	357
35	2.7	1.4	1169	11.65	328-355	359
36	4.3	2.2	846	8.43	306-344	374
37	3.9	2.0	903	9.00	306-372	365
38	3.0	1.5	853	8.50	344-355	365
39	4.6	2.4	1156	11.52	328-355	365
40	6.6	3.4	1945	19.38	328-355	365
41	5.8	3.0	1358	13.53	306-355	365
42	6.1	3.1	1070	10.66	306-355	379
43	6.3	3.2	1514	15.09	344-372	348

NOTE: The aftermost centerline bulkhead stem compression gage is located 345 ft (105 m) forward of the stern.

TABLE 6

SUMMARY OF MEASURED 01 DECK BENDING STRESS

RAM NUMBER	IMPACT VELOCITY		MAXIMUM BENDING STRESS		LOCATION	
	kts	m/s	psi	MPa	Frame	Ft Fwd. of Stern
14	3.2	1.6	-2123	-14.64	CF22	368
15	2.5	1.3	- 742	- 5.12	CF22	368
16	2.5	1.3	- 628	- 4.33	CF22	368
17	2.5	1.3	-1338	- 9.23	FR39	317
18	4.7	2.4	- 201	-13.90	CF43	338
19	2.0	1.0	-1777	-12.25	CF22	368
20	5.0	2.6	-1566	-10.80	FR39	317
21	5.2	2.7	-3464	-23.88	CF35	349
22	5.6	2.9	-3796	-26.17	FR39	317
23	4.4	2.3	-1798	-12.39	CF43	338
24	5.8	3.0	-1132	- 7.81	FR39	317
25	4.3	2.2	-1066	- 7.35	FR85	254
26	4.2	2.2	-1388	- 9.57	FR39	317
27	2.9	1.5	- 462	- 3.18	FR55	295
28	7.1	3.7	-1329	- 9.16	FR39	317
29	6.2	3.2	-1905	-13.13	FR85	254
30	5.4	2.8	- 923	- 6.37	FR85	254
31	4.2	2.2	- 554	- 3.82	FR55	295
32	4.0	2.1	- 614	- 4.23	FR55	295
33	6.0	3.1	-1428	- 9.85	FR39	317
34	3.8	2.0	-1149	- 7.92	FR39	317
35	2.7	1.4	-1495	-10.31	FR85	254
36	4.3	2.2	-1315	- 9.07	FR39	317
37	3.9	2.0	-1295	- 8.93	FR85	254
38	3.0	1.5	-1112	- 7.66	FR85	254
39	4.6	2.4	-1398	- 9.64	FR85	254
40	6.6	3.4	-3272	-22.56	FR85	254
41	5.8	3.0	-1811	-12.49	FR85	254
42	6.1	3.1	-1343	- 9.26	FR55	295
43	6.3	3.2	-1661	-11.45	FR85	254

Figures 13 and 19 give the strain gage time-histories for ram 36 showing two of these local load events. The tension spikes in these figures occur as the ice fragment passes over the strain gage. Figure 20 shows the bow force time-history that would be obtained if the two gages, B-3-FR55-P and B-3-FR39-S, were not removed from the analysis. The instances of large bow forces result from the erroneous data interpreted as a bending stress. By removing the first gage, B-3-FR55-P, from the analysis and using just the 01 Deck gages at frame 55 to compute the bending moment the first large spike in the bow force time-history disappears. This result is shown in Figure 21. Notice that the rest of the time-history remains essentially unaltered. Carrying this process one step further and using just the 01 Deck gages at frames 55 and 39 in the analysis gives a bow force time-history with both sets of spikes removed (Figure 22). Again, the rest of the time-history remains almost unchanged. This verifies the equivalence of the two different methods used in calculating the bending moment discussed earlier in this section.

This local load effect for gages installed along the waterline was observed in only seven of the thirty rams analyzed while the example discussed above gave the most dramatic changes in the bow force.

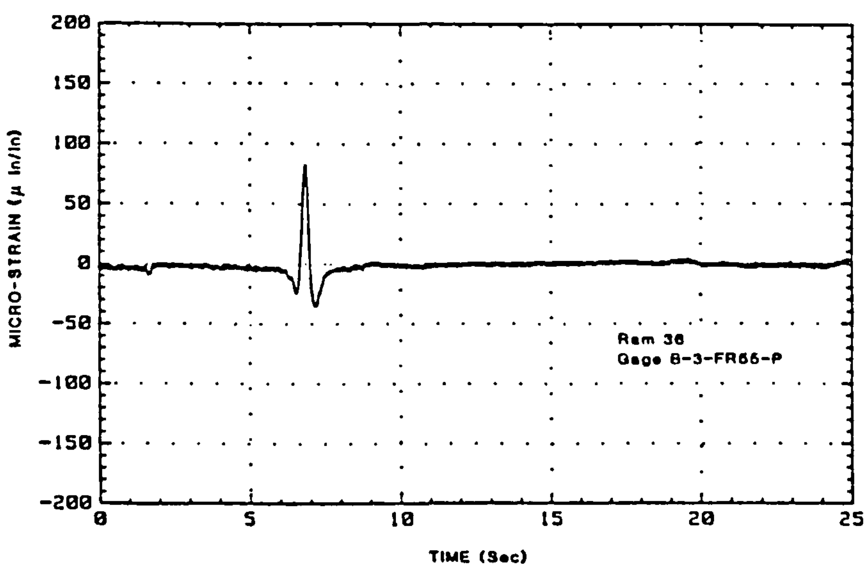

Figure 18
BENDING STRAIN TIME-HISTORY SHOWING LOCAL LOAD RESPONSE

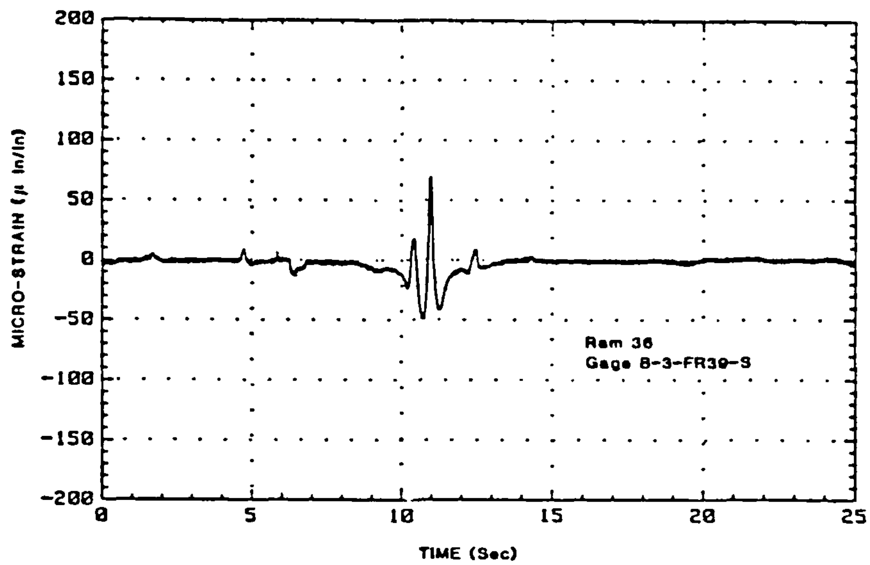

Figure 19
BENDING STRAIN TIME-HISTORY SHOWING LOCAL LOAD RESPONSE

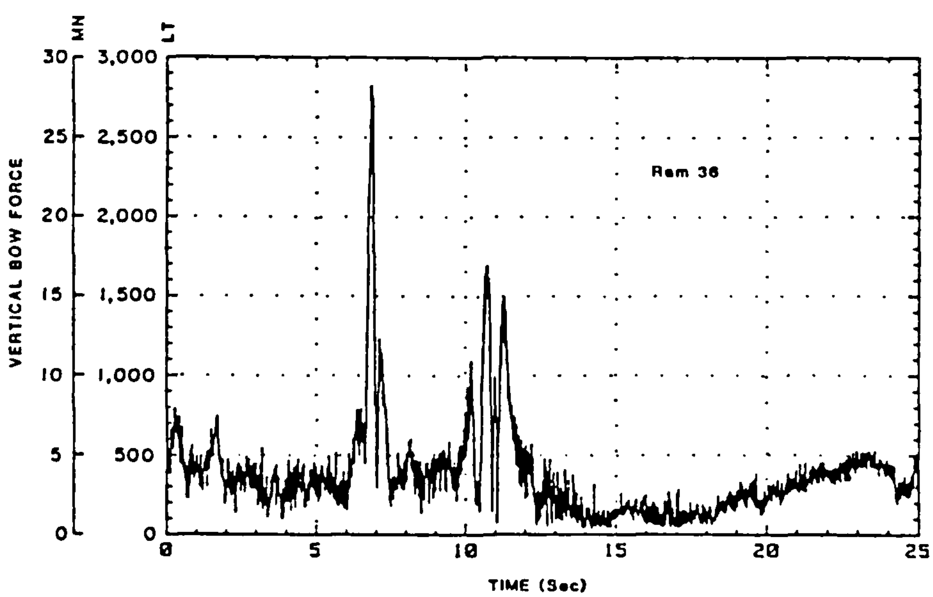

Figure 20
BOW FORCE TIME-HISTORY USING ALL BENDING GAGES

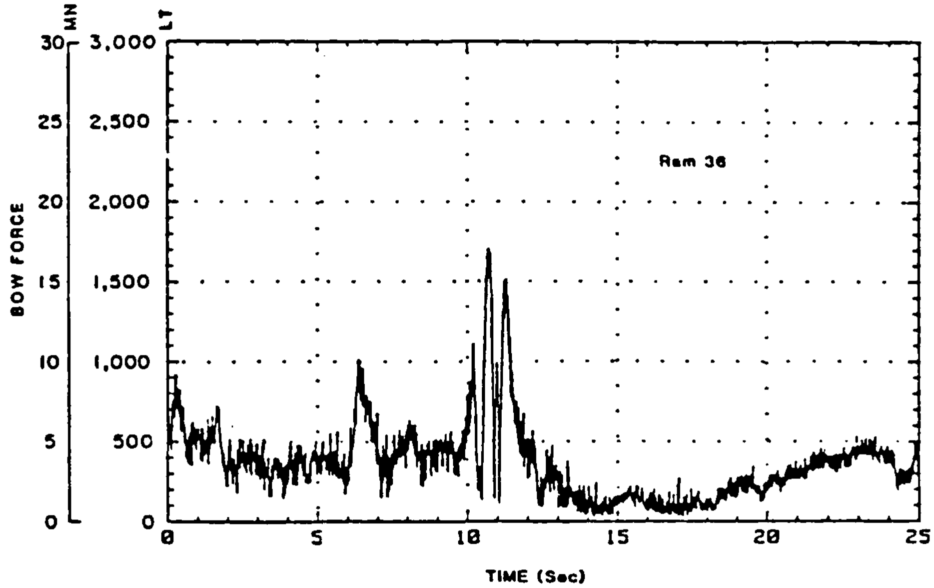

Figure 21
BOW FORCE TIME-HISTORY WITHOUT GAGE B-3-FR55-P

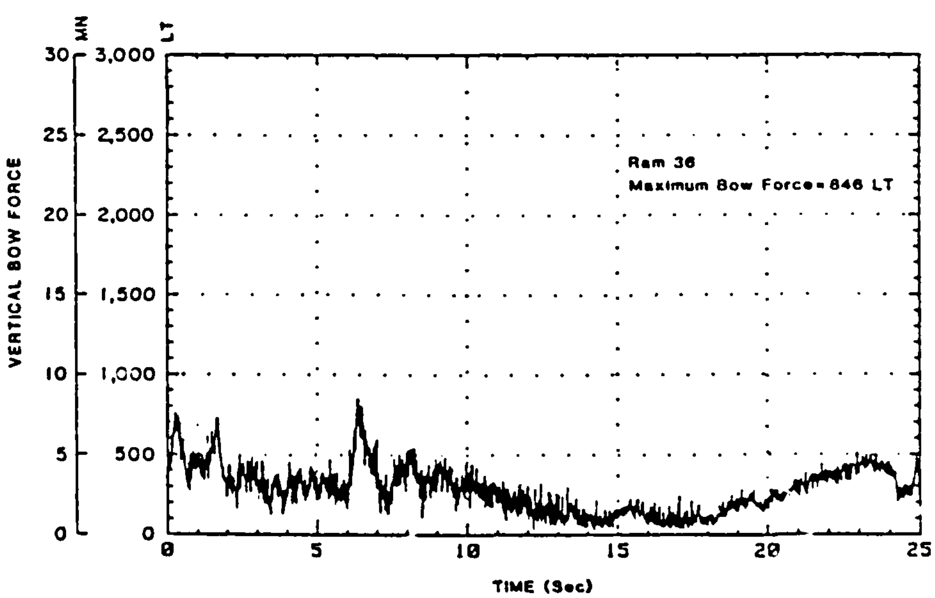

Figure 22
BOW FORCE TIME-HISTORY WITHOUT GAGES B-3-FR55-P
AND B-3-FR39-S

5. COMPARISON OF POLAR CLASS RESULTS WITH PREVIOUS REPORTS

5.1 Peak Vertical Bow Force Versus Impact Velocity

The results obtained from the full-scale impact tests onboard the USCGC POLAR STAR can be compared with previous predictions of vertical bow force on icebreaking vessels. Figure 23 gives a scatter plot of the vertical bow force versus the impact velocity for all impact events measured on both the POLAR STAR and the POLAR SEA. Added to this plot are several maximum vertical bow force prediction curves. The solid curve comes from a proposal by Johansson, Keinonen, and Mercer [16] for Arctic Class 10 vessels. They felt that the total maximum bow force was largely influenced by the ship's speed and mass and gave a recommended design equation of

$$F_{max} = V \cdot \Delta^{0.9}$$

where F_{max} = maximum force in MN
V = ship's speed or impact velocity in m/s
Δ = ship's maximum displacement in millions of kilograms

This is the force normal to the hull, and the vertical bow force component would therefore be the total bow force times the cosine of the angle of the stem bar.

$$F_{vert} = F_{max} \cdot \cos \alpha$$

$$F_{vert} = V \cdot \Delta^{0.9} \cdot \cos \alpha$$

For the POLAR Class the displacement is close to 11,000 LT (11,170 MT) at the design waterline of 28 ft (8.5 m) and the stem angle 5 feet (1.5 m) below this waterline is about 22.5°. The corresponding values used in the above equation are

$$\Delta = 11.17 \text{ millions of kg}$$
$$\alpha = 22.5°$$

which result in the solid curve on Figure 23. This curve shows Johansson's prediction which, with a couple of exceptions at the lower velocities, is a good upper bound for ramming velocities between 2.0 and 8.75 knots (1.0 and 4.5 m/s). It is important to note that Johansson's criteria was intended to include severe ice conditions such as impacting glacial ice, while the ice encountered during the POLAR Class trials consisted primarily of multiyear ridges and ridge fragments that broke upon impact. These ice conditions probably account for the lower values of bow force.

A second comparison can be made with the full-scale tests conducted onboard the CANMAR KIGORIAK in 1983. The inital test results were reported by Ghoneim, Johansson, Smyth, and Grinstead in Reference 17. They developed an envelope curve for their data which suggests that the bow force is proportional to the square root of the impact velocity.

$$F_{vert} = 2.34 \sqrt{V} \cdot \Delta^{0.9} \cdot \cos \alpha$$

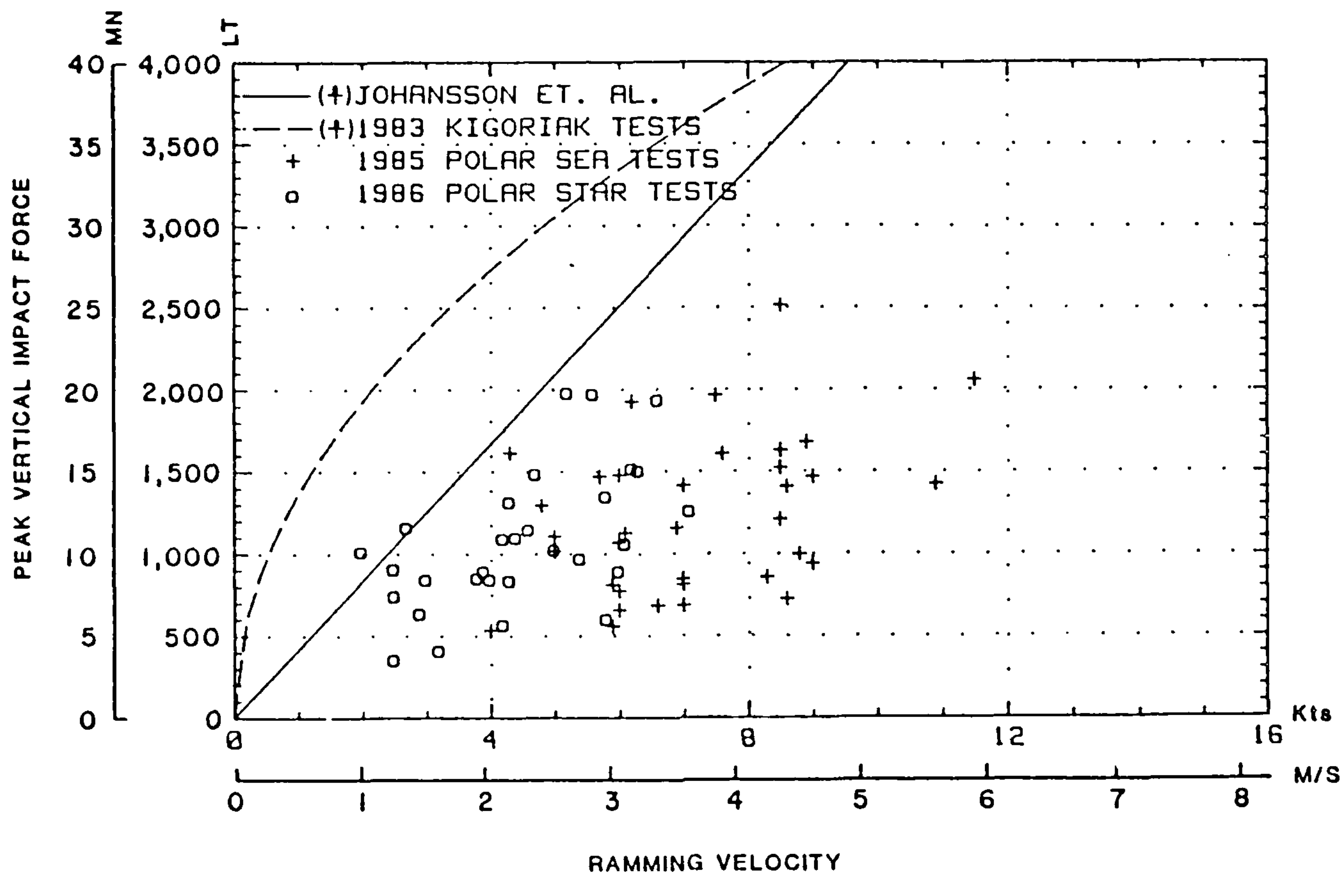

Figure 23

PEAK FORCE vs. VELOCITY RELATIONSHIP

(+) These curves have been adjusted to reflect the displacement and stem bar angle of the POLAR Class.

This equation is indicated for the POLAR Class by the dashed line in Figure 23 with the ship's displacement, Δ, again being given in terms of millions of kg to give a bow force in terms of MN. As a parametric relationship this equation was intended by Ghoneim, et al., to represent only a possible envelope curve based upon the portion of the data they had analyzed. It was not intended to reflect parameters such as bow shape. The ice conditions encountered during the KIGORIAK tests were much more severe than either the POLAR SEA or the POLAR STAR experienced with many of the rams being conducted against grounded first year and multiyear ridges. As the graph shows, the KIGORIAK curve certainly does provide an envelope to the POLAR Class data but it is much higher than Johansson's curve. The lower vertical bow force values obtained during the POLAR Class tests are again probably due to the lighter ice conditions although it would be difficult to say how much of an effect the different bow shapes may have had.

5.2 Vertical Bow Force Time-Histories

A typical time-history plot of the vertical bow force for the POLAR STAR was shown in Figure 10. A three second portion of this graph is illustrated in Figure 24 for comparison with a ramming event from the KIGORIAK impact trials [17]. Ghoneim and Keinonen [5], in discussing the typical ramming scenario for the KIGORIAK, identify five separate phases. These are the approach phase, the initial impact phase during which the ice crushes and the bow begins to ride up on the ice, the slide up phase, a second impact phase caused by the knife edge contacting the ice, and finally the slide down phase. Figure 25 clearly shows the two impact phases with the bow force dropping from 2360 long tons (23.5 MN) to zero, then rapidly increasing again up to 1200 long tons (12 MN). In this case, the period of zero ice load between the two impacts represents the bow rebounding off the ice surface and results in free vibration of the ship until reloading occurs. The model interprets this free vibration response as a bow force which leads to the "negative force" shown in the time-history between 1 and 1 1/2 seconds. Ghoneim, et al., observe that this force varies between $\pm$ 100 LT ($\pm$ 1.0 MN) which leads them to conclude that the error caused by vibration is of the order of 5% of the total vertical bow force [17].

Figure 24 uses the same time scale for comparison. After the initial impact of around 1650 long tons (16 MN) the bow force does drop, but it never reaches a state of zero ice load. That is, the bow-ice contact is maintained and the POLAR STAR does not "rebound" as KIGORIAK does. In fact, both the POLAR SEA and POLAR STAR bow force time-histories do not show this tendency to rebound on any of the rams analyzed to date. The displacement of the POLAR Class is almost 1.7 times that of the KIGORIAK which, when coupled with a different bow shape and ice conditions, may explain the difference in the two types of response.

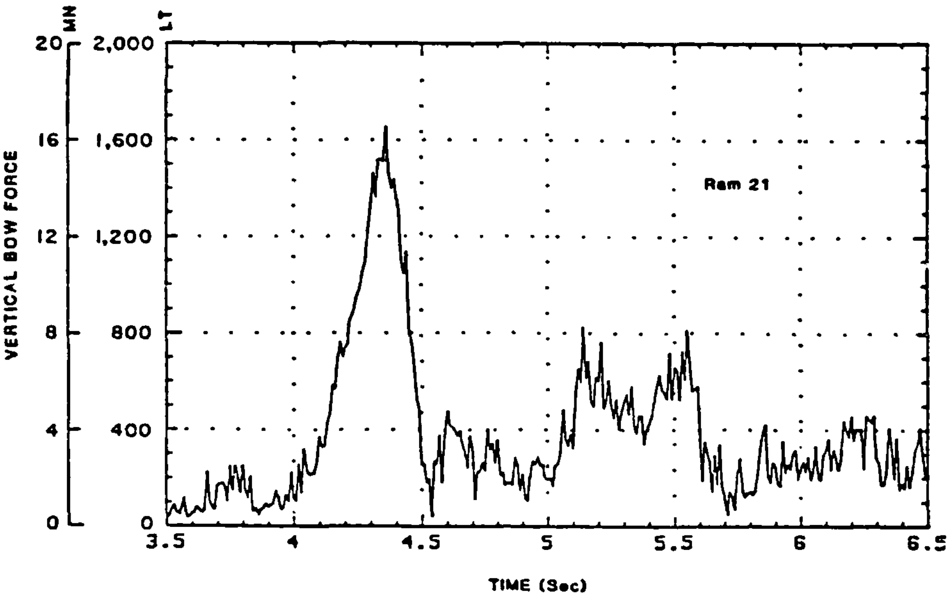

Figure 24
POLAR STAR VERTICAL BOW FORCE TIME-HISTORY

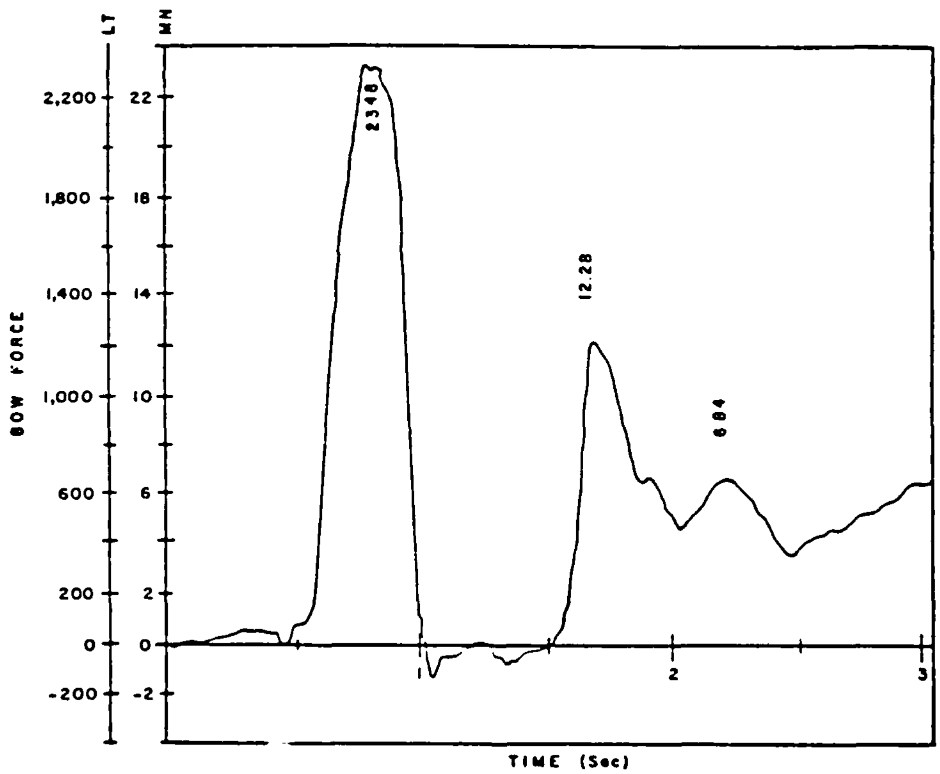

Figure 25
KIGORIAK BOW FORCE TIME-HISTORY (RAM KR426) [17]

5.3 Longitudinal Bending Moment and Shear Diagrams

The bending moment distributions for the POLAR STAR and the KIGORIAK, at the time of maximum force during the initial impact phase, are shown in Figures 26 and 27 respectively. There are several differences between these graphs. The maximum bending moment of the POLAR STAR occurs further forward (approximately 75% of the length of the vessel forward of the stern) than the KIGORIAK's (approximately midships).

In addition to this, notice that the bending moment for the POLAR STAR follows the idealized sketch given in Figure 3 except that the bending moment approaches zero over the first 40 ft. (12 m) of the vessel. Since bending gages were installed on the POLAR Class up to cant frame 17, which was forward of the anticipated maximum load location, the bending moment and shear force curves could be calculated forward of the load. In the instrumentation of the KIGORIAK, however, a slightly different approach was used [17]. It was felt that since the bow force was concentrated in the bow area, a frame instrumented to measure the shear force just aft of the load (frame 25 1/2 on the KIGORIAK) would be sufficient. It was assumed that the bending moment forward of the load location had negligible effect on the computations. This observation appears to be verified by Figure 26.

In the case of the KIGORIAK, once the bending moment and shear curves were obtained up to frame 25 1/2, the center of the load was estimated by employing a "best match" procedure between the two graphs. An extrapolation procedure was then used to obtain the bow force at the estimated load location. The shear distributions for the two ships (for the same rams used in Figures 26 and 27 and at the same time of maximum force during the initial impact phase) are shown in Figures 28 and 29. First note that the sign convention for the shear force is opposite in the two figures. The shear force distribution for the KIGORIAK was extended forward to the load location by the extrapolation procedure mentioned above, but does not go all the way to the bow (frame 30). The vertical line between frames 28 and 29 in Figure 29 represents the load location for this paritcular ram.

Returning to the shear force distribution for the POLAR SEA (Figure 28), it can be seen that near the location of the load the shear changes sign over approximately 50 ft (15 m). This gives a rough indication of the spreading of the ice load over the extent of the bow. At the point of maximum vertical force, a significant amount of crushing failure has occurred in the ice feature spreading the load over a large contact area.

Figure 30 shows a histogram of vertical bow force which combines the results for the POLAR Class impact tests. The histogram does show the beginnings of a regular distribution which could be used to develop a mathematical model describing the global ship-ice interaction process. It should be borne in mind, however, that such a model would only be adequate for the light ice conditions encountered during both years of testing.

An additional histogram could be developed to combine the POLAR Class results for the maximum bending stress, but the analysis of the POLAR STAR data computed the maximum compressive stress from all of the 01 Deck bending gages while the POLAR SEA analysis took into account only the 01 Deck gages at frame 39.

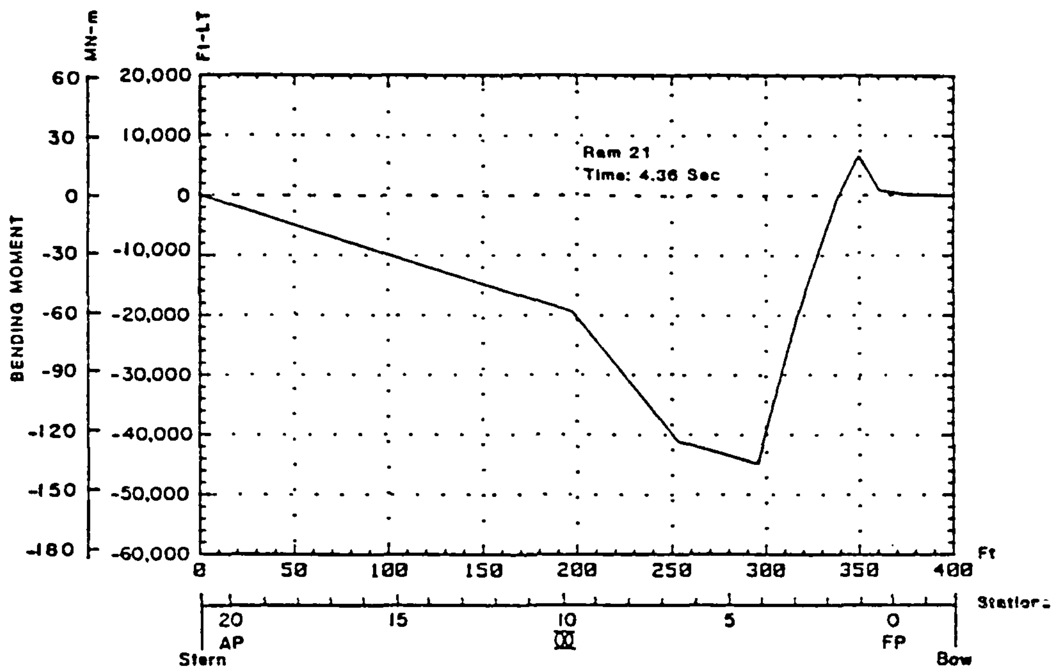

Figure 26

POLAR STAR BENDING MOMENT DISTRIBUTION

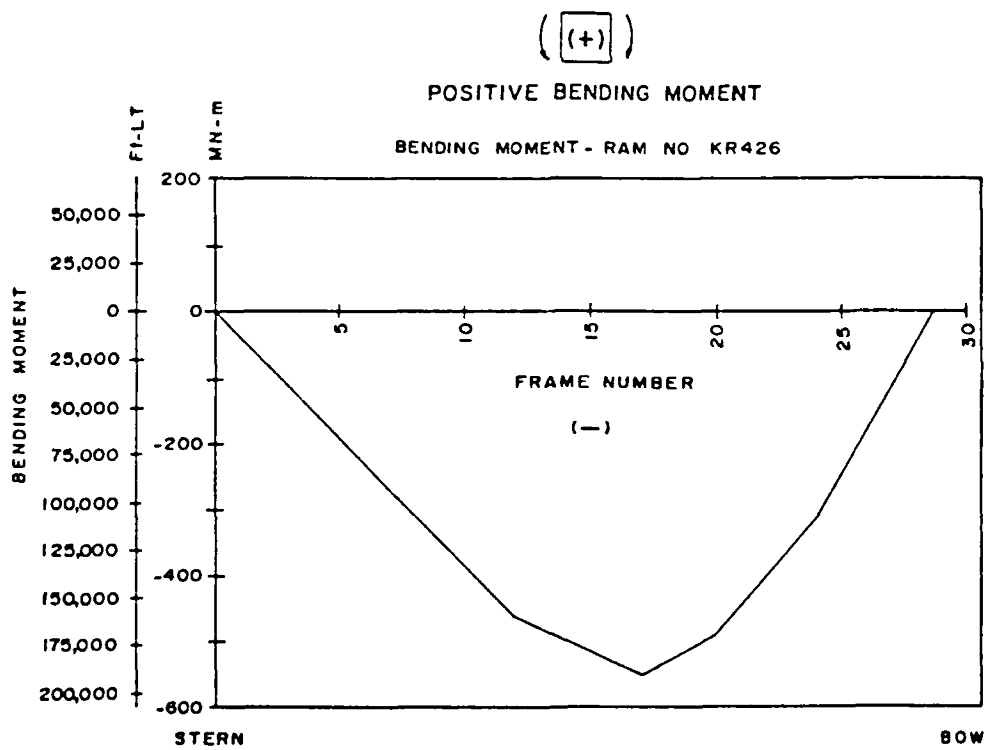

Figure 27

KIGORIAK BENDING MOMENT DISTRIBUTION [17]

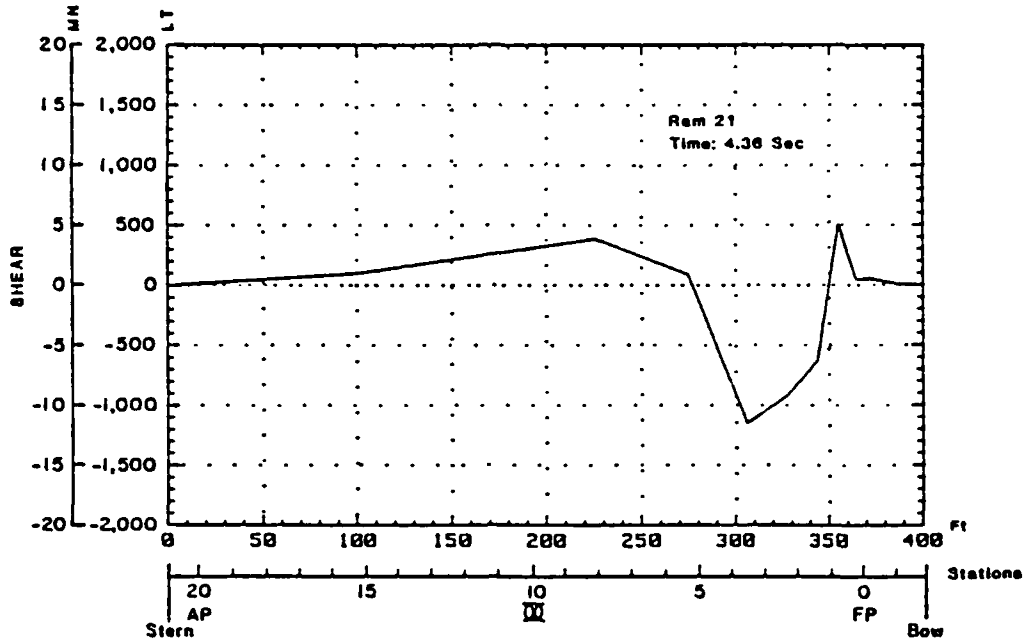

Figure 28
POLAR STAR SHEAR FORCE DISTRIBUTION

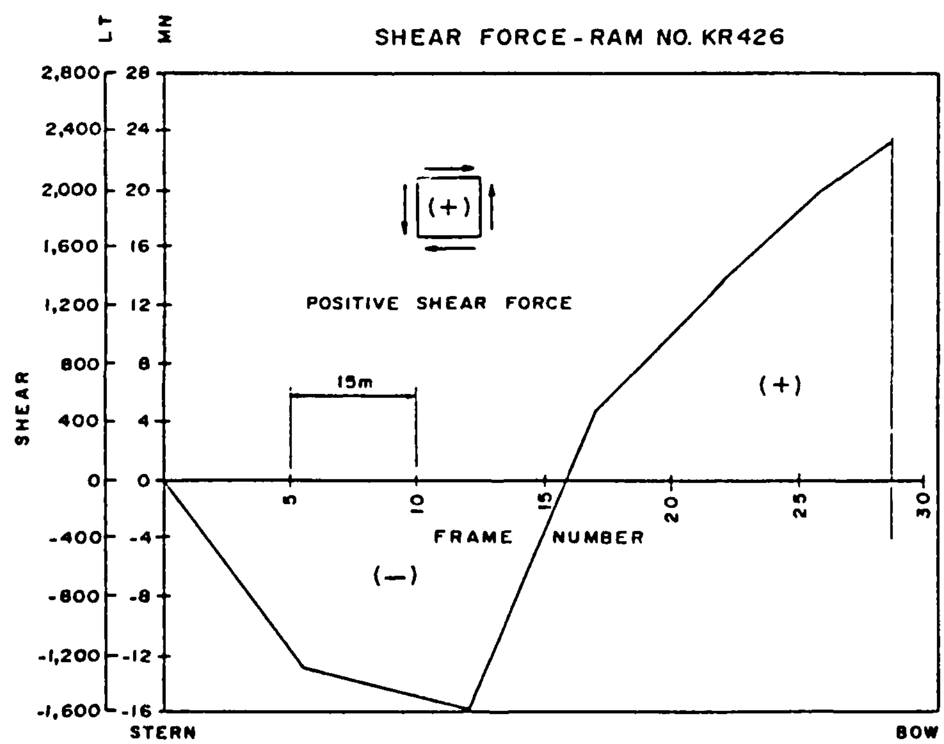

Figure 29
KIGORIAK SHEAR FORCE DISTRIBUTION [17]

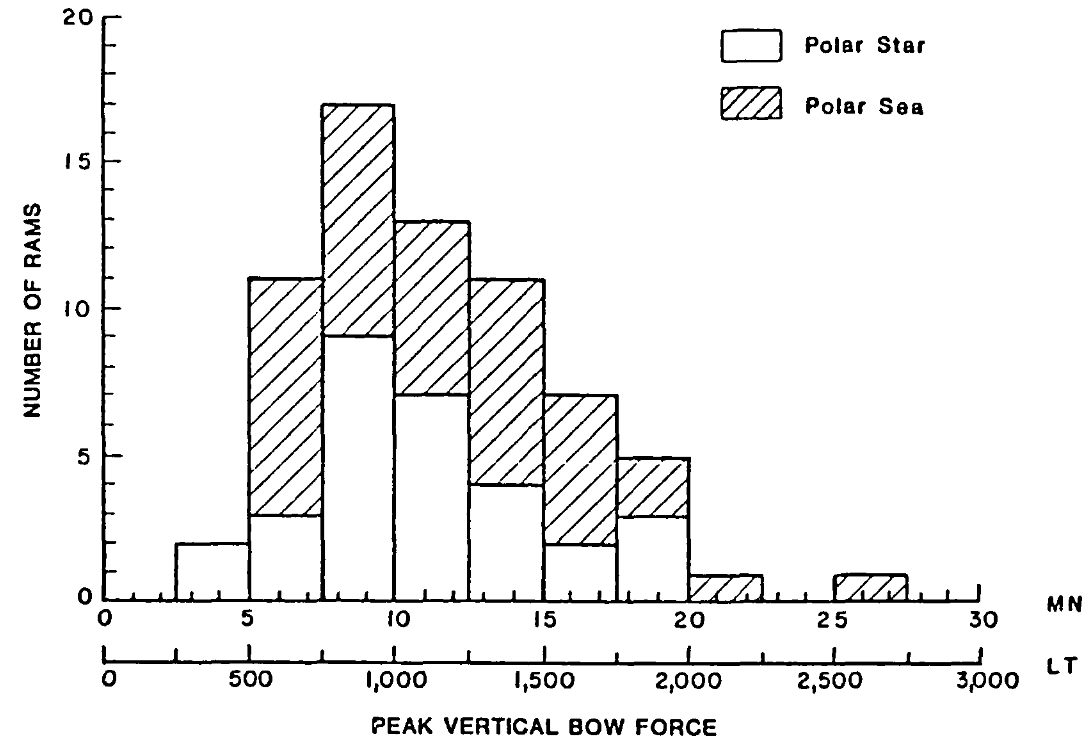

Figure 30
HISTOGRAM OF POLAR CLASS PEAK VERTICAL BOW FORCE

6. EVALUATION OF THE ACCURACY OF THE GLOBAL LOAD MEASURING SYSTEM

There are a number of potential sources of error that should be considered in order to estimate the overall accuracy in computing the global bow force. Each of the major errors is investigated in turn and combined with the other errors using the standard techniques of error analysis [18]. Starting with the equation for the bending moment where just the 01 Deck bending stress is used and inserting all the variables, we have

$$M = \frac{\sigma \cdot I}{Y} = \frac{\varepsilon \cdot E \cdot I}{Y}$$

$$M = \frac{\varepsilon' \cdot f \cdot E \cdot I}{Y}$$

where f is the transformation factor relating the strain parallel to the deck edge to the principal strain along the centerline and Y is the distance from the neutral axis to the gage elevation at an instrumented frame. The derivation of this equation is contained in Appendix B.

The error associated with measuring the strain, ε', can be estimated from the sampling rate and the accuracy to which peak amplitudes of a signal are measured. Assuming a quarter sine wave with a frequency of 2.5 Hz to represent the rise in strain, as mentioned in Section 2, and using a sampling rate of 100 samples/second, 40 digital samples can be obtained during one cycle at the highest frequency. The digital measurement can therefore occur a maximum of 4.5° away from the peak in the worst case (360°/(40x2)). This yields a maximum error in sampling the peak amplitude of ± 0.31%.

Next, the expression for the transformation factor f contains a $\cos^2\theta$ term where θ is the angle the strain gage is positioned off of the centerline. If the uncertainty in placing the gage and measuring the angle is about 2°, and assuming a θ value of 22° (i.e. near the bow), then the uncertainty in $\cos(\theta)$ is about ± 1.47%. The uncertainty associated with the transformation factor would then be twice this amount.

Uncertainties associated with the moment of inertia, I, are more difficult to determine. For the frames forward of the superstructure inertias were computed manually from the ship's plans and an estimated error of ± 2.5% was used. The neutral axis was judged to be accurate to within ± 0.5 ft. Using a value of 40 feet for the neutral axis near the bow, then the resulting uncertainty is about 1.25%.

Since these uncertainties are based on independent measurements they can be added in quadrature to arrive at the uncertainty in calculating the bending moment.

$$\Delta M/M = [\,(0.31)^2 + (2x1.47)^2 + (2.5)^2 + (1.25)^2\,]^{0.5}$$

$$= 4.07\%$$

Next, a specific ram was selected (ram 40), to observe how the uncertainty in the bending moment propagated through the equations for shear and bow force. The 4.07 percent computed above was applied to the four bending moments just fore and aft of the two shear forces used in the calculation of the vertical bow force. The uncertainty for just one of these shear forces is composed of the errors brought about by the uncertainty in the two bending moments. These two errors were added in quadrature.

$$\Delta S_i \approx [(\Delta M_i/\Delta X)^2 + (\Delta M_{i+1}/\Delta X)^2]^{0.5}$$

Finally, the uncertainty for the two shear forces were also added in quadrature to estimate the uncertainty of the bow force. The final result for ram 40 was as follows:

$$\Delta F \approx [(\Delta S_i)^2 + (\Delta S_{i+1})^2]^{0.5}$$

$$\Delta F \approx 183.2 \text{ LT}$$

$$F = 1945 \text{ LT}$$

which implies $\Delta F/F \approx 9.4\%$

Several other rams where analyzed using the same procedure and in each case the uncertainty was less than 10%. This overall uncertainty, however, takes into account only the errors associated with the measurements of the individual terms that make up the expression for the bending moment. Thus the uncertainty in the measurement of the bending moment applies only to values of the bending moment at the instrumented frames. It does not include any error which may arise from measuring the bending moment at a finite number of points. Therefore an additional uncertainty is present when the shear force distribution is represented by the slope of the straight line segmented bending moment distribution. A more reasonable, but qualitative, assessment of the overall uncertainty in the bow force would probably be ± 15%.

The error associated with the location of the center of the ice load is unrelated to the uncertainty in estimating the bow force. This was determined from the compression gages installed from cant frames 14 to 38. The spacing of the gages allowed the load center to be estimated with an accuracy of ± 16 in (± 41 cm).

7. CONCLUSIONS

The following is a list of the conclusions from this work. It should be noted that both of the POLAR Class deployments to gather ice load data encountered generally light ice conditions. Ideal ice conditions for the test would have large, thick multiyear floes that could be rammed repeatedly without breaking apart.

1. The use of bending gages provided a good estimate of the longitudinal bending moment and shear force distributions. This instrumentation method uses fewer strain gages than attempting to measure the shear force directly.

2. The centerline bulkhead compression gages provided an excellent indication of the location of the center of the ice load during the initial impact phase. As the penetration increases, however, much of the ice load is shifted aft along each side of the bow, thus moving the center of the load aft of the position indicated by the compression gages.

3. For the ice conditions encountered, the global impact ice forces on the POLAR Class are not localized loads but spread over much of the bow.

4. The superstructure is effective in bending and should not be ignored in design calculations.

5. The maximum bending stress was found to be primarily at the three instrumented frames in the vicinity of the forward part of the superstructure (frames 39, 55, and 85). This is in contrast to the POLAR SEA report which only gave the maximum bending stresses found at frame 39 [9].

6. The loading rate was measured to be as high as 5000 LT/s (50 MN/s), considerably less than the KIGORIAK's loading rate of 15000 LT/s (150 MN/s) [17].

7. The vessel did not "rebound" after the first impact with the ice as was observed in the KIGORIAK tests [17].

8. The dominant response of the vessel was at the first mode of vibration (3 Hz).

9. The maximum calculated vertical bow force was 1989 LT (19.82 MN) which is lower than the maximum of 2506 LT (24.97 MN) observed during the POLAR SEA impact tests [9].

10. The measured vertical bow forces for the POLAR Class were compared with and found to be lower than the predictive equations of Johansson [16] and Ghoneim [17]. This is undoubtedly a result of the light ice conditions encountered, but no conclusion can be drawn concerning the effectiveness of the bow shape.

11. The maximum bending stress measured was 2123 psi (14.64 MPa) in compression which is lower than the 6078 psi (41.91 MPa) measured on the POLAR SEA [9] and well below the 45,600 psi (310 MPa) yield strength for the deck steel.

12. The maximum bending stresses obtained during the two POLAR Class global ice loads deployments are not really comparable. Analysis of the POLAR STAR data computed the maximum compressive stress from all of the 01 Deck bending gages while the POLAR SEA analysis took into account only the 01 Deck gages at frame 39.

13. The uncertainty in calculating the bending moment at any of the instrumented frames is approximately ± 4%. The propagation of this error based on a finite number of points results in a bow force uncertainty of ± 10%. Since the bending moment distribution should really be a smooth continuous curve, a reasonable estimate for the overall uncertainty is more likely to be ± 15%.

8. RECOMMENDATIONS

Recommendations based on this study fall into several categories; additional analysis, improvements to the instrumentation, and additional data collection.

Additional analysis can be done with the data already collected on unsymmetric ramming events to estimate the amount and location of torsion in the hull girder. This would be done by examining the strain difference between port and starboard gages on the same instrumented frame. It is also suggested that the data from the POLAR SEA impact tests be reexamined to determine the maximum 01 Deck bending stress and its longitudinal location for each ram. These results could then be combined with the values given in this report.

One of the recommendations from the 1985 POLAR SEA global ice loads report [9] suggested that future instrumentation programs on the POLAR Class shift the centerline strain gages outboard to the deck edges since the data from these gages was found to be unreliable due to stress concentration influences. This recommendation was carried out in positioning the gages aboard the POLAR STAR, however, the gages placed near the deck edge on the 3rd Deck (near the design waterline) occasionally picked up the local load effect of broken ice pieces dragging along the ship's hull. Future instrumentation programs aboard the POLAR Class should strive to position the below deck gages to avoid both of these problems.

Additional multiyear ice data should be collected with the POLAR Class in order to build up a data base for more complete analysis. In particular, ramming events collected against large, hard multiyear ice features are needed before any conclusions can be reached regarding the relationship between icebreaker impact velocity and the maximum bow force.

REFERENCES

1. Noble, P.G., Tam, W.K., Menon, B., and Bayly, I.M., "Ice Forces and Accelerations on a Polar Class Icebreaker", POAC, 1979.

2. Ghoneim, G.A.M. and Smyth, A.M., "Finite Element Beam Modelling of Ship Structures under Ice Induced Forces", IAHR Symposium on Ice, Hamburg, August, 1984.

3. Masakatsu Matsuishi, Jun-Ichi Ikeda, Hajime Kawkami, and Masao Hirago, "Ship Ice Floe Collision Analysis Considering the Elastic Deflection of Hull Girder", Ice-Tech 84, SNAME, Calgary, May, 1984.

4. Varsta, P., "Modelling of Impact between Ship Hull and Ice", POAC 83, Vol. 2, pp. 760-777.

5. Ghoneim, G.A.M., and Keinonen, A.J., "Full Scale Impact Tests of Canmar Kigoriak In Thick Ice", POAC, April 1983.

6. Ghoneim, G.A.M., Edgecombe M.H., and Grinstead,J., "System Development for Measurement of Full Scale Ship Ice Impact Forces", Ice-Tech 84, SNAME, May 1984.

7. Churcher, A., Kolomocjev, A., and Hubbard, G., "Design of the Robert LeMeur Ice Breaking Supply Ship", SNAME, Pacific Northwest Section, Vancouver, 1983.

8. Iyer, S.H., "Calibration Testing of M.V. Arctic for the Measurement of Icebreaking Loads", Workshop on Sea Ice Field Measurement, St. John's, Newfoundland, April 29 -May 01, 1980.

9. Minnick, P.V., St. John, J.W., Cowper, B., and Edgecombe, M. "The 1985 Global Ice Impact Tests on the USCGC POLAR SEA", ARCTEC ENGINEERING, Inc. Report No. 1092C/1095C, November 1986, for the Ship Structure Committee (SR-1313).

10. Keinonen, A.J., "Ice Loads on Ships in the Canadian Arctic", WEGEMT, 1983.

11. Glen, I.F., and Daley, C., "Ice Impact Loads on Ships", Arctic Section, SNAME, Calgary, May 1982.

12. Glen, I.F., Daley, C., Edworthy, J., and Gareau, G., "Studies Supporting Update of the CASPPR Regulations Group 1 and 2", Report 586A by Arctec Canada Limited for Canadian Coast Guard, 1982.

13. St. John, J.W., Daley, C., and Blount, H., "Ice Loads and Ship Response to Ice", Report SR-1291 by ARCTEC, Incorporated and ARCTEC CANADA Limited for U.S. Maritime Administration, Ship Structure Committee, and The Canadian Transport Development Center, 1984.

14. Glen, I.F., Majid, I., Tam, G., and Menon, B., "Winter 1981 Trafficability Tests of the Polar Sea," Volume IX "Ice Induced Vibration Measurements and Development of a Model for Icebreaking Excitation Forces," ARCTEC CANADA Limited Report No. 792C-5, ARCTEC, Incorporated, Report No. 583C-3, April, 1982.

15. Blount, H., Glen, I.F., Comfort, G., and Tam, G., "Results of Full Scale Measurements aboard CCGS Louis S. St. Laurent During a 1980 Fall Arctic Probe," Volume 1, ARCTEC CANADA Limited, Report No. 737C for Canadian Ccoast Guard, July 1981.

16. Johansson, B.M., Keinonen, A.J., and Mercer, B., "Technical Development of an Environmentally Safe Arctic Tanker", Ice Tech 81, SNAME Spring Meeting/Star Symposium, Ottawa, June 1981.

17. Ghoneim, G.A.M., Johansson, B.M., Symth, A.J., Grinstead, J., "Global Ship Ice Impact Forces Determined from Full-Scale Tests and Analytical Modelling of the Icebreakers Canmar Kigoriak and Robert LeMeur, TSNAME, November 1984.

18. Schenck, H. Jr., "Theories of Engineering Experimentation," McGraw-Hill Book Company, Inc., New York, 1961.

APPENDIX A

SENSOR/CHANNEL SPECIFICATIONS AND LOCATIONS

This appendix gives some of the specific details associated with the operation and installation of the data acquisition system onboard the POLAR STAR.

In the initial configuration of the system maximum expected values had to be estimated for the strains and other engineering quantities in order to calibrate and interpret the measurements received. Using the strain gages as an example, it was estimated that the maximum peak strain expected to occur with the highest impact loads was approximately 500 microstrain. This full scale value was used to adjust the the gain setting on the signal filter/amplifiers to provide a maximum output of ± 10 volts to a analog-to-digital subsystem. The A-to-D system used was a HP 6940B Multiprogrammer with enough scanning boards to handle up to 48 channels of data. Associated with the analog-to-digital process was a conversion factor of 10 volts/2000 A-to-D units which places some limits on the resolution of the resulting data. For a full scale of 497.512 microstrain/10 volts on all the strain gages this resolution corresponds to a value of 0.2487 microstrain/A-to-D unit. A similar procedure was carried out for the accelerometers and the doppler velocity radar to arrive at the calibration factors listed in Table A1. All of the strain gages were wired as opposite-active arm bridges and had an excitation of 10 volts.

The control, storage and processing data collection functions were performed by the Hewlett-Packard series 200 model 9816 desk top computer with an internal memory of approximately 4.3 megabytes. The computer was used to program and receive the data from the HP 6940B Multiprogrammer. Prior to each ramming event the computer programmed the HP 6940B so that it would scan through all of its 48 data channels (including one null channel) 100 times each second for 25 seconds. When the proper cue was received from the computer the scanning would commence. With each scan the multiprogrammer received the filtered data, converted it to digital form, and transfered it to the computer's memory. Afterwards the measurements were transfered from computer memory onto a 3.5 inch floppy disk for storage; one ram event for each disk.

The signal processing filters, analog-to-digital multiprogrammer, and the computer were all set up in the windlass room aboard the POLAR STAR. This compartment was selected because of its central location with respect to laying of the necessary cables to each of the strain gages, and because the out of the way location would not interfere with shipboard activities. The equipment rack also contained a video screen giving the view from aloft conn of the bow of the vessel and the area forward of the bow. Extra components were available for the entire system in case the failure of one or more of the essential elements occurred.

The installation of electronic equipment and strain gages onboard the POLAR STAR was carried out in July of 1986; approximately two months prior to the deployment. After arrival in the Beaufort Sea and before any ramming tests were conducted the entire system was checked out. This investigation led to three strain gages that were found to be defective (probably due to water exposure). Two of the gages were located on the 01 weather deck and were replaced or repaired. The third was one of the centerline compression gages used to locate the ice load along the stem bar. This particular gage was located in the lowest part of the 3-E-0-W tank; the same place where a defective gage was found during the POLAR SEA trials [9]. Fortunately, this gage was found to work when rewired as a single arm bridge and the calibration factor was doubled accordingly. The refurbished gage system was found to provide clean, noise free data.

The notation used for the gage/channel identification is made up of four elements. The first identifies the gage as a bending or compression type. The second element gives the deck (or stembar) location which is followed by the frame number. The last character (P, S, or C) means port, starboard or centerline.

TABLE A1

POLAR STAR IMPACT TESTS FALL 1986
SENSOR SPECIFICATIONS

CHAN #	CHAN ID	CALIBRATION FACTOR	GAGE FACTOR	EXIT. VOLTAGE	BRIDGE TYPE	UNITS
1	B-01-FR85S	2.487E-7	2.01	10.00	2.00	strain
2	B-01-FR85P	2.487E-7	2.01	10.00	2.00	strain
3	B-01-FR55S	2.487E-7	2.01	10.00	2.00	strain
4	B-01-FR55P	2.487E-7	2.01	10.00	2.00	strain
5	B-01-CF43S	2.487E-7	2.01	10.00	2.00	strain
6	B-01-CF43P	2.487E-7	2.01	10.00	2.00	strain
7	B-01-FR39S	2.487E-7	2.01	10.00	2.00	strain
8	B-01-FR39P	2.487E-7	2.01	10.00	2.00	strain
9	B-01-CF35S	2.487E-7	2.01	10.00	2.00	strain
10	B-01-CF35P	2.487E-7	2.01	10.00	2.00	strain
11	B-01-CF27S	2.487E-7	2.01	10.00	2.00	strain
12	B-01-CF27P	2.487E-7	2.01	10.00	2.00	strain
13	B-01-CF22S	2.487E-7	2.01	10.00	2.00	strain
14	B-01-CF22P	2.487E-7	2.01	10.00	2.00	strain
15	B-01-CF17S	2.487E-7	2.01	10.00	2.00	strain
16	B-01-CF17P	2.487E-7	2.01	10.00	2.00	strain
17	C-SB-CF28C	2.487E-7	2.01	10.00	2.00	strain
18	C-SB-CF26C	2.487E-7	2.01	10.00	2.00	strain
19	B-1P-CF43S	2.487E-7	2.01	10.00	2.00	strain
20	B-1P-CF43P	2.487E-7	2.01	10.00	2.00	strain
21	C-SB-CF38C	2.487E-7	2.01	10.00	2.00	strain
22	C-SB-CF36C	2.487E-7	2.01	10.00	2.00	strain
23	B-3-CF35-S	2.487E-7	2.01	10.00	2.00	strain
24	B-3-CF35-P	2.487E-7	2.01	10.00	2.00	strain
25	B-SB-CF35C	2.487E-7	2.01	10.00	2.00	strain
26	C-SB-CF32C	2.487E-7	2.01	10.00	2.00	strain
27	B-SB-CF27C	2.487E-7	2.01	10.00	2.00	strain
28	C-SB-CF24C	2.487E-7	2.01	10.00	2.00	strain
29	B-2-CF17-C	2.487E-7	2.01	10.00	2.00	strain
30	C-SB-CF14C	2.487E-7	2.01	10.00	2.00	strain
31	B-01FR128S	2.487E-7	2.01	10.00	2.00	strain
32	B-01FR128P	2.487E-7	2.01	10.00	2.00	strain
33	NULL					
34	B-3-FR55-S	2.487E-7	2.01	10.00	2.00	strain
35	B-3-FR55-P	2.487E-7	2.01	10.00	2.00	strain
36	B-3-FR39-S	2.487E-7	2.01	10.00	2.00	strain
37	B-3-FR39-P	2.487E-7	2.01	10.00	2.00	strain
38	B-3-CF43-S	2.487E-7	2.01	10.00	2.00	strain
39	B-3-CF43-P	2.487E-7	2.01	10.00	2.00	strain
40	Velocity	7.719E-3	0.00	10.00	0.00	knots
41	AccZ Heave	1.064E-3	0.00	10.00	0.00	g
42	AccY Sway	5.263E-4	0.00	10.00	0.00	g
43	AccX Surge	-5.319E-4	0.00	10.00	0.00	g
44	C-SB-CF20C	2.487E-7	2.01	10.00	2.00	strain
45	C-SB-CF18C	2.487E-7	2.01	10.00	2.00	strain
46	C-SB-CF16C	2.487E-7	2.01	10.00	2.00	strain
47	C-SB-CF34C	2.487E-7	2.01	10.00	2.00	strain
48	C-SB-CF30C	2.487E-7	2.01	10.00	2.00	strain

TABLE A2

POLAR STAR IMPACT TESTS FALL 1986

SENSOR SPECIFICATIONS

		LONGITUDINAL		VERTICAL		ANGLE	TRANSFORMATION
CHAN #	CHAN ID	Ft.	m	Ft.	m.	(Deg.)	FACTOR
1	B-01-FR85S	253.7	77.3	54.7	16.7	1.0	1.000
2	B-01-FR85P	253.7	77.3	54.7	16.7	1.0	1.000
3	B-01-FR55S	295.3	90.0	56.3	17.2	6.5	1.017
4	B-01-FR55P	295.3	90.0	56.3	17.2	6.5	1.017
5	B-01-CF43S	338.3	103.1	58.1	17.7	18.0	1.140
6	B-01-CF43P	338.3	103.1	58.1	17.7	18.0	1.140
7	B-01-FR39S	316.7	96.5	57.1	17.4	12.0	1.059
8	B-01-FR39P	316.7	96.5	57.1	17.4	12.0	1.059
9	B-01-CF35S	349.3	106.5	58.7	17.9	20.0	1.178
10	B-01-CF35P	349.3	106.3	58.7	17.9	20.0	1.178
11	B-01-CF27S	360.7	109.9	59.0	18.0	21.0	1.199
12	B-01-CF27P	360.7	109.9	59.0	18.0	21.0	1.199
13	B-01-CF22S	368.5	112.3	59.4	18.1	22.0	1.221
14	B-01-CF22P	368.5	112.3	59.4	18.1	22.0	1.221
15	B-01-CF17S	375.0	114.3	59.7	18.2	23.0	1.245
16	B-01-CF17P	375.0	114.3	59.7	18.2	23.0	1.245
17	C-SB-CF28C	359.5	1.9.6	28.2	8.6	0.0	1.000
18	C-SB-CF26C	362.4	110.5	29.1	8.9	0.0	1.000
19	B-1P-CF43S	338.3	103.1	21.0	6.4	28.5	1.416
20	B-1P-CF43P	338.3	103.1	21.0	6.4	28.5	1.416
21	C-SB-CF38C	345.1	105.2	22.1	6.7	27.0	1.362
22	C-SB-CF36C	348.0	106.1	23.5	7.2	0.0	1.000
23	B-3-CF35-S	349.3	106.5	29.4	9.0	26.5	1.346
24	B-3-CF35-P	349.3	106.5	29.4	9.0	26.5	1.346
25	B-SB-CF35C	349.3	106.5	22.7	6.9	0.0	1.000
26	C-SB-CF32C	353.9	107.9	26.0	7.9	0.0	1.000
27	B-SB-CF27C	360.7	109.9	27.0	8.2	0.0	1.000
28	C-SB-CF24C	365.3	111.3	29.9	9.1	0.0	1.000
29	B-2-CF17-C	375.0	114.3	37.6	11.5	0.0	1.000
30	C-SB-CF14C	379.5	115.7	33.4	10.2	0.0	1.000
31	B-01FR128S	197.3	60.1	53.2	16.2	-2.0	1.002
32	B-01FR128P	197.3	60.1	53.2	16.2	-2.0	1.002
33	NULL						
34	B-3-FR55-S	295.3	90.0	28.4	8.7	13.0	1.070
35	B-3-FR55-P	295.3	90.0	28.4	8.7	13.0	1.070
36	B-3-FR39-S	316.7	96.5	28.8	8.8	20.0	1.178
37	B-3-FR39-P	316.7	96.5	28.8	8.8	20.0	1.178
38	B-3-CF43-S	338.3	103.1	29.1	8.9	25.0	1.299
39	B-3-CF43-P	338.3	103.1	29.1	8.9	25.0	1.299
40	Velocity	175.0	53.5	51.5	15.7	0.0	1.000
41	AccZ Heave	358.7	109.3	54.0	16.5	0.0	1.000
42	AccY Sway	358.7	109.3	54.0	16.5	0.0	1.000
43	AccX Surge	358.7	109.3	54.0	16.5	0.0	1.000
44	C-SB-CF20C	370.9	113.1	30.9	9.4	0.0	1.000
45	C-SB-CF18C	373.9	114.0	32.0	9.8	0.0	1.000
46	C-SB-CF16C	376.7	114.8	32.3	9.8	0.0	1.000
47	C-SB-CF34C	350.9	107.0	24.8	7.6	0.0	1.000
48	C-SB-CF30C	356.7	108.7	27.0	8.2	0.0	1.000

APPENDIX B

DETAILS OF THE ANALYSIS PROCEDURE

CALCULATION OF BENDING STRESS

$\sigma(Rdg)$ = [Data(Rdg, Chn) - Base-line (Chn)]x(Calib(Chn))x(f)x(E)

$\sigma(Rdg)$	=	Bending Stress Rdg= Reading number (100/second)
Data (Rdg, Chn)	=	Data from A/D Subsystem Chn = Channel number (42 channels)
Base-line (Chn)	=	Base line, calculated as the average of 100 readings before impact occurs.
Calib (Chn)	=	Calibration constant (converts A/D counts to strain).
E	=	Elastic Modulus 30×10^6 psi (2.07E+11 Pa)
f	=	Factor for transformation of stress parallel to side shell to stress parallel to center line of vessel.

The transformation factor f which relates the stress parallel to the deck edge to the principal stress parallel to the centerline was calculated from the equation for strain at a point.

$$\epsilon x' = \epsilon x \cdot (\cos\theta)^2 + \epsilon y \cdot (\sin\theta)^2 + \gamma \cdot \sin\theta \cdot \cos\theta$$

If ϵx and ϵy are the strains in the principal directions, then the shearing strain, γ, is equal to zero. In this case it is assumed that the principal strain ϵx lies along or is very close to the centerline of the ship.

$$\epsilon x' = \epsilon x \cdot (\cos\theta)^2 + \epsilon y \cdot (\sin\theta)^2$$

$$\epsilon x' = \epsilon x \cdot (\cos\theta)^2 + \epsilon y \cdot (1 - (\cos\theta)^2)$$

Using $\epsilon y = -\upsilon \cdot \epsilon x$

$$\epsilon x' = \epsilon x \cdot (\cos\theta)^2 - \upsilon \cdot \epsilon x \cdot (1 - (\cos\theta)^2)$$

$$\epsilon x' = \epsilon x \cdot [(\cos\theta)^2 \cdot (1 + \upsilon) - \upsilon]$$

$$\epsilon x = \epsilon x' / [(\cos\theta)^2 \cdot (1 + \upsilon) - \upsilon]$$

$$\epsilon x = \epsilon x' \cdot f$$

where $\epsilon x'$ = measured strain parallel to side shell
ϵx = principal strain parallel to the centerline
γ = shear strain = 0
θ = angle between the ship's centerline and the tangent line to side shell at the gage location
υ = Poisson's ratio = 0.29

Next Hooke's law for a plane stress state is used with the assumption that for the ship in bending the stress in the transverse direction is much less than the longitudinal stress. Therefore

$$\sigma(Rdg) = \epsilon x \cdot E$$

$$\sigma(Rdg) = \epsilon x' \cdot f \cdot E$$

CALCULATION OF BENDING MOMENT

Frame 55, 39
Cant frames 43, 35 $M=(\epsilon 2-\epsilon 3)x(E)x(I)/D$

Frames 128, 85
Cant frames 27,22, 17 $M=(\epsilon 01)x(E)x(I)/Y$

M	=	bending moment (negative if 01 deck is in compression)
$\epsilon 01$	=	average bending strain in 01 deck at instrumented frame
$\epsilon 2$	=	average bending strain in 2nd deck at instrumented frame
$\epsilon 3$	=	average bending strain in 3rd deck at instrumented frame
E	=	elastic modulus of the deck plating
I	=	transverse sectional inertia
Y	=	distance from the neutral axis to the 01 deck
D	=	vertical distance between gages located at the same frame

NOTE: The deck bending gages located on the centerline were not used in the bending moment calculation, because local stress fields occurred when the ice force was located at the frame containing these gages.

CALCULATION OF SHEAR FORCE VALUES

S(X) = -(M2-M1)/(X2-X1)

S(x)	=	the shear force at x=X1 + (X2-X1)/2
M1	=	the bending moment at x=X1
M2	=	the bending moment at x=X2
X1	=	the longitudinal location of bending moment M1
X2	=	the longitudinal location of bending moment M2

LOCATION OF THE CENTER OF THE LOAD

Loc = Loc_comp(Max_comp)

The location of the center of the ice load was taken to be at the location of the stem bar compression gage undergoing the largest amount of compression.

CALCULATION OF VERTICAL FORCE ON THE BOW

A. If bending gages forward of location of load

Bow_f	=	ABS [S(x1)] + ABS [S(x2)]
Bow_f	=	the vertical ice force on the bow
S(x1)	=	shear force aft of the location of the load
S(x2)	=	shear force forward of the location of the load
ABS	=	absolute value of quantity in brackets

B. If no bending gages forward of location of load

Bow_f	=	ABS[S(x1)]+(Mass)x(acc) ≈ ABS(S(x1))
Bow_f	=	vertical ice force on bow
S(x1)	=	shear aft of location of load
Mass	=	mass of bow section forward of ice force
acc	=	vertical acceleration of bow section

NOTE: The maximum inertial force [(mass)x(ACC)], for the case of no bending gages forward of the location of the load, is approximately 30 LT (0.3 MN).

APPENDIX C

DESCRIPTION OF THE GLOBAL LOAD ANALYSIS SOFTWARE

General Description

The program developed for the USCGC POLAR STAR Impact Tests was derived from the program written for the M.V. KIGORIAK and the M.V. ROBERT LEMEUR Impact Tests conducted in 1983 and is, with only slight modifications, the same program that was used on the POLAR SEA in 1985. The main function of the program is to calculate and plot the global vertical load time history on the bow of the POLAR STAR. The following calculations can be performed by the program:

- longitudinal shear force and bending moment distribution
- neutral axis location
- vertical ice force on bow
- maximum and minimum values calculated
- longitudinal location of maximum and minimum bending and shear values
- location of center of ice load on bow

The analysis software was quite versatile in its mode of application. While a full length report containing everything from graphs of the output from each strain gage to the final time-history of the vertical bow force took about a hour to generate, the program allowed for much quicker results if desired. Once the data disk was read by the computer, any of the strain gage time histories could be viewed and plotted. Also, any time segment out of the 25 second sampling interval could be selected for calculation of the bending moment, shear, or bow force to be displayed and/or plotted. This latter mode of operation reduced the computations down to a few minutes and was used primarily during the system checkout phase to determine operational readiness of the instrumentation.

The hardware required for the analysis program is as follows:

- HP 9816 Computer
- HP 9121 Disk Drive
- HP 2225A Think Jet Printer
- 2.2 MBytes of Memory

The HP Basic 3.0 operating system is required also.

A general soft key menu flow chart is illustrated in Figure C1.

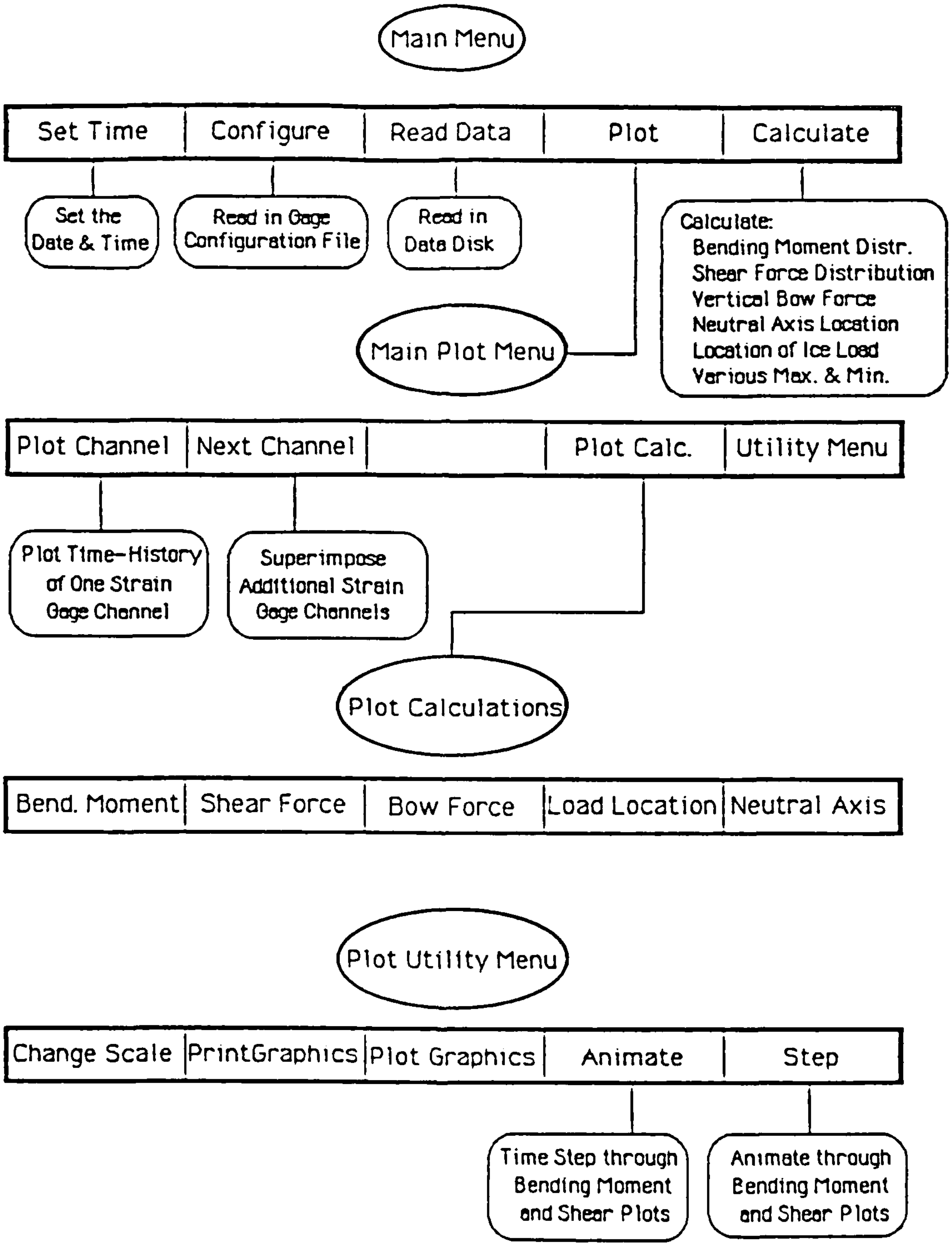

Figure C1

GLOBAL LOAD ANALYSIS FLOWCHART

APPENDIX D

REPRESENTATIVE SAMPLES OF DATA

NOTE: These graphs are arranged into three groups. The first group is the data from the bending gages arranged by frame number. This is followed by the velocity and accelerometer data, and finally, the compression gages.

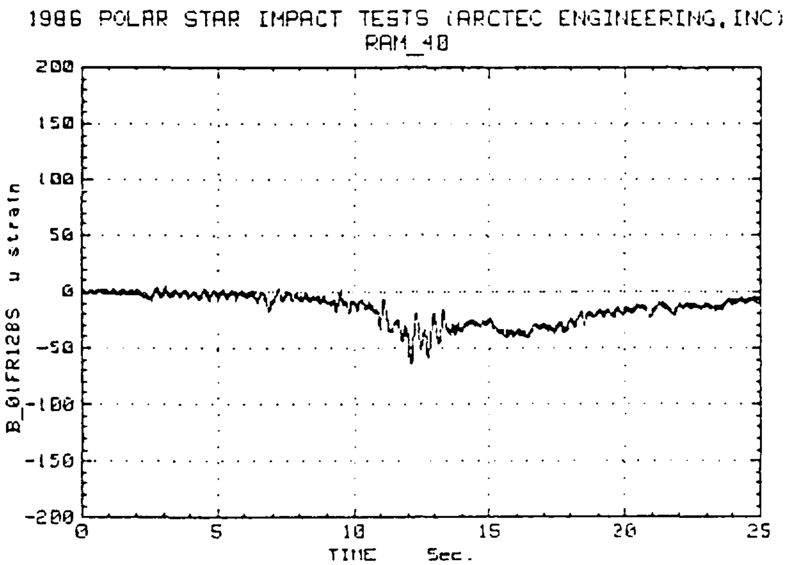
1986 POLAR STAR IMPACT TESTS (ARCTEC ENGINEERING, INC)
RAM_40
B_01FR128S u strain
TIME Sec.

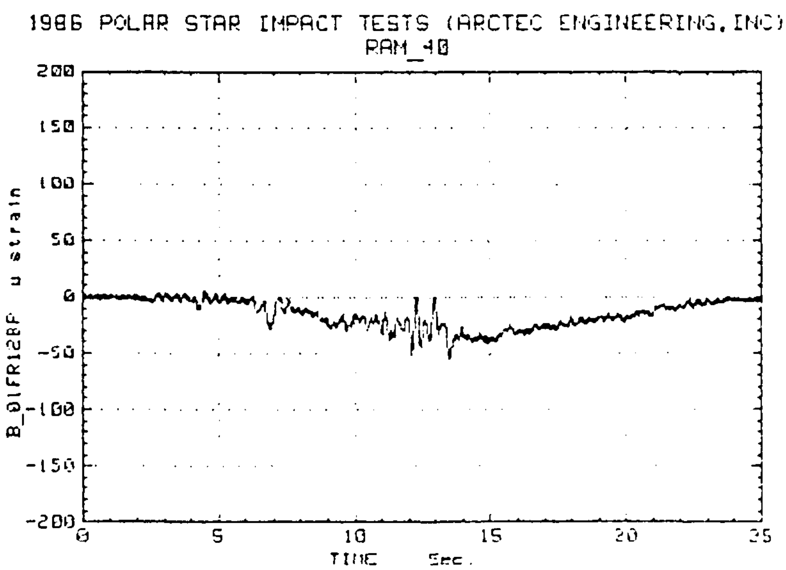
1986 POLAR STAR IMPACT TESTS (ARCTEC ENGINEERING, INC)
RAM_40
B_01FR128F u strain
TIME Sec.

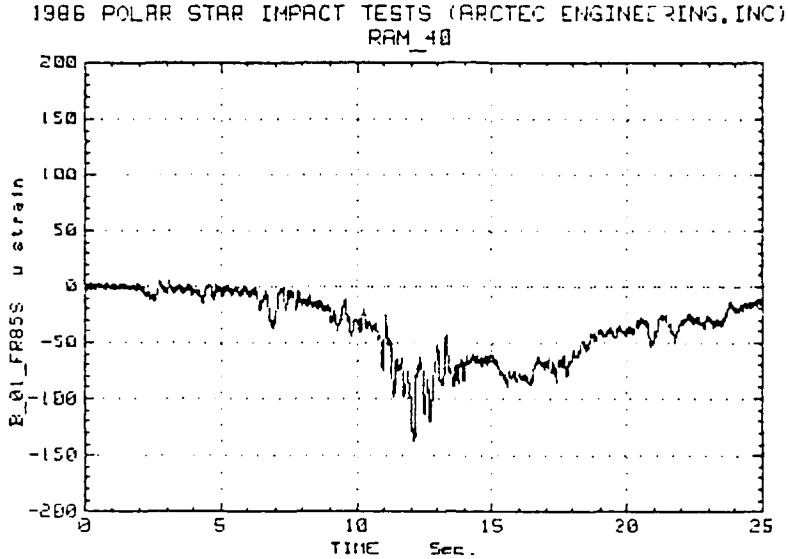

1986 POLAR STAR IMPACT TESTS (ARCTEC ENGINEERING, INC)
RAM_40
E_01_FR85S u strain
TIME Sec.
200
150
100
50
0
-50
-100
-150
-200
0
5
10
15
20
25

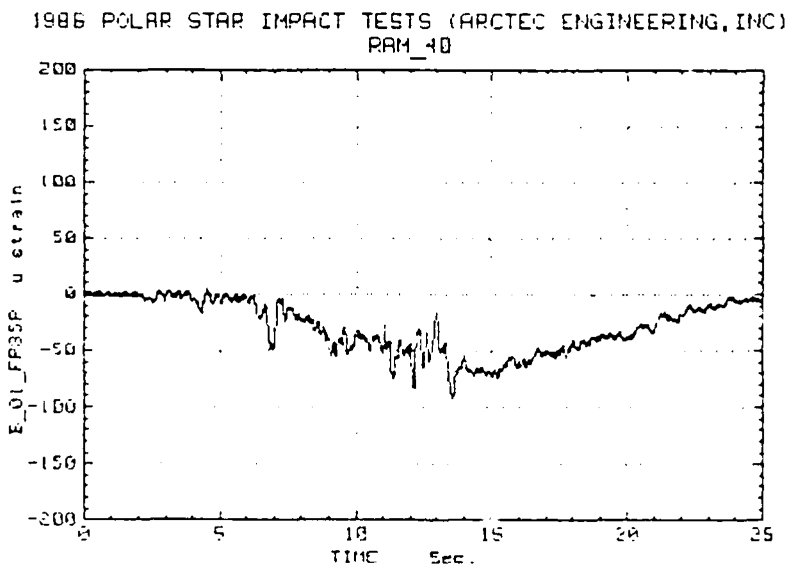

1986 POLAR STAR IMPACT TESTS (ARCTEC ENGINEERING, INC)
RAM_40
E_01_FR35P u strain
TIME Sec.
200
150
100
50
0
-50
-100
-150
-200
0
5
10
15
20
25

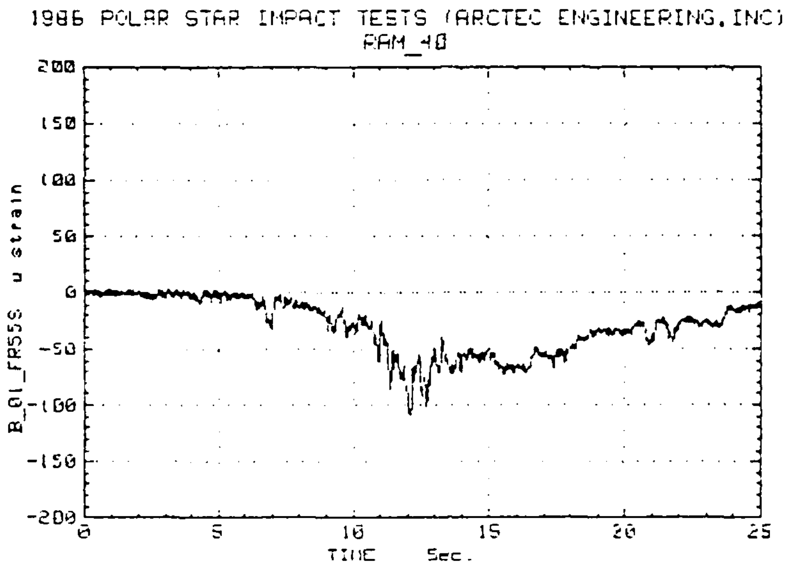
1986 POLAR STAR IMPACT TESTS (ARCTEC ENGINEERING, INC)
RAM_40
B_01_FR55S u strain
TIME Sec.

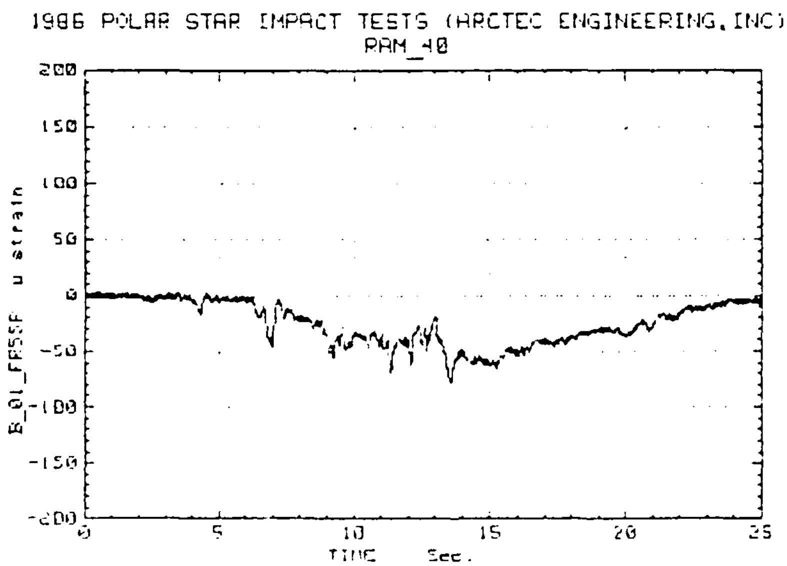
1986 POLAR STAR IMPACT TESTS (ARCTEC ENGINEERING, INC)
RAM_40
B_01_FR55F u strain
TIME Sec.

1986 POLAR STAR IMPACT TESTS (ARCTEC ENGINEERING, INC)
RAM_40

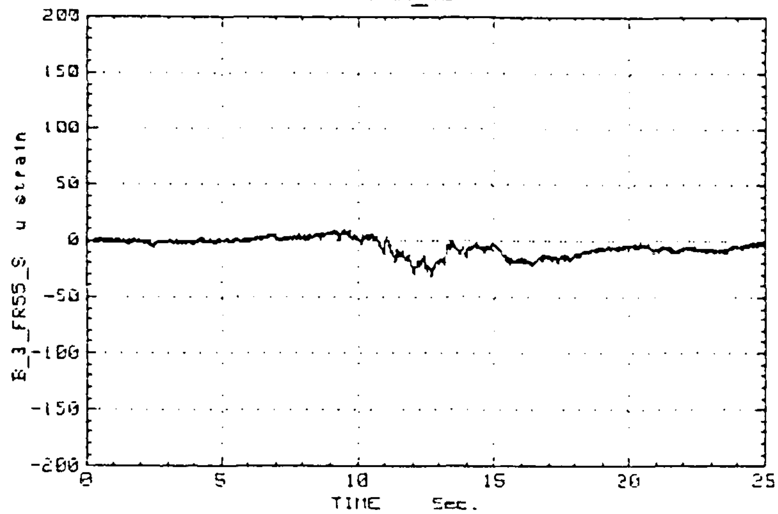

1986 POLAR STAR IMPACT TESTS (ARCTEC ENGINEERING, INC)
RAM_40

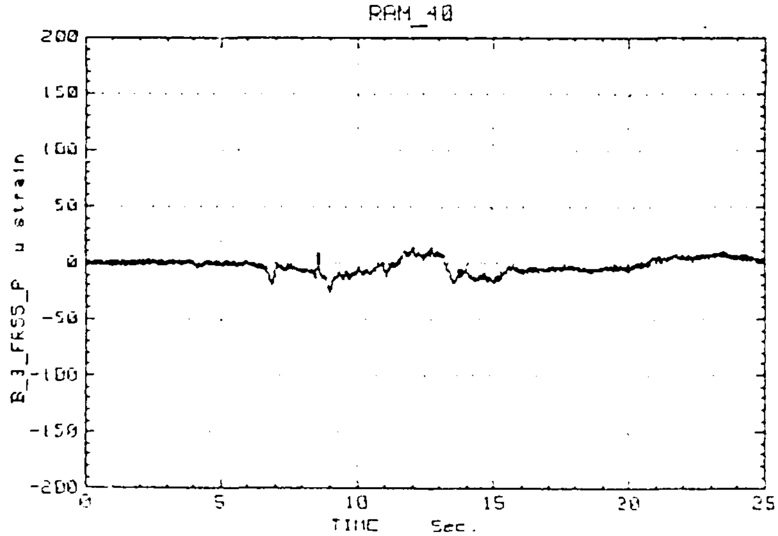

1985 POLAR STAR IMPACT TESTS (ARCTEC ENGINEERING, INC)
FRM_40

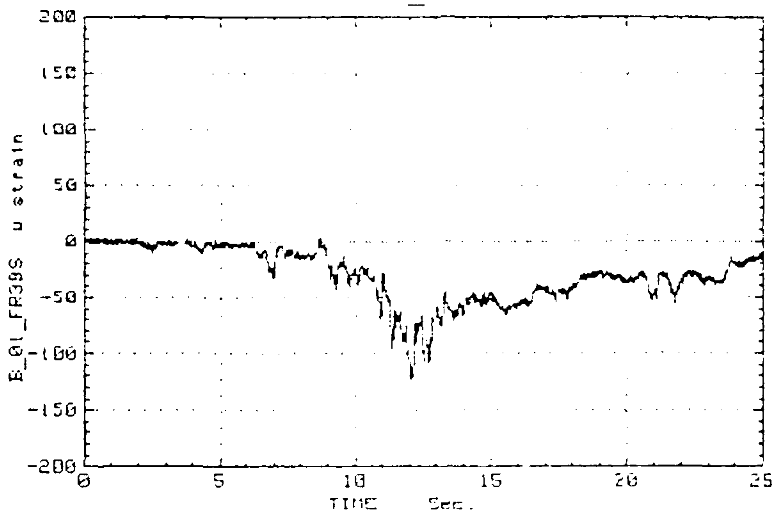

1985 POLAR STAR IMPACT TESTS (ARCTEC ENGINEERING, INC)
FRM_40

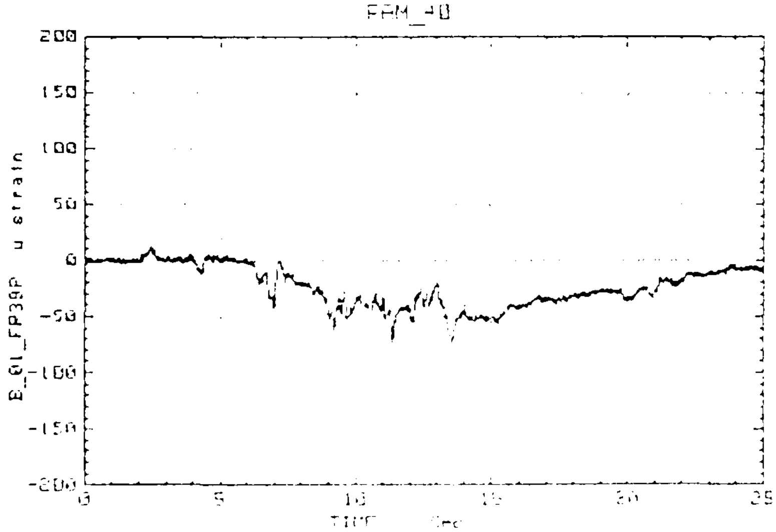

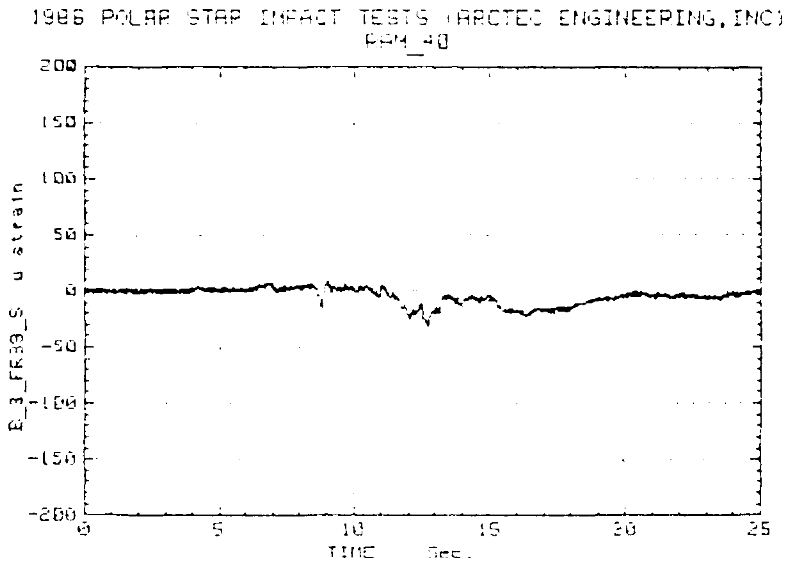
1986 POLAR STAR IMPACT TESTS (ARCTEC ENGINEERING,INC)
RAM_40
B_3_FR33_S u strain
TIME Sec.

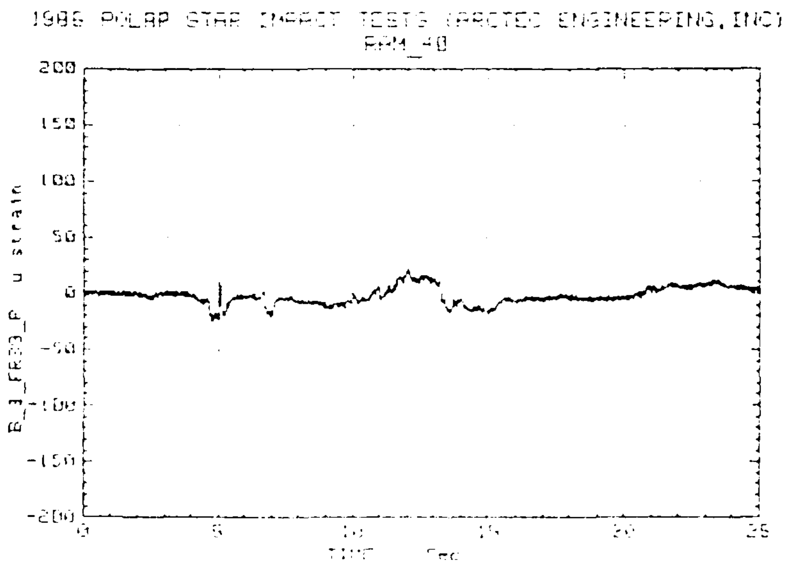
1986 POLAR STAR IMPACT TESTS (ARCTEC ENGINEERING,INC)
RAM_40
B_3_FR33_P u strain
TIME Sec.

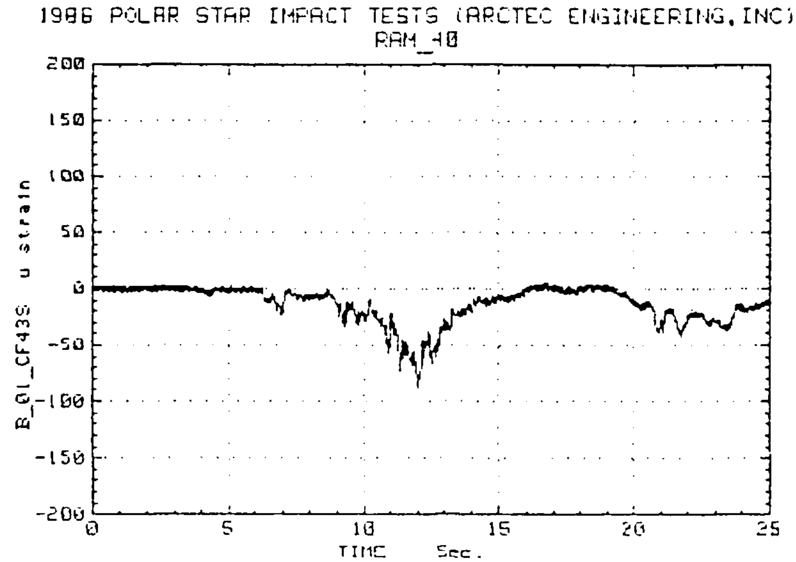

1986 POLAR STAR IMPACT TESTS (ARCTEC ENGINEERING, INC)
RAM_40
B_01_CF43S u strain
TIME Sec.

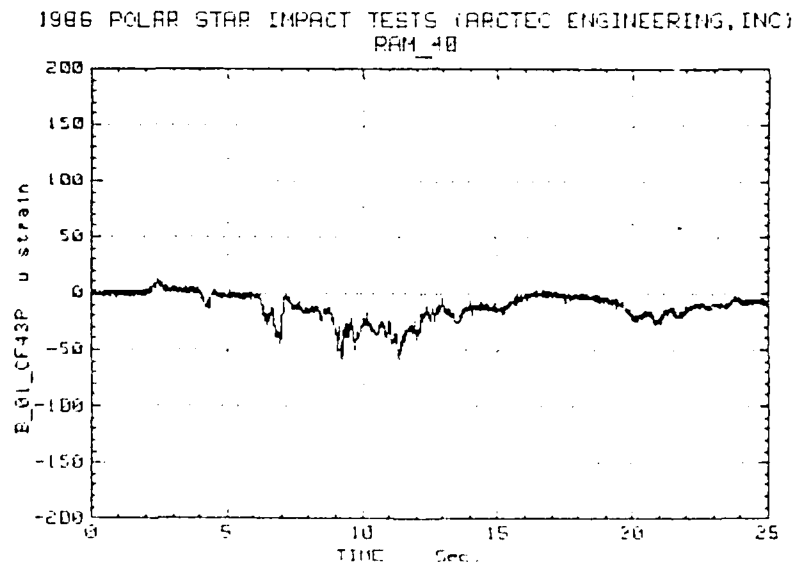

1986 POLAR STAR IMPACT TESTS (ARCTEC ENGINEERING, INC)
RAM_40
B_01_CF43P u strain
TIME Sec.

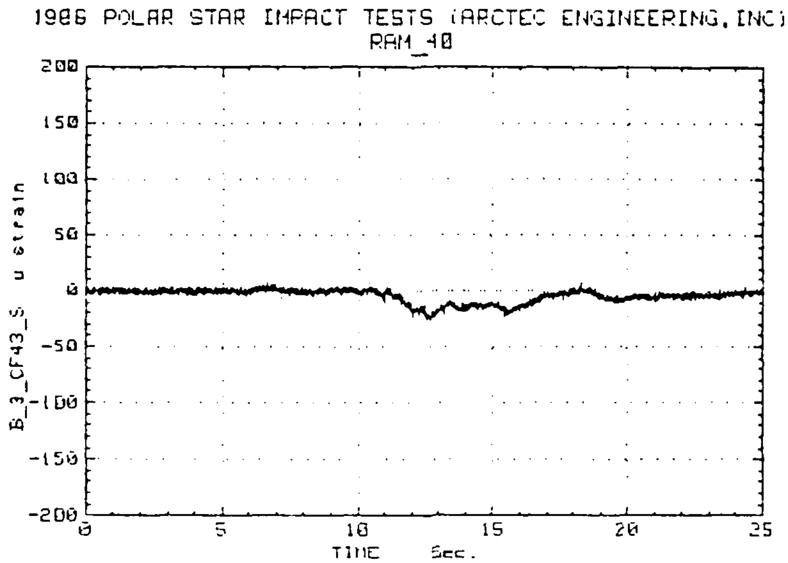
1986 POLAR STAR IMPACT TESTS (ARCTEC ENGINEERING, INC)
RAM_40
B_3_CF43_S u strain
TIME Sec.

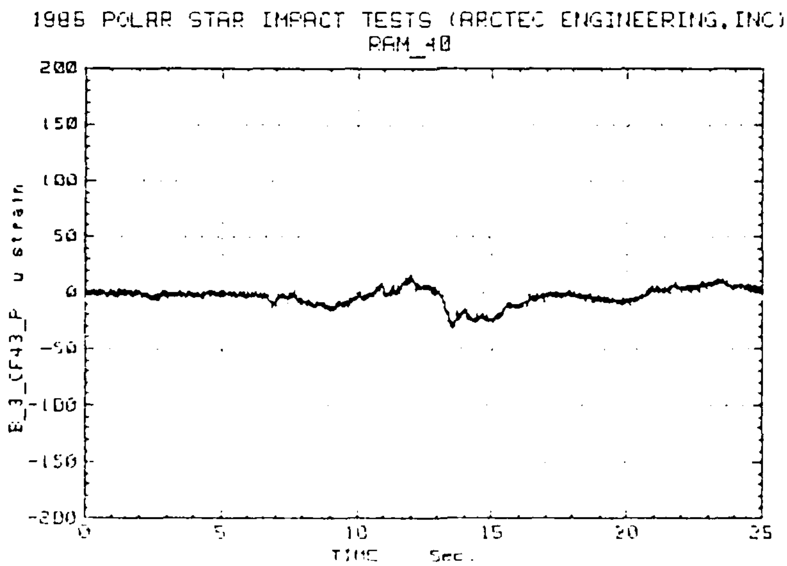
1986 POLAR STAR IMPACT TESTS (ARCTEC ENGINEERING, INC)
RAM_40
B_3_CF43_P u strain
TIME Sec.

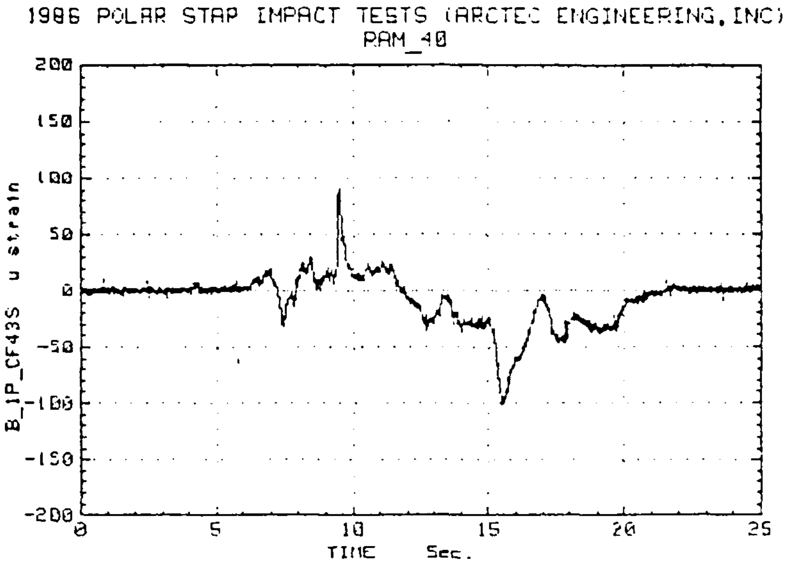

1986 POLAR STAR IMPACT TESTS (ARCTEC ENGINEERING, INC)
RAM_40
200
150
100
50
0
-50
-100
-150
-200
B_1P_CF43S u strain
0
5
10
15
20
25
TIME Sec.

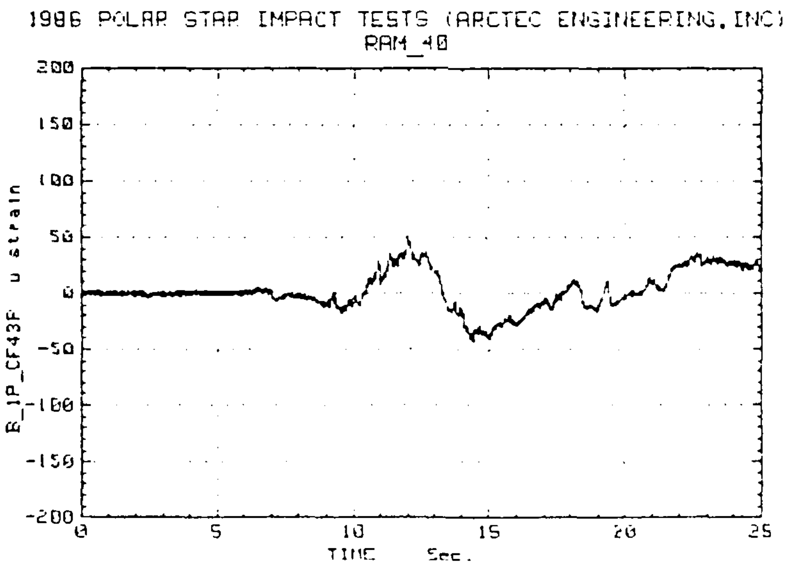

1986 POLAR STAR IMPACT TESTS (ARCTEC ENGINEERING, INC)
RAM_40
200
150
100
50
0
-50
-100
-150
-200
B_1P_CF43F u strain
0
5
10
15
20
25
TIME Sec.

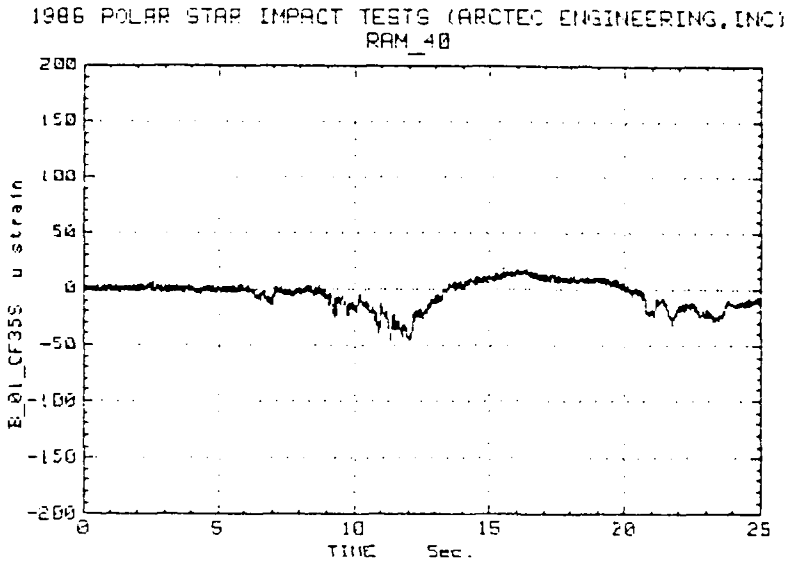
1986 POLAR STAR IMPACT TESTS (ARCTEC ENGINEERING, INC)
RAM_40
B_01_CF35S u strain
TIME Sec.

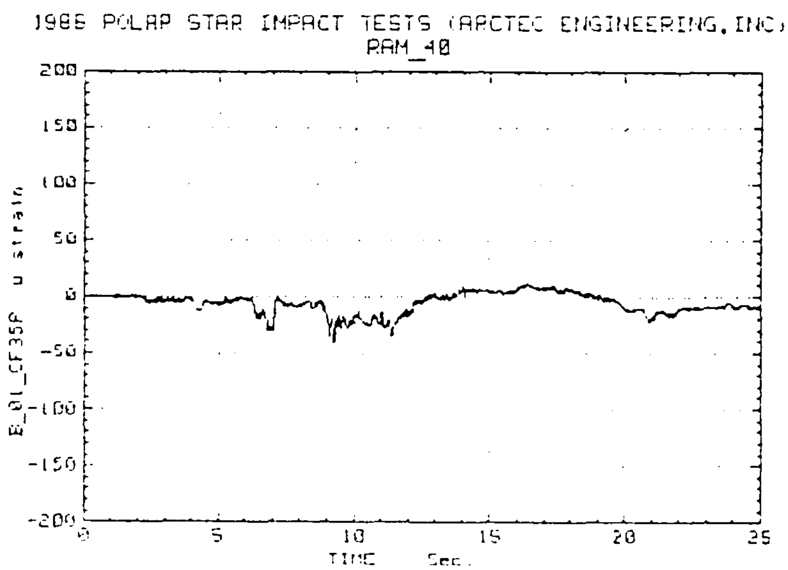
1986 POLAR STAR IMPACT TESTS (ARCTEC ENGINEERING, INC)
RAM_40
B_01_CF35P u strain
TIME Sec.

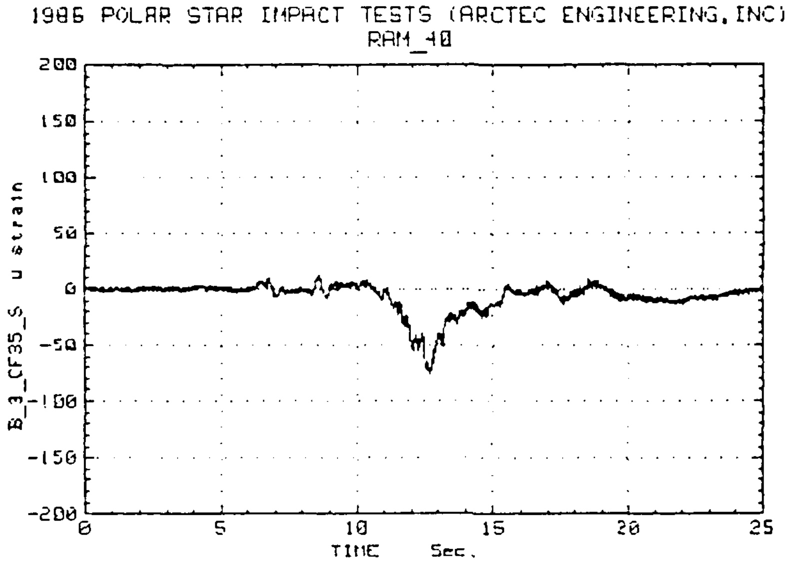
1986 POLAR STAR IMPACT TESTS (ARCTEC ENGINEERING, INC)
RAM_40
B_3_CF35_S u strain
TIME Sec.

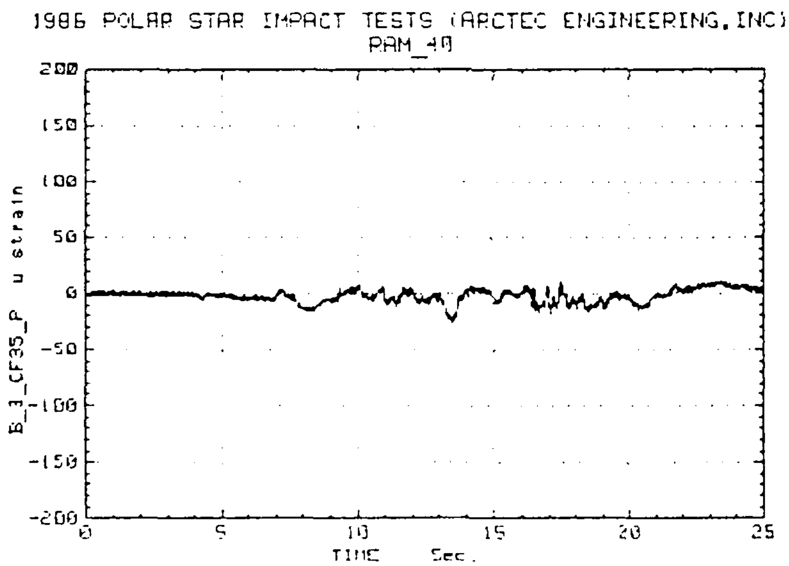
1986 POLAR STAR IMPACT TESTS (ARCTEC ENGINEERING, INC)
RAM_40
B_3_CF35_P u strain
TIME Sec.

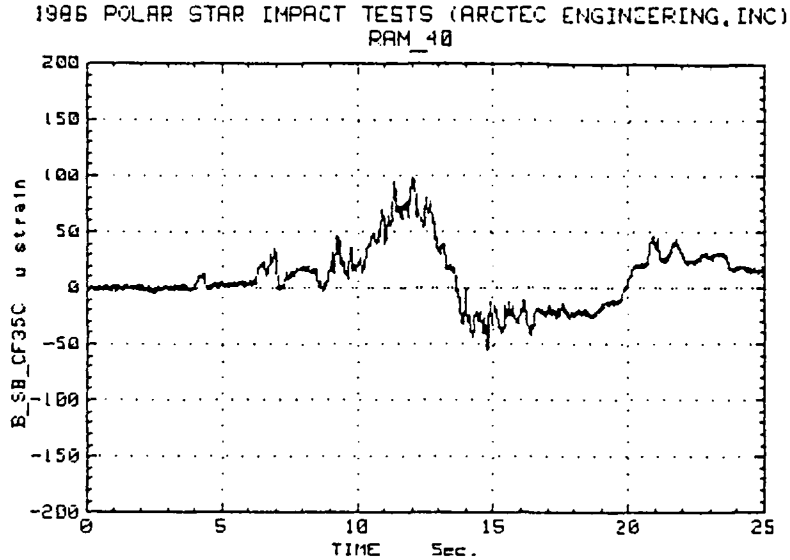
1986 POLAR STAR IMPACT TESTS (ARCTEC ENGINEERING, INC)
RAM_40
B_SB_CF35C u strain
TIME Sec.

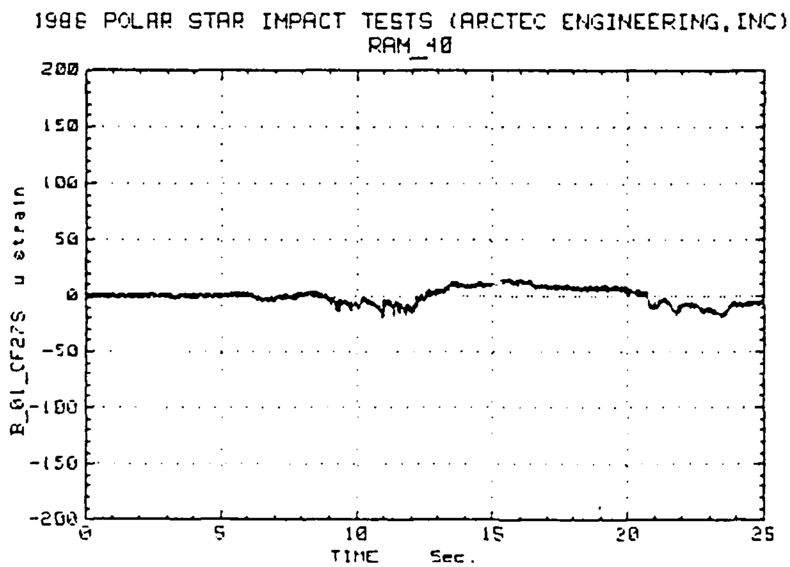
1986 POLAR STAR IMPACT TESTS (ARCTEC ENGINEERING, INC)
RAM_40
B_BL_CF27S u strain
TIME Sec.

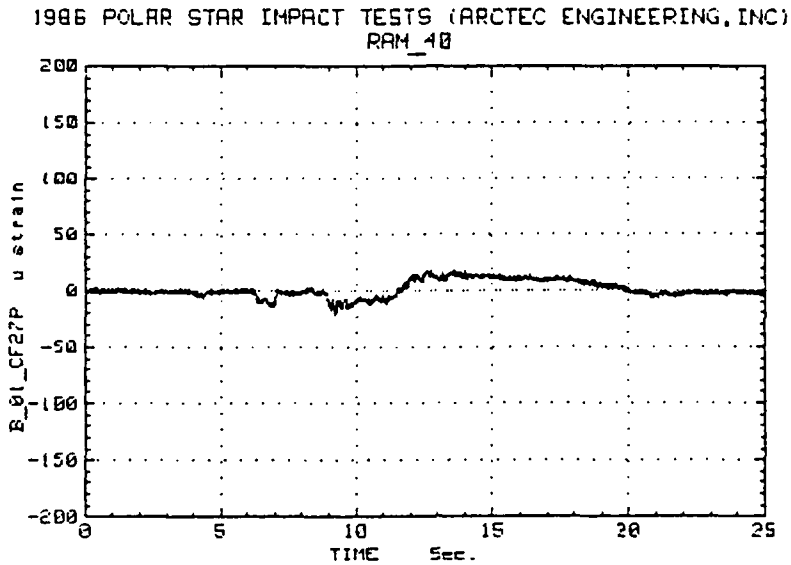
1986 POLAR STAR IMPACT TESTS (ARCTEC ENGINEERING, INC)
RAM_40
B_01_CF27P u strain
TIME Sec.

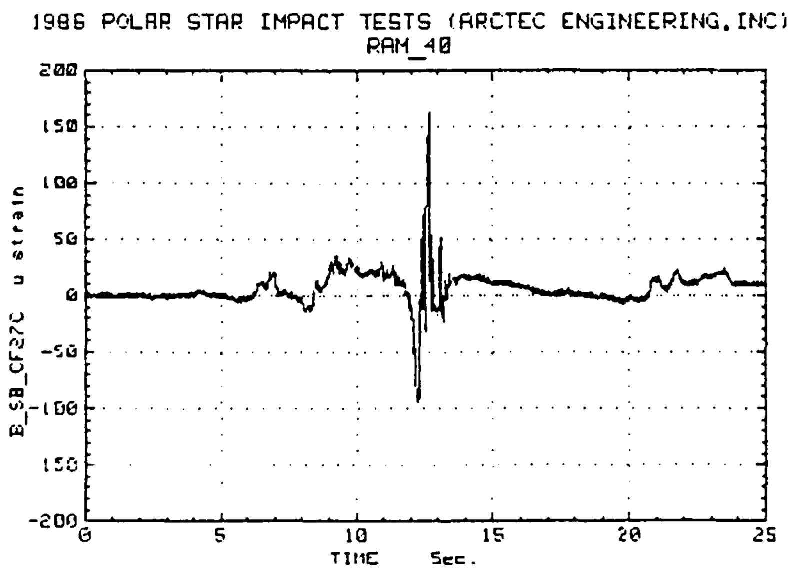
1986 POLAR STAR IMPACT TESTS (ARCTEC ENGINEERING, INC)
RAM_40
B_SB_CF27C u strain
TIME Sec.

1986 POLAR STAR IMPACT TESTS (ARCTEC ENGINEERING, INC)
RAM_40

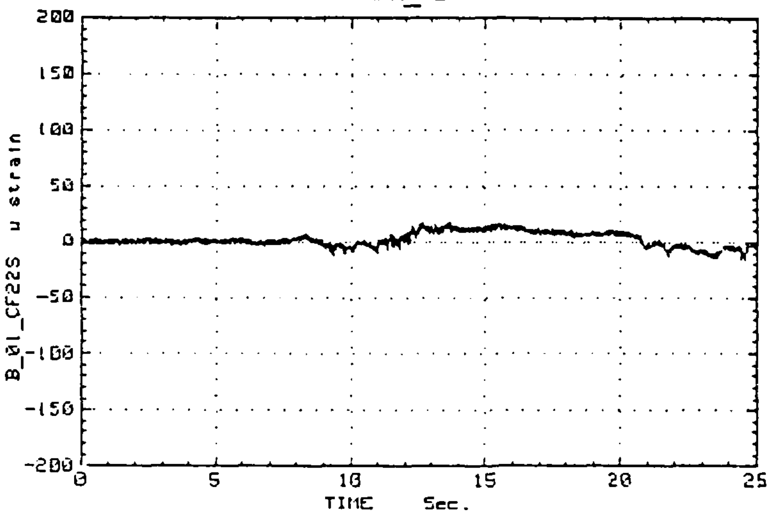

1986 POLAR STAR IMPACT TESTS (ARCTEC ENGINEERING, INC)
RAM_40

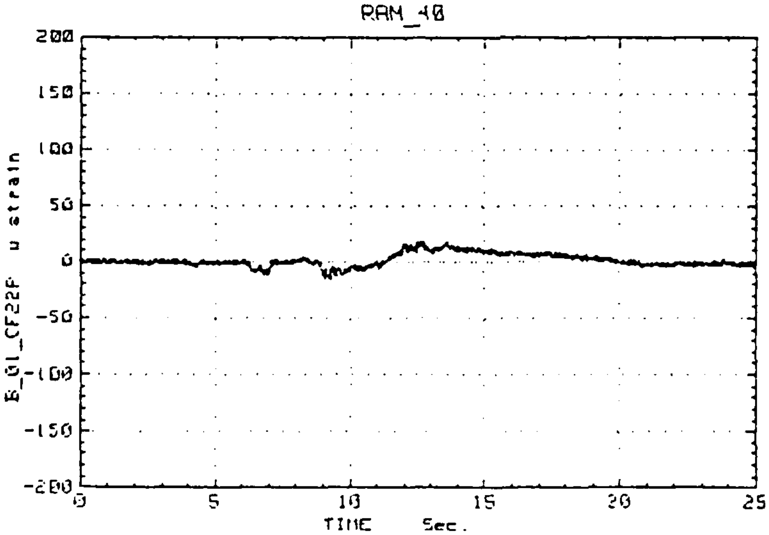

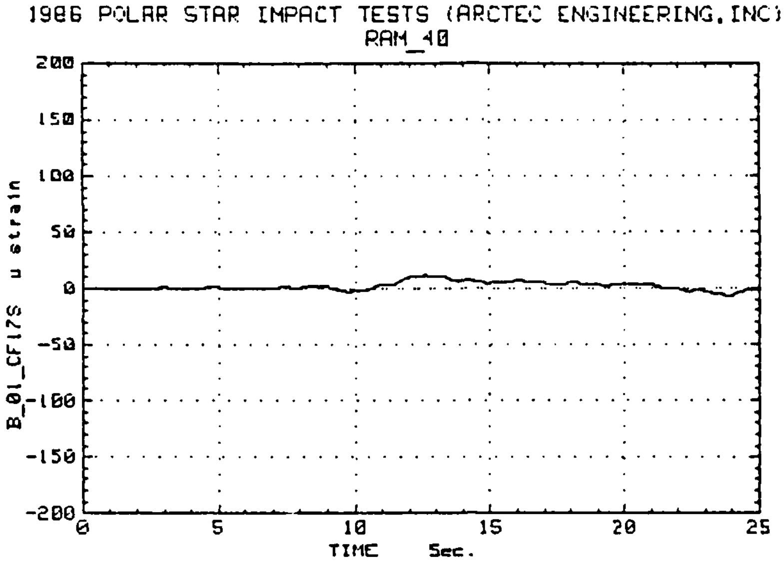
1986 POLAR STAR IMPACT TESTS (ARCTEC ENGINEERING, INC)
RAM_40
B_01_CF17S u strain
TIME Sec.

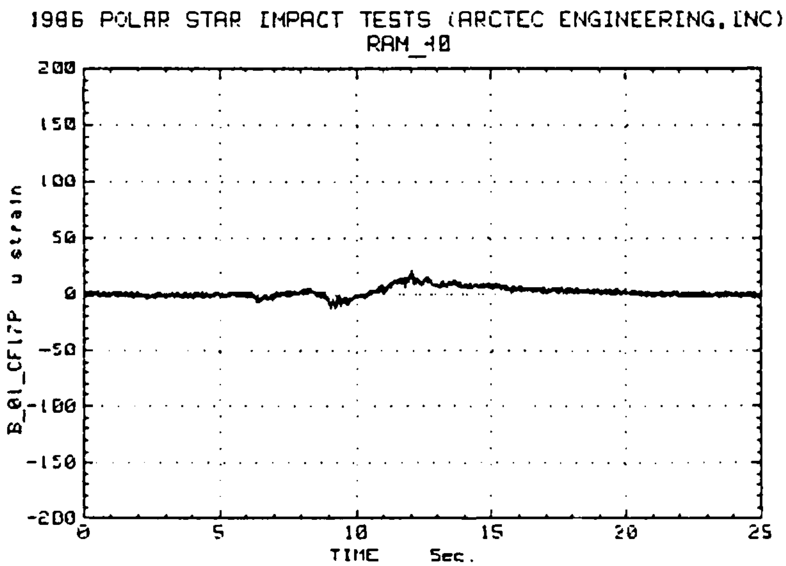
1986 POLAR STAR IMPACT TESTS (ARCTEC ENGINEERING, INC)
RAM_40
B_01_CF17P u strain
TIME Sec.

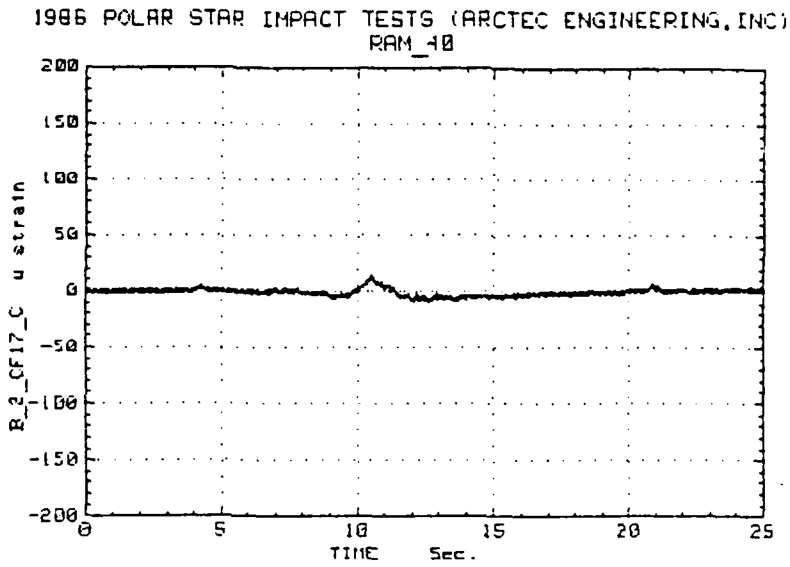
1986 POLAR STAR IMPACT TESTS (ARCTEC ENGINEERING, INC)
RAM_40
B_2_CF17_C u strain
200
150
100
50
0
-50
-100
-150
-200
0
5
10
15
20
25
TIME Sec.

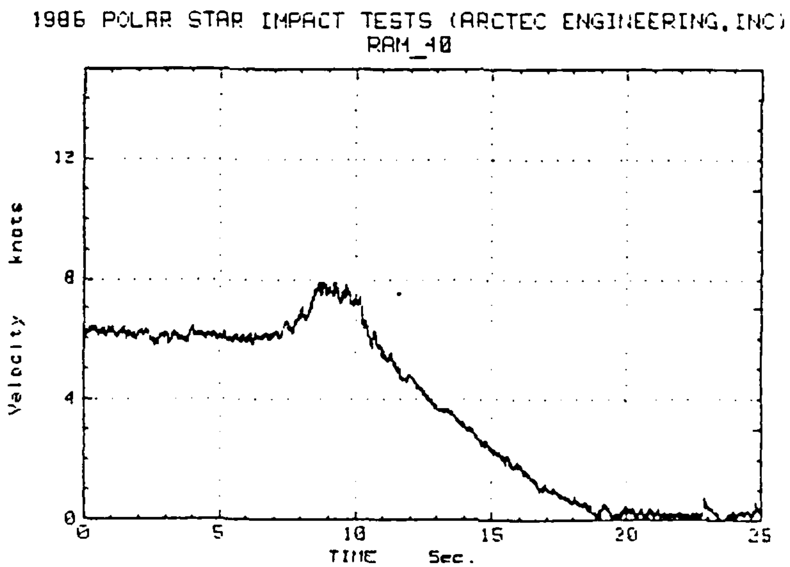
1986 POLAR STAR IMPACT TESTS (ARCTEC ENGINEERING, INC)
RAM_40
Velocity knots
12
8
4
0
0
5
10
15
20
25
TIME Sec.

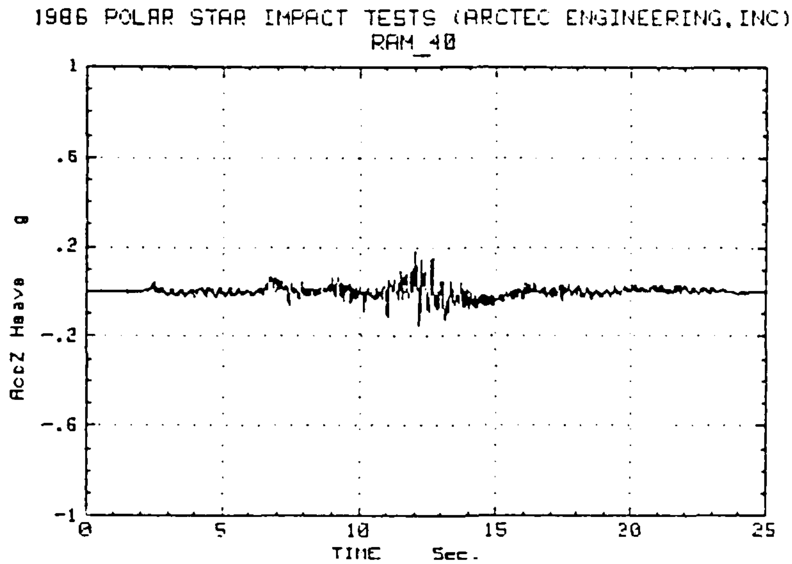
1986 POLAR STAR IMPACT TESTS (ARCTEC ENGINEERING,INC)
RAM_40
AccZ Heave g
TIME Sec.

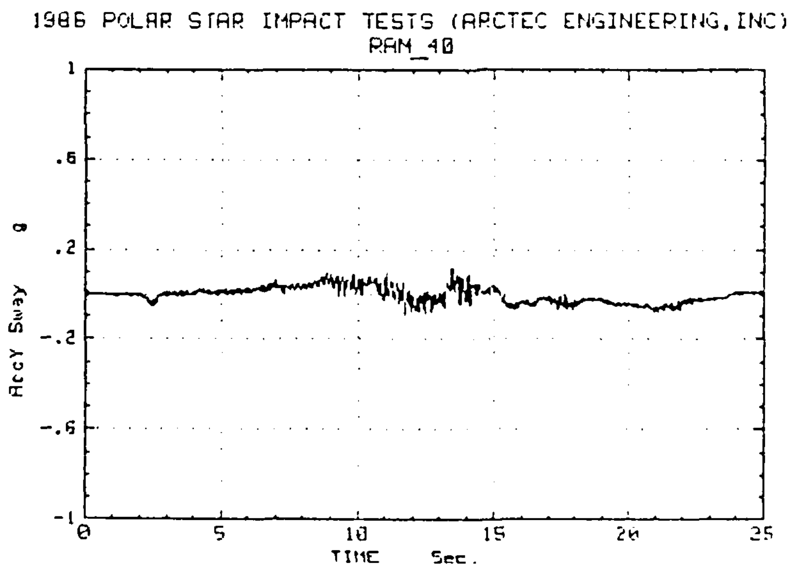
1986 POLAR STAR IMPACT TESTS (ARCTEC ENGINEERING,INC)
RAM_40
AccY Sway g
TIME Sec.

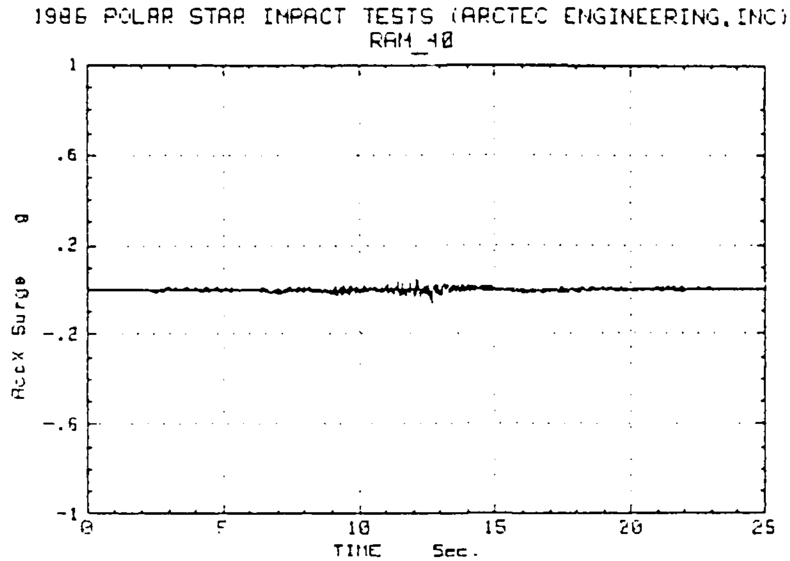
1986 POLAR STAR IMPACT TESTS (ARCTEC ENGINEERING, INC)
RAM_40
AccX Surge g
1
.6
.2
-.2
-.6
-1
0
5
10
15
20
25
TIME Sec.

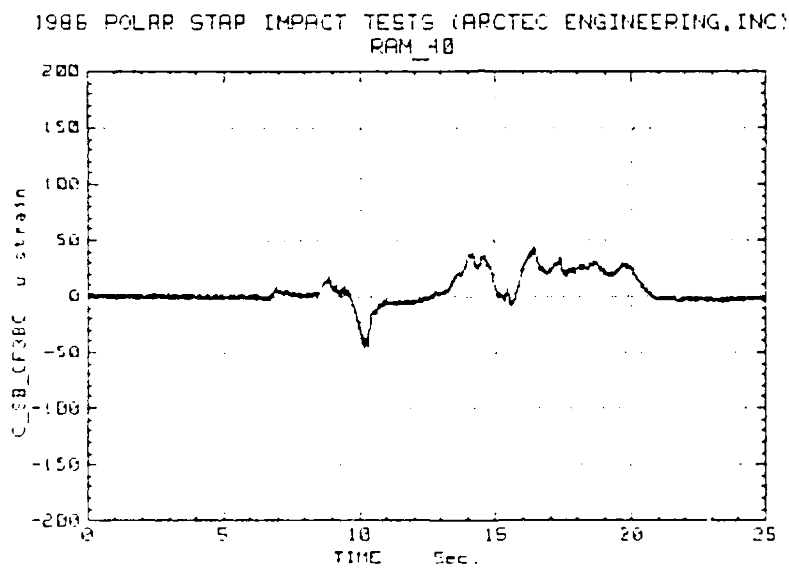
1986 POLAR STAR IMPACT TESTS (ARCTEC ENGINEERING, INC)
RAM_40
C_SB_CF3BC u strain
200
150
100
50
0
-50
-100
-150
-200
0
5
10
15
20
25
TIME Sec.

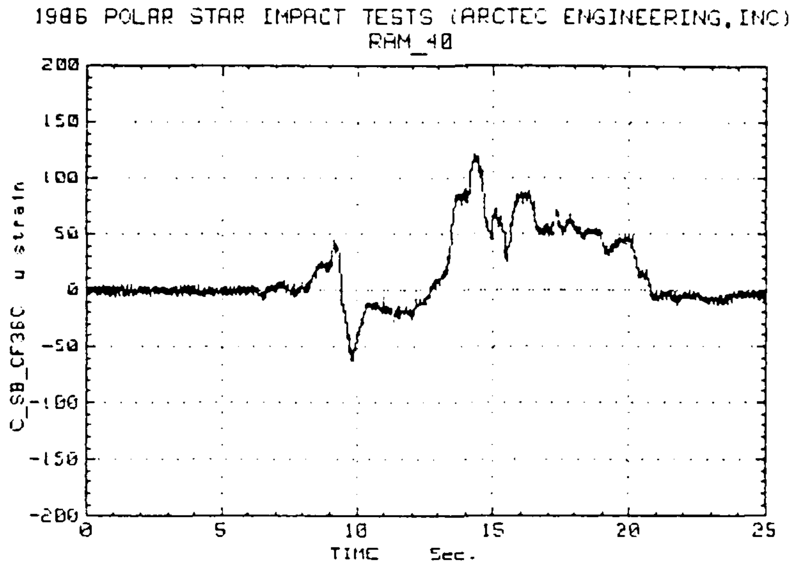
1986 POLAR STAR IMPACT TESTS (ARCTEC ENGINEERING, INC)
RAM_40
C_SB_CF36C u strain
TIME Sec.
200
150
100
50
0
-50
-100
-150
-200
0
5
10
15
20
25

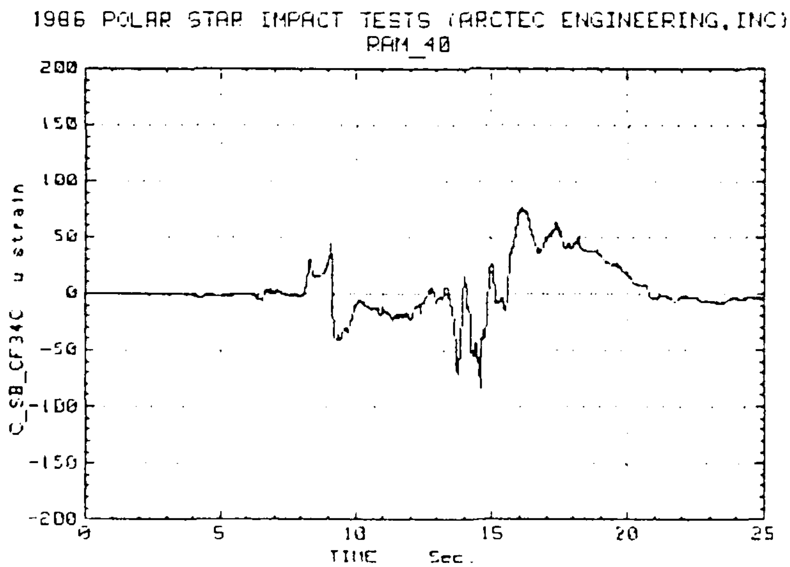
1986 POLAR STAR IMPACT TESTS (ARCTEC ENGINEERING, INC)
RAM_40
C_SB_CF34C u strain
TIME Sec.
200
150
100
50
0
-50
-100
-150
-200
0
5
10
15
20
25

1986 POLAR STAR IMPACT TESTS (ARCTEC ENGINEERING, INC)
RAM_40

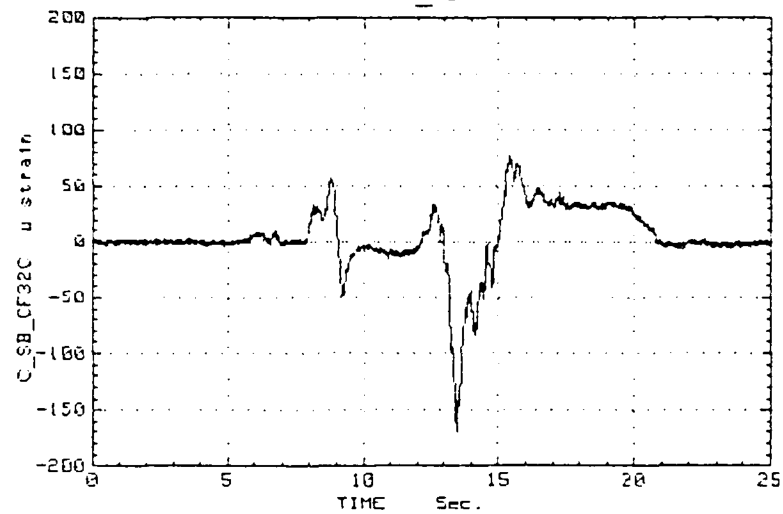

1986 POLAR STAR IMPACT TESTS (ARCTEC ENGINEERING, INC)
RAM_40

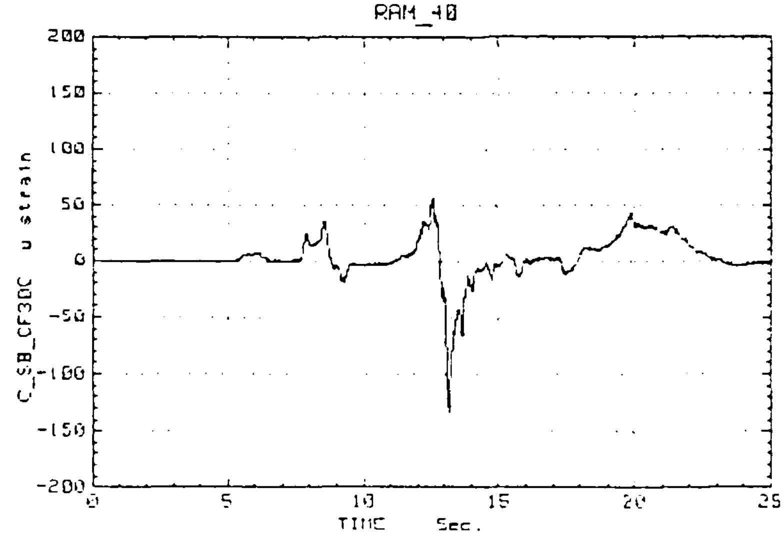

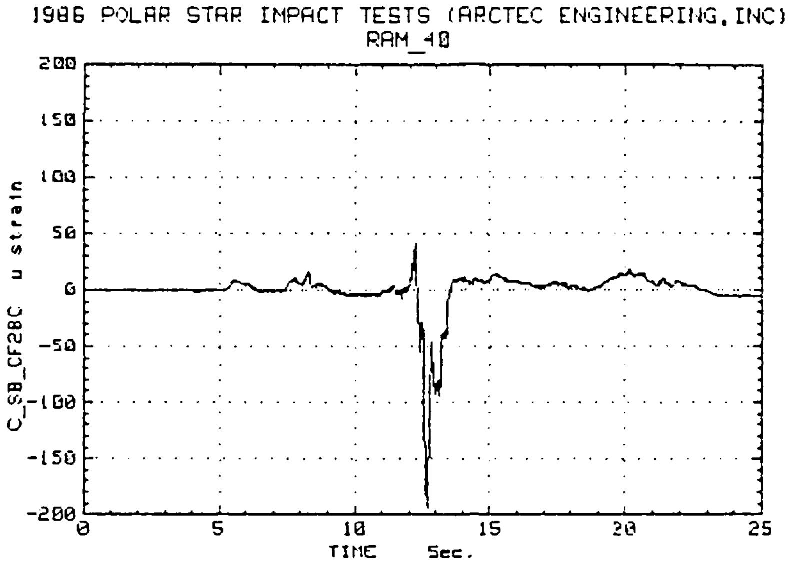
1986 POLAR STAR IMPACT TESTS (ARCTEC ENGINEERING, INC)
RAM_40
C_SB_CF28C u strain
200
150
100
50
0
-50
-100
-150
-200
0
5
10
15
20
25
TIME Sec.

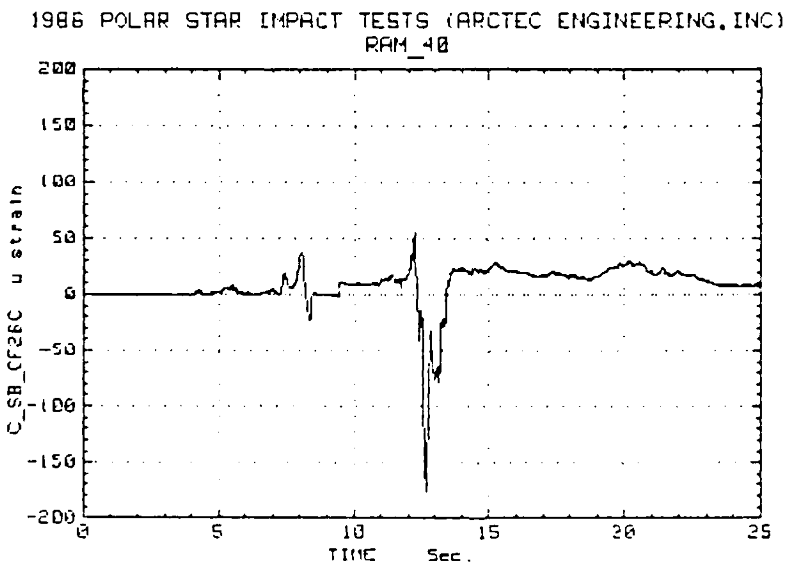
1986 POLAR STAR IMPACT TESTS (ARCTEC ENGINEERING, INC)
RAM_40
C_SB_CF26C u strain
200
150
100
50
0
-50
-100
-150
-200
0
5
10
15
20
25
TIME Sec.

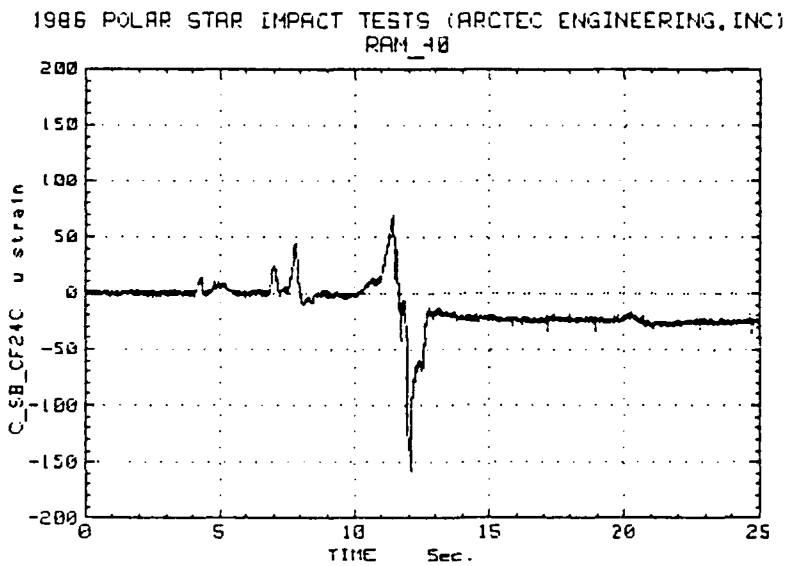

1986 POLAR STAR IMPACT TESTS (ARCTEC ENGINEERING, INC)
RAM_40
C_SB_CF24C u strain
TIME Sec.
200
150
100
50
0
-50
-100
-150
-200
0
5
10
15
20
25

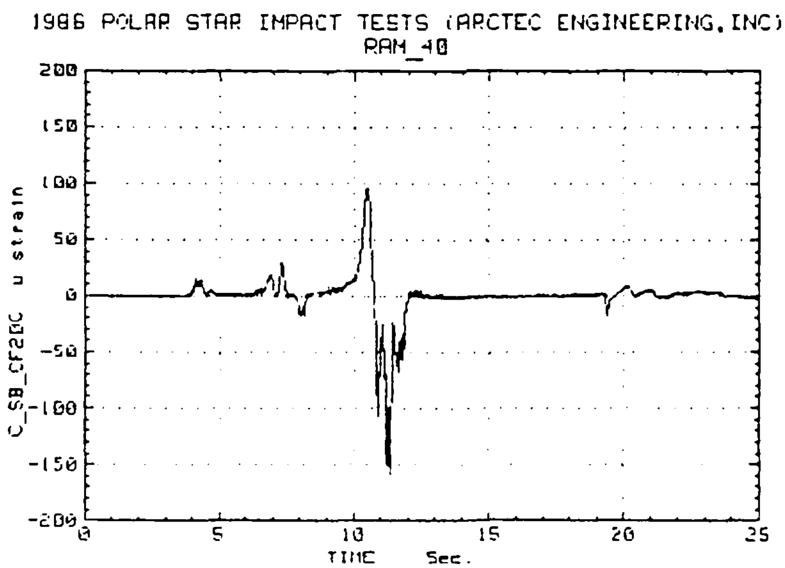

1986 POLAR STAR IMPACT TESTS (ARCTEC ENGINEERING, INC)
RAM_40
C_SB_CF20C u strain
TIME Sec.
200
150
100
50
0
-50
-100
-150
-200
0
5
10
15
20
25

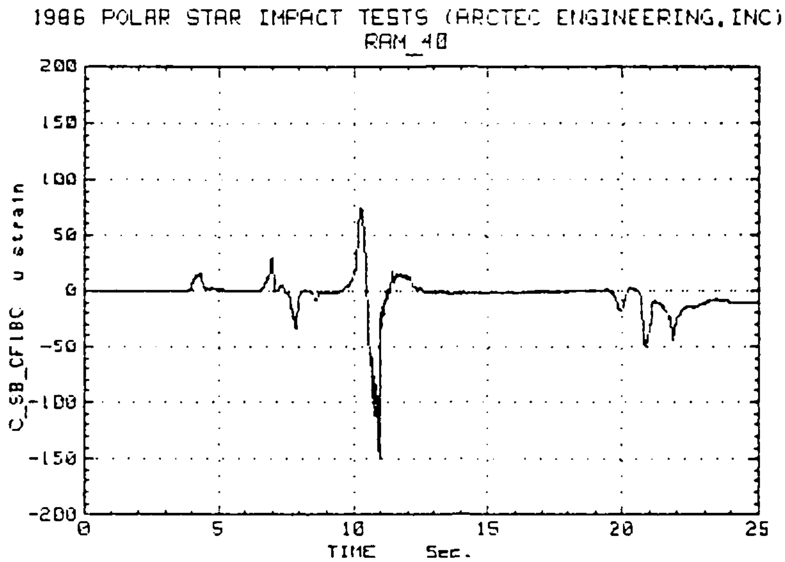
1986 POLAR STAR IMPACT TESTS (ARCTEC ENGINEERING, INC)
RAM_40
C_SB_CF18C u strain
TIME Sec.

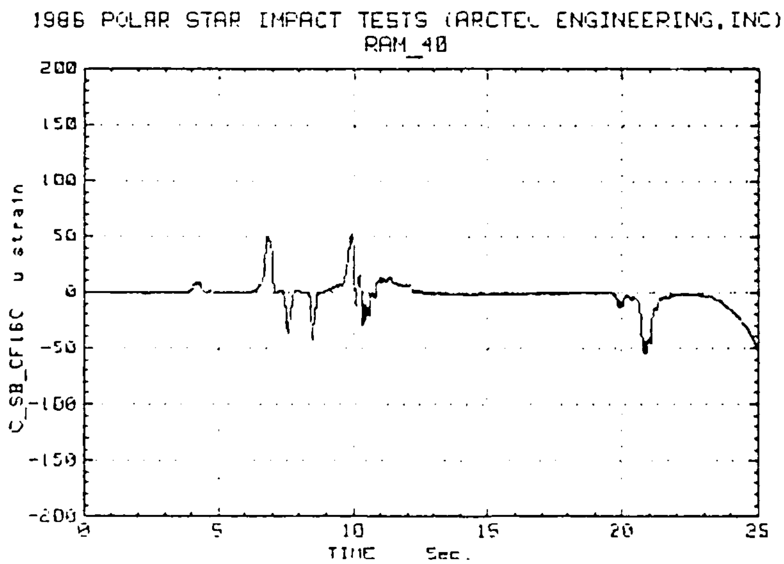
1986 POLAR STAR IMPACT TESTS (ARCTEC ENGINEERING, INC)
RAM_40
C_SB_CF16C u strain
TIME Sec.

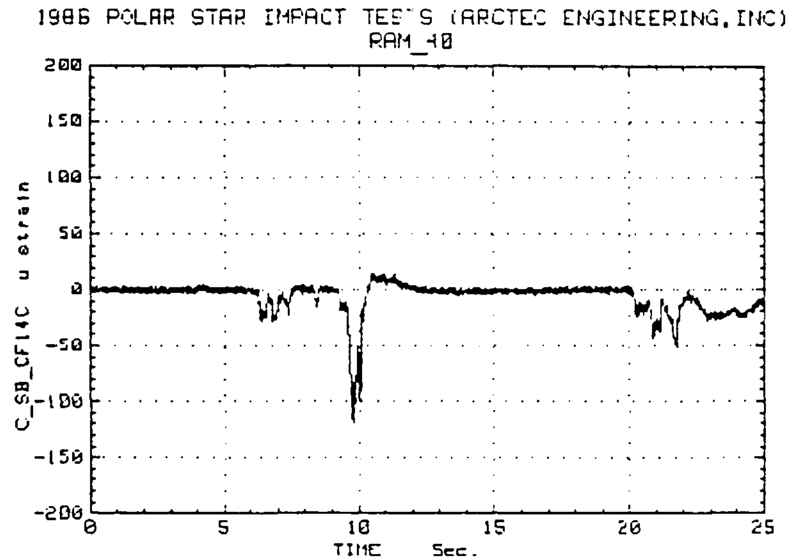
1986 POLAR STAR IMPACT TESTS (ARCTEC ENGINEERING, INC)
RAM_40
C_SB_CF14C u strain
TIME Sec.
200
150
100
50
0
-50
-100
-150
-200
0
5
10
15
20
25

COMMITTEE ON MARINE STRUCTURES

Commission on Engineering and Technical Systems

National Academy of Sciences - National Research Council

The COMMITTEE ON MARINE STRUCTURES has technical cognizance over the interagency Ship Structure Committee's research program.

LOADS WORK GROUP

MATERIALS WORK GROUP

SHIP STRUCTURE COMMITTEE PUBLICATIONS

SSC-329 Ice Loads and Ship Response to Ice by J. W. St. John, C. Daley, and H. Blount 1985

SSC-330 Practical Guide for Shipboard Vibration Control by E. F. Noonan, G. P. Antonides and W. A. Woods 1985

SSC-331 Design Guide for Ship Structural Details by C. R. Jordan and R. P. Krumpen, Jr. 1985

SSC-332 Guide for Ship Structural Inspections by Nedret S. Basar & Victor W. Jovino 1985

SSC-333 Advance Methods for Ship Motion and Wave Load Prediction by William J. Walsh, Brian N. Leis, and J. Y. Yung 1989

SSC-334 Influence of Weld Porosity on the Integrity of Marine Structures by William J. Walsh , Brian N. Leis, and J. Y. Yung 1989

SSC-335 Performance of Underwater Weldments by R. J. Dexter, E. B. Norris, W. R. Schick, and P. D. Watspon 1986

SSC-336 Liquid Slosh Loading in Slack Ship Tanks; Forces on Internal Structures and Pressures by N. A. Hamlin 1986

SSC-337 Part 1 - Ship Fracture Mechanisms Investigation by Karl A. Stambaugh and William A. Wood 1987

SSC-337 Part 2 - Ship Fracture Mechanisms - A Non-Expert's Guide for Inspecting and Determining the Causes of Significant Ship Fractures by Karl A. Stambaugh and William A. Wood 1987

SSC-338 Fatigue Prediction Analysis Validation from SL-7 Hatch Corner Strain Data by Jen-Wen Chiou and Yung-Kuang Chen 1985

SSC-339 Ice Loads and Ship Response to Ice - A Second Season by C. Daley, J. W. St. John, R. Brown, J. Meyer, and I. Glen 1990

SSC-340 Ice Forces and Ship Response to Ice - Consolidation Report by C. Daley, J. W. St. John, R. Brown, and I. Glen 1990

SSC-341 Global Ice Forces and Ship Response to Ice by P. Minnick, J. W. St. John, B. Cowper, and M. Edgecomb 1990

SSC-342 Global Ice Forces and Ship Response to Ice - Analysis of Ice Ramming Forces by Yung-Kuang Chen, Alfred L. Tunik, and Albert P-Y Chen 1990